MATHEMATICAL MODELING OF IMMUNE SYSTEM DYNAMICS DURING FLU INFECTION AND REINFECTION

CATHERINE ENGERT

Department of Mathematics and Statistics
FACULTY OF SCIENCE
McGill University, Montreal

APRIL 2025

A thesis submitted to McGill University
in partial fulfillment of the
requirements for the degree of
Master of Science

ABSTRACT

Immunological memory is a key feature of the human immune system's ability to clear seasonal influenza infections, but we lack detailed and quantitative understanding of the mechanisms that regulate the maintenance of immunological memory over time and activation of memory cells upon reinfection. In this thesis, we develop an 11-delay differential equation within-host model of influenza A virus, which describes three infection phases: the innate and adaptive immune responses, and the generation of immunological memory. We mathematically study a 3-equation submodel of viral dynamics, a 5-equation submodel of the innate immune response to viral infections, and the full 11-equation model. One of the main features of this model is the lack of a unique disease-free steady state, which is due to the interferon (IFN) positive feedback regulation and varying levels of immunological memory. The study of endemic-disease equilibria shows that the existence of memory T cells keeps viral titers low over time. Numerical simulations of the model confirm that the innate immune response is integral to early control of the infection while killer T cells and immunological memory are crucial for limiting the total number of infected cells. This holds for infections of varying infectiousness and viral replication strength.

Various findings regarding the immune response upon re-exposure to the virus follow from numerical simulations of successive infections: (1) very high levels of pre-existing immunity are not able to clear infections without triggering the adaptive immune response, but (2) they do considerably reduce the magnitude of the infection, and (3) repeated re-exposures to virus induce a quicker antibody response and keep antibody levels high. Modeling of various vaccination and natural infection scenarios suggest that these results hold, even when considering decreasing immunity, which results from mutations of the influenza A virus or time elapsed between infections.

We also adapt our model to consider sex-biased differences in the immune response. Increasing T cell and antibody production as well as IFN positive feedback in females results in much shorter infections of lower magnitude and increased inflammation. Conversely, decreasing T cell and antibody production and increasing virus-induced IFN production in males results in infections of decreased magnitude, but of similar length and inflammation as the original simulations. This suggests that such a model could be used to study sex-biased differences in immunological dynamics, but more data is needed to better quantify these differences.

ABRÉGÉ

La mémoire immunitaire est une composante essentielle du système immunitaire, en ce qui a trait à l'élimination d'infections de la grippe saisonière. Cependant, les mécanismes qui régulent le maintien de la mémoire immunitaire et l'activation de cellules mémoire lors d'une réinfection restent à élucider et quantifier. Dans ce mémoire, nous développons un modèle mathématique intra-hôte du virus de l'influenza A, composé de 11 équations différentielles à retards. Ce modèle décrit trois phases de la réponse immunitaire: la réponse immunitaire innée, la réponse immunitaire adaptative (acquise) et la formation de la mémoire immunitaire. Nous étudions mathématiquement un sous-modèle composé de 3 équations, décrivant la dynamique virale de l'influenza A; un sous-modèle composé de 5 équations, décrivant la réponse immunitaire innée aux infections virales; et le modèle complet composé de 11 équations. L'une des principales qualités qui caractérise ce modèle est la non-unicité de l'état d'équilibre correspondant à l'absence d'infection, qui résulte de la modélisation des méchanismes de rétroaction positive de l'interferon (IFN) et des différents niveaux de mémoire immunitaire. L'étude des états d'équilibre endémique de la maladie démontre que l'existence des lymphocytes T mémoire permet d'obtenir une borne supérieure de la charge virale à long-terme. Les simulations numériques du modèle appuient l'hypothèse selon laquelle la réponse immunitaire innée permet de contrôler la croissance initiale de l'infection, tandis que les lymphocytes T cytotoxiques et la mémoire immunitaire déterminent le nombre total de cellules infectées. Nous démontrons d'ailleurs que ces conclusions s'imposent indépendemment de l'infectiosité de la maladie ou de la vitesse à laquelle le virus se réplique.

Les simulations numériques d'infections successives permettent de tirer plusieurs conclusions concernant la réponse immunitaire en cas d'expositions multiples au virus: (1) une mémoire immunitaire préexistante, engendrée par des niveaux élévés de cellules mémoire, ne peut éliminer une infection sans déclencher de réponse immunitaire adaptative (acquise), mais (2) la mémoire immunitaire réduit considérablement la gravité de l'infection, et (3) des expositions répétées au virus promeut une production d'anticorps plus rapide et maintiennent des taux élevés d'anticorps. La modélisation et la simulation de plusieurs scénarios qui incluent à la fois des vaccinations et des infections naturelles suggèrent que ces résultats sont valides, même si l'on prend en considération que immunité décline avec le temps, entre les infections, et que les mutations du virus de l'influenza A sont

fréquentes.

Nous adaptons également notre modèle pour tenir compte de la différenciation de la réponse immunitaire selon le sexe. Une augmentation de la production de cellules T et d'anticorps ainsi que de la rétroaction positive de l'IFN chez les femelles se traduit par des infections beaucoup plus courtes, de moindre gravité, et par une augmentation de l'inflammation chez les femelles. Inversement, une diminution de la production de cellules T et d'anticorps et une augmentation de la production d'IFN induite par le virus chez les hommes entraînent des infections de moindre gravité, mais d'une durée et d'une inflammation similaires à celles des simulations initiales. Cela suggère qu'un tel modèle pourrait être utilisé pour étudier l'impact des différences sexuées sur les dynamiques du système immunitaire, mais davantage de données expérimentales sont nécessaires pour mieux quantifier ces différences.

CONTRIBUTION TO ORIGINAL KNOWLEDGE

In Chapter 2, I derive a new model, described by (2.1.1), of within-host influenza A infection, which to the best of our knowledge is the only within-host delay differential equation (DDE) model of influenza A which explicitly includes innate immunity as well as T-cell mediated immunity and B-cell/antibody mediated immunity, which make up the adaptive immune response. Using piecewise-smooth DDEs, the model (2.1.1) explicitly describes 3 phases of infection, each of which is reached a different threshold is met: the innate immune response, the adaptive immune response, and the generation of immunological memory post-infection. We study the stability of disease-free equilibria of a 3-equation submodel of viral dynamics and show characterize the conditions under which the disease-free and endemic disease steady states stable, which is directly linked to the epidemiological R_0. We numerically study the stability of two types of disease-free equilibria of a 5-equation submodel of the innate immune response to infection: the healthy disease-free equilibrium and the chronic inflammation equilibrium. We study the disease-free equilibria of the full 11-equation model of the innate and adaptive immune responses to acute infection and find that the absence of memory T cells is a necessary condition for the persistence of high viral titers.

In Chapter 3, we use this model to study different reinfection scenarios and study open questions in mathematical modeling of influenza. We find that high levels of pre-existing immunity considerably reduce the magnitude of the infection, and repeated re-exposures to virus induce a quicker antibody response and keep antibody levels high. It is to the best of our knowledge the first within-host differential equation model to study the impact of multiple vaccinations on long-term immunity and how repeated vaccinations impact infection time courses. In Chapter 3, we also adapt this model to study sex-disparities in the innate and adaptive immune responses for males and females, which is one of the first models to do so.

CONTRIBUTION OF AUTHORS

Catherine Engert developed the original model in this thesis and performed all of the mathematical analysis and numerical simulations under Dr Antony Humphries' supervision. Catherine Engert wrote this thesis under Dr Antony Humphries' supervision.

LIST OF ABBREVIATIONS

Abbreviation	Full Name
Ab	Antibody
ASC	Antigen Secreting Cell
AVP	Antiviral Protein
DIB	Discontinuity-Induced Bifurcation
dpi	Days Post-Infection
CTL	Cytotoxic T Cell
DDE	Delay Differential Equation
DF	Disease Free
E	Endemic
H, HA	Hemagglutinin
IFN	Interferon
IL	Interleukin
IR	Immune Response
N, NA	Neuraminidase
NK	Natural Killer
ODE	Ordinary Differential Equation
PWS	Piecewise-Smooth

LIST OF FIGURES

LIST OF TABLES

CONTENTS

ACKNOWLEDGMENTS

I would like to express my sincere gratitude to my advisor, Prof. Tony Humphries, for his support, feedback, and encouragement to explore freely the wonders and intricacies of mathematical modeling. I have learned so much these last years owing to his insightful suggestions and guidance. I would also like to thank everyone else who has been part of our group during the last two years for their help, especially Wendy for guiding me through the chaos of Matlab.

I want to acknowledge the funding I have received from CAMBAM and the Department of Mathematics and Statistics at McGill. I would also like to acknowledge everyone else I've had the opportunity of crossing paths with in the last two years, at McGill, à l'Université de Montréal et à l'extérieur du monde des mathématiques for the support, encouragement, and kindness that have provided a stimulating and inclusive environment in which I was able to flourish.

En particulier, Zahra, par ses judicieuses questions, ses propositions de films, et ce lien qui nous unit d'une sincère et étroite amitié, ainsi que Yixin, par son soutien, ses réserves inépuisables de thé et ses rires, ont ensoleillé mes journées.

Finally, I would like to thank my parents for their many hugs, their enduring love, confidence, and support: my dad for his good humor and curiosity et ma mère pour son enthousiasme et ses précieuses relectures.

CHAPTER 1

INTRODUCTION

In this thesis, I develop a time-dependent delay differential equation model of the human immune system response to natural influenza A infections and reinfections. This 11-equation model takes into account both the innate and adaptive immune responses, which are broadly the first and second phases of the immune response, respectively. To do so, this model will describe the underlying mechanisms and kinetics of viral infections at a cellular level, that is the interactions between different cell types. The model can be divided into three nestled sub-models: the basic viral dynamics (three equations), the innate immune response (five equations), and the full model, including the adaptive immune response (11 equations). The mathematical study of these three different models will allow for a better understanding of the relative contribution and impact of each phase of the immune response during infection. The goal is to simulate different scenarios of infection and reinfection, through natural infection and inoculation, to gain insights into disease time courses, as experimental data for immunological quantities for these scenarios is very limited. Moreover, one of my model's objectives is also to gain a better understanding of how viral time courses are impacted by the delays in the different physiological processes that occur during a flu infection. This model will also be applied to study the difference between male and female individuals, which is little studied in mathematical immunology.

An overview of the different components of the immune response to flu infections is presented in Sections 1.1, 1.2, and 1.3. Previous models of influenza A infections are reviewed in Section 1.4, and Section 1.5 introduces delay differential equation modeling specifically. Section 1.6 presents an overview of numerical simulations, and 1.7 serves as an outline for the work presented in the following chapters this thesis.

1.1 General Immune Response to Flu Infections

Individuals are infected with the flu or influenza A by inhaling respiratory droplets (saliva or mucus) containing influenza virions (virus particles) produced by an infected person exhaling. These virions bind to receptors of healthy epithelial cells, i.e. the cells that line internal organs and body cavities, of the respiratory tract. By doing so, the virions are infecting new cells, which can then produce more virions [1]. This triggers an immune response (IR), made up of two distinct components: (1) the innate immune response and (2)

the adaptive immune response. The innate immune response is the first line of the defense of the immune system. Innate immune cells and molecules are physical and chemical barriers that initiate an immune response by rapidly recognizing antigens, i.e. foreign pathogens. The innate immune response is crucial for early control of an infection. The innate immune response is short lasting and non-specific, i.e. innate immune cells and molecules target and bind to molecules that are common in many viruses and bacteria but they cannot distinguish between different microorganisms. The innate immune response mostly relies on the production of phagocytes and proteins, such as cytokines, a type of protein that affects the behavior of other cells. There are various types of cytokines, which include interferons (IFNs) and interleukins (ILs). The action of innate immune cells and molecules is not always sufficient to eliminate the infection. When this occurs, the adaptive immune response is initiated [2–4].

The adaptive immune response includes a naive or primary component and a memory component. The primary adaptive immune response is triggered when antigen levels exceed a certain threshold and initiated by the innate immune cells [3, 5–7]. The primary adaptive immune response usually takes effect several days post-infection [3, 8, 9]. It is long lasting, more versatile and very specific, i.e. adaptive immune cells can distinguish between and respond to a wide variety of foreign pathogens. The adaptive immune response also relies on cytokine action but its main effects are the result of T-cell and B-cell actions. Moreover, the adaptive immune response is the most important component in immunological memory, which is the immune system's ability to more rapidly recognize previously encountered pathogens. The memory property of the adaptive immune system leads to increased protection because the immune response upon re-infection with the same pathogen is stronger than the immune response provoked by the primary (first) infection [2, 3].

These different components of the immune response peak at different times over the course of infection, with the innate immune response peaking before the adaptive immune response. The peak times of each type of cell, molecule or agent that make up the primary immune response are shown in Table 1.1.

In the case of influenza A infections, the immune response begins when immune cells bind to two antigenic (foreign) proteins found on the surface of virions: hemagglutinin (H or HA) and neuraminidase (N or NA), whose properties determine the sub-type or strain of influenza (e.g. H1N1, H3N2, etc.) [2]. Inoculation and infection usually induce a response based on the recall of previously acquired immune memory (backboosting antibody response, reactivation of memory T cells), which is strongest for an infecting strain that is similar to those of previous infections [10]. For influenza, there are, however, major

Cell or Molecule Type	Range of Values	Reference
Free Virus	2-3	[8, 10–12]
	4-5	[13]
IFNs	2-3	[10, 14]
	2-5	[11]
Effector CD8+ T Cells	7-10	[1, 8, 15, 16]
Effector CD4+ T Cells	6-7	[17]
Effector B cells	7	[10, 18]
Antibody	8-10, 25	[8, 12, 18]

Table 1.1: *Time of Peak of Different Cell Types During Primary Influenza A Infections in Days Post-infection (dpi).*

differences between the immune responses mounted after a natural infection and after vaccination. On one hand, the adaptive immune response induced by a natural infection targets both HA and NA proteins and generates a response of the same magnitude against both. On the other hand, the most common currently licensed influenza A vaccines, which are live attenuated and recombinant vaccines, are HA-based and generate little to no response against NA. This is not ideal because generating an anti-NA immune response results in less severe disease [10].

Post-infection, the waning of antibody titers and the evolution of the virus lead to decreasing immunity. The protection resulting from antibodies also declines such that three to seven years post-infection, an individual is only half as protected from infection when compared to immediately post-infection [10].

1.2 Innate Immune System and Interferons

When an infection occurs, viruses are initially recognized by several innate immune receptors located on the surface of host cells or within these cells [5]. Once activated, these receptors induce innate immune cells and infected cells to produce macrophages, which in turn produce pro-inflammatory cytokines, such as ILs and IFNs, which allows for early control of the infection [5, 19, 20]. In addition, mcrophages can destroy virions through phagocytosis and are an important component of T cell activation [5, 13, 21]. There exist three different types of IFNs. Type I IFNs can reduce the production of virus by infected cells by binding to receptors on the surface of infected cells. This leads to infected cells producing different proteins that inhibit virus replication inside the cell. They can also induce an antiviral state in susceptible, uninfected cells, i.e. make them resistant

to infection [13, 19, 20, 22]. Type II and III IFNs' also have antiviral properties but their precise mechanisms of action have not been characterized as well [19, 23, 24]. Moreover, IFNs stimulate certain components of the innate immune system, such as the production of natural killer (NK) cells (which kill infected cells) [13, 20]. IFNs are also required to activate the short-lived adaptive immune response [20]. When the IFN response occurs sufficiently early in an infection, there is rapid viral clearance which results in a subclinical infection, i.e. an asymptomatic and undetectable infection, or in mild disease. Subclinical infections can be cleared by an innate immune response without inducing an adaptive immune response [5]. In contrast, when the IFN response is delayed, there is persistent viral infection and inflammation which leads to more severe disease [22].

1.3 ADAPTIVE IMMUNE RESPONSE

The adaptive immune response, activated in part by IFNs and other innate immune components, is comprised of high-affinity and antigen-specific T-cell and B-cell responses. In fact, T cells and B cells can recognize a diversity of antigens and mount a targeted response to each pathogen.

1.3.1 *Helper T Cells, Cytotoxic T Cells & Memory T Cells*

During an infection, mature naive CD4+ T cells bind to viral antigen and acquire effector functions to become helper T cells. These cells are required to activate almost all adaptive immune responses. They activate B cells, which leads to antibody secretion and the production of macrophages [9]. Moreover, when mature naive CD8+ T cells bind to viral antigen, they differentiate into effector CD8+ T cells also called cytotoxic T cells (CTLs) or killer T cells. They are then activated by helper T cells, i.e. they acquire effector functions and the ability to migrate to infection sites within a week of their activation by antigen [25]. Once activated, a CTL "hunts" for target cells, i.e the CTL (1) surveys many cells and recognizes infected cells; (2) kills a target cell by binding to the target cell; and (3) the target cell disintegrates and the CTL hunts for new target cells [13, 26]. It is usually supposed that CTLs cannot hit multiple cells simultaneously [26]. The proliferation of CTLs in response to antigenic stimulation can elicit a stronger CTL response (positive feedback loop) which in turn down regulates the virus population, which down regulates the CTL response [27].

During the infection, the T-cell population expands, but it returns to normal levels post-infection, after the deletion of 90 to 95% of effector CD8+ T cells. The remaining 5 to 10% become memory T cells after a few weeks [28–30]. The CD8+ T cells peak 10-fold

higher than CD4+ T cells, but CD4+ T cells peak earlier and the CD4+ T-cell population declines faster [15].

The population of pathogen-specific memory T cells is maintained through homeostatic regulation for years or decades, even in the absence of persistent antigen (bystander stimulation). Upon re-infection with the same pathogen or similar pathogens and re-exposure to antigen, these cells rapidly gain effector functions to kill infected cells [5, 25, 28, 30]. As an individual ages and is exposed to different pathogens, the memory T-cell compartment expands and there is competition for growth factors and anatomical space between memory T cells and naive T cells which limits naive CD8+ T cells' homeostatic proliferation. This could lead to there being fewer T cells available to fight pathogens [5].

These processes also depend on ILs. In fact, ILs and paradoxal IL signaling are an essential part of the immune response resulting in a broad range of T-cell action. For example, IL-12 increases the proliferation, differentiation and the formation of CTLs. IL-2 intensifies antigen specific CD8+ T-cell response and induces T-cell death. IL-7 and IL-15 are required for the formation and maintenance of memory T cells. Moreover, different types of ILs are required for homeostatic regulation of CD4+ T cells [25, 28, 31–33].

1.3.2 *Effector & Memory B Cells and Antibodies*

Exposure to viral antigen after an influenza infection activates naive B cells. After being activated, these B cells differentiate into short-lived effector B cells (plasmablasts), with the action of helper T cells. These plasmablasts can then produce naive or low-affinity virus-specific antibodies which bind to virions and neutralize them [10, 13, 18, 34, 35]. A small fraction of these activated naive B cells also differentiate into long-lived plasma cells after selection for high-affinity B cell receptors in germinal centers. Plasma cells continuously secrete antibody that maintains long-term antibody levels, conferring long-term protection and immunity from disease [10, 18, 35]. Most B cells die post-infection, when there is no longer antigen stimulation, with only a small proportion of long-lived antibody-secreting cells (ASCs) or plasma cells [34] remaining. The mechanisms that explain the persistence of these cells without persistent antigenic stimulation are unclear [10, 18, 35].

Upon activation naive B cells can also differentiate into another type of long-lived cells: memory B cells. Memory B cells do not secrete antibodies, but have the ability to rapidly proliferate and differentiate into plasmablasts on antigen re-encounter, a process heavily reliant on T-cell help [10, 18, 34]. The plasmablasts that result from memory B-cell differentiation secrete mature or high-affinity antibody [10]. Hence, antibodies are secreted by two distinct cell types: short-lived plasmablasts or long-lived plasma cells (i.e. not directly from memory B cells) [10, 13, 18].

1.4 PREVIOUS MATHEMATICAL MODELS OF INFLUENZA

Since the early 20th century, ordinary differential equation (ODE) compartmental models have been used to model between-host population dynamics of infectious diseases, to inform public health decisions. One of the first within-host model of influenza, that is a model describing viral dynamics between cells of a single individual, was developed by Larson et al. in 1976 [36]. This model, consisting of seven compartments and five parameters, was able to accurately reproduce viral titers in mice but its parameters could not be related to biological mechanisms.

1.4.1 *Viral Dynamics Models*

Simple ODE models have been used to quantify cell dynamics in infectious disease because they are relatively easy to fit to data. Basic viral dynamics, which form the base of these ODE models are described in Nowak and May [27] as

$$\dot{V(t)} = kY(t) - uV(t) \tag{1.4.1}$$

$$\dot{X(t)} = \lambda - dX(t) - \beta X(t)V(t) \tag{1.4.2}$$

$$\dot{Y(t)} = \beta X(t)V(t) - aY(t) \tag{1.4.3}$$

with variables $V(t)$ the free virus cell population; $X(t)$, the uninfected, susceptible cell population; and $Y(t)$, the infected cell population with the following parameters: k, the virion production rate; u the death rate of free virus; λ, the birth rate of uninfected cells; d, the death rate of uninfected cells; β, the infection rate constant; a, the death rate constant of infected cells. These equations have been shown to accurately reproduce the exponential growth of viral titers that is measured experimentally [1].

In 2006, Baccam et al. [37] used (1.4.1)-(1.4.3) to model influenza kinetics taking $\lambda = dX(t)$. In this case, (1.4.2) reduces to

$$\dot{X(t)} = -\beta X(t)V(t)$$

and we say the model is target-cell limited.

Target-cell limited models have the trivial steady state $(V^*, X^*, Y^*) = (0, 0, 0)$, which indicates the infection is cleared because all target (susceptible) cells have been infected by virions and have died [13]. Models are constructed in this way because the regeneration and natural death of target cells have long time scales (months) which have little impact on the rapid dynamics of influenza (days). However, this assumes that either (1) all cells are infected or (2) the initial number of target cells X^0 is defined as the number of cells

that will become infected. The first assumption is false as in most cases influenza infects no more than 50% to 60% of the lungs [12].

Target cell limited models do not explicitly account for the immune response. This supposes that either (1) the immune response is negligible or (2) it is constant and implicitly defined by the parameters u and a, which represent the rate of loss of infectious cells Y and virus V, respectively.

Nonetheless, these equations have been shown to accurately reproduce the exponential growth of viral titers that is measured experimentally [1, 11]. Many other target-cell limited ODE models developed since have also been shown to accurately reproduce viral dynamics [1, 12, 37–39]. Moreover, because most variables and parameters in Baccam et al's model [37] represent biological quantities and processes (e.g. viral clearance rate, cell lifespan), the parameter values obtained from fitting the model to experimental data provided new insights on influenza kinetics.

In the last 20 years, the development of within-host ODE and delay differential equation (DDE) models of influenza has greatly accelerated. This has led to the development of more complex models which have allowed for greater theoretical investigations of cell dynamics and the impact of the immune response on viral time courses [8, 12, 32, 40–43].

1.4.2 *Immune Response Models*

The 1994 model of Bocharov et al. [44] is widely recognized as one of the first within-host model of influenza to include the immune response [1, 13]. This 10-dimensional ODE model included compartments for helper T cells, CTLs, B cells, antibodies and interferon (IFN) and was parameterized using the known biology of influenza infections. However, the model was not validated using experimental data.

In [37], the model described by (1.4.1)-(1.4.3) was also extended to include an IFN compartment, representing the immune response. Parameterizing this model with experimental data resulted in fits that were not statistically significantly better than the ones obtained with the 3-dimensional model described by (1.4.1)-(1.4.3), which includes no immune response. However, the model in [37] could reproduce a double peak in virus load, which occurs in some patients, whereas the model in (1.4.1)-(1.4.3) could not. More generally, basic influenza models that do not account for the immune response are unable to reproduce a variety of scenarios. For example, dose-dependent dynamics, i.e. infections where the viral load is low, or infections in immunocompromised individuals cannot be modeled without adding an immune response component [11]. Since the mid-2000s, many models which include the immune response, and the differences between the innate and adaptive immune responses, have been developed [2]. These models include the

Cell or Molecule Type	Range of Values	Unit	Reference
Free Virus	10^6	$\text{TCID}_{50}\cdot\text{mL}^{-1}$	[1]
Infected Cells	$2.625 \cdot 10^9$ - $5.25 \cdot 10^9$	cells	[11, 12, 41, 45]
IFNs	$10 - 100$	$\text{pg} \cdot \text{ml}^{-1}$	[14]
Effector CD8+ T Cells	$5 \cdot 10^4$ - 10^6	cells	[8, 16, 29]
Effector CD4+ T Cells	$5 \cdot 10^3$ -10^5	cells	[15]
Effector B cells	$\sim 10^3$	$\text{cells} \cdot \mu\text{L}^{-1}$	[46]
Antibody	$4 \cdot 10^2$ - $8 \cdot 10^2$	$\text{pg} \cdot \text{ml}^{-1}$	[8]

Table 1.2: *Typical Peak Values of Different Cell Types During Influenza A Infections.*

3-dimensional virus-triggered innate immune signaling model developed by Tan et al. [40] which is described in Section 2.1.2.

The main challenge with models which include an immune response component is the lack of diverse and quantitative data. This is mostly due to the fact that influenza infections occur over a very short time period and most data from human patients only contains a few time points representing immunological measurements such as cytokine or antibody levels, making it hard to parameterize mathematical models [12, 13].

However the peak values of most immune components have been experimentally measured and can be found in Table 1.2. In Table 1.2, the viral load is measured in units of 50% tissue culture infectious dose TCID_{50} (or TCID_{50}/mL), which represents infectious viral load only (total virus is measured by viral RNA levels). TCID_{50} has been used in previous models [1, 11, 12]. The T-cell populations describe the T-cell populations in the lungs and the B-cell concentrations are in liters, which is the right order of magnitude for B cells in the lungs.

1.5 DELAY DIFFERENTIAL EQUATION MODELING

The mathematical modeling of many biological phenomena entails taking into account various delays in physiological processes, such as the delay between infection and production of immune cells, or the delay between infection and the production of virions by the infected host. Classical time-dependent ODE models that seek to model these delays often introduce an additional compartment or variable representing a latent state, assuming that the latent and infected periods are exponentially distributed [1]. For example, when including a latent or eclipse phase, $E(t)$, the model described by (1.4.1)-(1.4.3) becomes

$$\dot{V(t)} = kY(t) - uV(t) \tag{1.5.1}$$

$$\dot{X(t)} = \lambda - dX(t) - \beta X(t)V(t) \tag{1.5.2}$$

$$\dot{E(t)} = \beta X(t)V(t) - cE(t) \tag{1.5.3}$$

$$\dot{Y(t)} = cE(t) - aY(t) \tag{1.5.4}$$

with the new variable E and new parameter c. In this case, cells become infected after an average time c^{-1} has elapsed. The assumption that the latent and infected periods are exponentially distributed was shown to incorrectly reproduce influenza kinetics. As such, the implementation more appropriate delays could lead to more accurate model behavior and parameter value estimates [1].

The introduction of additional compartments to represent multiple steps (or cascades) within a process, as in (1.5.1)-(1.5.4) where X produces E which in turn produces Y, can lead to an increase in the number of parameters in more complex models [47]. This can make it harder to have quantifiable parameters with biological significance, especially if multiple delays are considered. DDE models, while less common in mathematical modeling of immunological processes than classical ODE models, allow us to avoid these issues [2].

Similarly to ODE models, we can define an initial value problem for autonomous DDEs in $\mathbb{R}^n$. The following definitions are taken from Smith [48]. Let $\tau > 0$, the delay, be a real number. Let $C = C([-\tau, 0], \mathbb{R}^n)$, the state space of the dynamical system, be the space of continuous functions from $[-\tau, 0]$ into $\mathbb{R}^n$, with the norm

$$\|\phi\| = \sup\{|\phi(\theta)| : -\tau \leq \theta \leq 0\}, \quad \phi \in C.$$

Then, the initial value problem for an initial condition ϕ is

$$\begin{aligned} x'(t) &= f(x, x_t), \quad t \geq 0 \\ x_0 &= \phi \end{aligned} \tag{1.5.5}$$

where $x'(t)$ represents the right hand derivative of $x(t)$ and $f : C \to \mathbb{R}^n$ is a given function. We say $x(t)$ is a solution to the initial value problem if it satisfies (1.5.5). Then, in a dynamical systems framework, the trajectory of the solution to (1.5.5) is the curve $t \to x_t$. For $x(t) \in C([-\tau, S], \mathbb{R}^n)$, $S \geq 0$, then for any $t \in [0, S]$, we define $x_t \in C$, the state of the dynamical system at time t by

$$x_t(\theta) = x(t + \theta), \quad -\tau \leq \theta \leq 0. \tag{1.5.6}$$

The state of the system is defined this way because to know the value of $x(s)$ for $t \leq s \leq S$, we must know all the values $x(\eta)\ \forall\ \eta \in [t - \tau, t]$. By rewriting $\theta = \eta - t$, we

obtain (1.5.6).

If in addition to continuity, we assume f is Lipschitz in the state variable x_t on each bounded subset of $\mathbb{R} \times C$, then there exists a unique solution to the initial-value problem (1.5.5) [48].

The delays that occur most frequently in the modeling literature are discrete or constant delays [49]. In this case, (1.5.5) can be written

$$\begin{aligned} x'(t) &= f(x, x(t-\tau)) \\ x(t) &= \phi(t), \quad -\tau \leq t \leq 0. \end{aligned} \tag{1.5.7}$$

If $\tau = 0$, (1.5.7) is simply an ODE initial-value problem. When there are multiple delays, (1.5.7) becomes

$$x'(t) = f(x, x(t-\tau_1), \cdots, x(t-\tau_n)) \tag{1.5.8}$$

with $\tau_1 \geq \cdots \geq \tau_n$.

We can define $f(x, x(t-\tau)) = f(x, y)$. Theorem 3.1 in [48] states that if f, f_x and ϕ are continuous, then there exists $\sigma > 0$ such that there exists a unique solution of (1.5.7) on $[-\tau, \sigma]$. This can be generalized to the case with multiple delays, (1.5.8) [48].

Many DDEs model intrinsically nonnegative quantities arising from biological problems. As such, ensuring nonnegative initial conditions lead to nonnegative solutions is an important aspect of DDE modeling. From Theorem 3.4 of [48], for $x \in \mathbb{R}^n$, if there exists a unique solution of the initial-value problem (1.5.8) under continuity of f and f_x, and $x_i = 0$ implies $f_i \geq 0$, then provided $\phi \geq 0 \, \forall t \in [-\tau, 0]$, then $x(t) \geq 0 \, \forall t \geq 0$ for which it is defined.

$x(t) = x^* \in \mathbb{R}^n$ is a steady state solution of (1.5.5) if and only if $f(\hat{x}^*) = 0$, where $\hat{x}^* \in C$ is the constant function equal to x^*. The equilibria of (1.5.8) are the same as that of the corresponding ODE

$$x'(t) = f(x(t), \cdots, x(t)).$$

Like ODEs, but unlike PDEs, DDEs have the principle of linearized stability. Thus, similarly to ODE systems, the local stability of these equilibria can be determined by linearizing the system about the equilibria. The following derivation follows Smith [12].

If $x(t)$ is a solution of (1.5.5), to linearize about x^*, we consider the solution

$$x(t) = x^* + y(t)$$

where $y(t)$ is a small perturbation to the solution $x(t)$. Then $y(t)$ is a solution of

$$y'(t) = f(\hat{x}^* + y_t).$$

We assume that f can be written in the form

$$f(\hat{x}^* + \phi) = L(\phi) + g(\phi), \quad \phi \in C$$

where $L : C \to \mathbb{R}^n$ is a bounded linear function and $g : C \to \mathbb{R}^n$ is "higher order", i.e.

$$\lim_{\phi \to 0} \frac{|g(\phi)|}{\phi} = 0.$$

If we neglect the higher order term, we obtain the linearized equation about the equilibrium $\hat{x}^*$,

$$z'(t) = L(z_t). \tag{1.5.9}$$

For the DDE defined in (1.5.7), the linearized equation (1.5.9) simplifies to

$$L(z_t) = f_x(\hat{x}^*)x(t) + f_y(\hat{x}^*)x(t-\tau) \tag{1.5.10}$$

where we define $f(x, x(t-\tau)) = f(x, y)$. This can be generalized to a DDE with multiple discrete delays of the form in (1.5.8). In this case, we have

$$L(z_t) = f_x(\hat{x}^*)x(t) + \sum_{j=1}^{n} f_{y_j}(\hat{x}^*)x(t-\tau_j) \tag{1.5.11}$$

where we define $f(x, x(t-\tau_1), \cdots, x(t-\tau_n)) = f(x, y_1, \cdots, y_n)$.

For $z(t) = e^{\lambda t}v$, $v \neq 0$ to be a solution of (1.5.9), with λ complex and v a vector with complex components, we must have

$$\lambda v = L(e^{\lambda}v) = L_\lambda$$

where L_λ is an $n \times n$ matrix. For DDEs with a single discrete delay, as defined in (1.5.7), we have

$$L_\lambda = f_x(\hat{x}^*)v + f_y(\hat{x}^*)e^{-\lambda\tau}v.$$

We can generalize this to DDEs with multiple discrete delays as defined in (1.5.8) and we obtain

$$L_\lambda = f_x(\hat{x}^*)v + \sum_{j=1}^{n} f_{y_j}(\hat{x}^*)e^{-\lambda\tau_j}v.$$

Then $z(t)$ is a solution of (1.5.9) if λ is a root of the characteristic polynomial

$$\det(\lambda I - L_\lambda) = 0.$$

The delays often result in more complex characteristic polynomial that typically have

infinitely many roots. From Theorem 4.8 in [48], let $\Delta(\lambda) = 0$ be the characteristic polynomial corresponding to (1.5.9), which is the linearized system of (1.5.5) and suppose that

$$-\sigma := \max_{\Delta(\lambda)=0} \Re(\lambda) < 0.$$

Then x^* is a locally asymptotically stable steady state of (1.5.5). If $\Re(\lambda) > 0$ for some λ, then the equilibrium is unstable.

Sufficiently large delays can also lead to delay-induced instability or delay-induced oscillations. A solution $x(t)$ to (1.5.5) is oscillatory with respect to a steady state x^* if $x(t) - x^*$ has arbitrarily large zeros: for some $s \in \mathbb{R}$, for a solution of (1.5.5), defined for $t \geq s$ for every $t_0 > s, \exists\, t_1 > t_0$ such that $x(t_1) - x^* = 0$ [21]. If it is locally asymptotically stable for all delays, then we say x^* has delay-independent stability.

1.5.1 *Piecewise-Smooth Delay Differential Equations*

The mathematical modeling of infections requires the modeling of distinct phases representing various biological processes. For example, in my mathematical model, which will be developed in Chapter 2, the adaptive immune system is not activated until virus levels cross a certain threshold. In this context, piecewise-smooth (PWS) functions can be used to define the distinct phases. More generally, PWS functions are often used to represent biological processes that are described by smooth nonlinear functions. The use of PWS functions can simplify the model and lead to easier mathematical analysis [50].

The following definitions are taken from Bernardo et al. [51]. A PWS flow is described by a finite set of smooth ODEs

$$\dot{x} = F_i(x, \mu), \quad \text{for } x \in S_i$$

where $\bigcup_i S_i = \mathcal{D} \subset \mathbb{R}^n$ and each S_i is non-empty. The intersection

$$\sum_{ij} := \bar{S}_i \bigcap \bar{S}_j$$

is either an $\mathbb{R}^{n-1}$-dimensional manifold included in the boundaries ∂S_i and ∂S_j or it is the empty set. Each F_i is smooth in both the state x and the parameter set μ for any open subset of S_i and defines a smooth flow $\Phi_i(x, t)$ within any open set $U \supset S_i$. If $\sum_{ij}$ is non-empty, it is called a discontinuity set or switching manifold. The degree of smoothness of a PWS ODE in the switching manifold $\sum_{ij}$ is determined by the highest order r such that the Taylor series expansions of $\Phi_i(x, t)$ and $\Phi_j(x, t)$ agree up to terms of $\mathcal{O}(t^{r-1})$. If $F_i(x) \neq F_j(x)$ for $x \in \sum_{ij}$, then the degree of smoothness of the PWS ODE is one. This type

of system is said to be of Filippov type. If $F_i(x) = F_j(x)$ but $F_{i,x} \neq F_{j,x}$, then the degree of smoothness is two. Systems with smoothness of degree two or higher are said to be PWS continuous systems. PWS systems give rise to various types of bifurcations on the switching manifold called discontinuity-induced bifurcations (DIBs). These can occur, for example, when an equilibrium point lies on a discontinuity set or there are limit cycles near or tangent to the discontinuity set.

For example, for an ODE with a single discontinuity set, we have

$$\dot{x} = \begin{cases} F_1(x, \mu), & \text{if } x \in S_1 \\ F_2(x, \mu), & \text{if } x \in S_2 \end{cases} \tag{1.5.12}$$

where F_1 generates the flow Φ_1 and F_2 generates the flow Φ_2. The single boundary can be written as the zero of a smooth function H such that (1.5.12) can be written as

$$\dot{x} = \begin{cases} F_1(x, \mu), & \text{if } H(x) \leq 0 \\ F_2(x, \mu), & \text{if } H(x) > 0. \end{cases} \tag{1.5.13}$$

As shown in Barton [50], this can be extended to PWS DDEs with a finite number of discrete delays:

$$\dot{x(t)} = \begin{cases} F_1(x(t), x(t-\tau_1), \ldots, \mu) & \text{if } H(x(t), x(t-\tau_1), \ldots) \leq 0 \\ F_2(x(t), x(t-\tau_1), \ldots, \mu) & \text{if } H(x(t), x(t-\tau_1), \ldots) > 0. \end{cases} \tag{1.5.14}$$

1.6 Numerical Simulations

The goal of numerically simulating DDEs is to approximate solutions of initial value problems for which we cannot find exact solutions and to study the qualitative behavior of equilibria using the characteristic roots of linearized systems. DDE models are generally more complex to simulate numerically than ODE models but restricting a model to DDEs with discrete delay results in a more robust numerical solution [2, 49].

For the initial-value problem defined in (1.5.7), the following definitions are adapted from Bellen and Zennaro [52] and Shampine [49]. On the interval $[0, T]$, we consider step sizes $h_n > 0$ and mesh points $\Delta = \{t_0, t_1, \ldots, t_n, \ldots, t_N = T\}$. Considering $t_0 = 0$ and $t_n = t_{n-1} + h_n$ for $n \geq 1$, for all $t_n \in \Delta$ we either have that $t_n - \tau < 0$ or $t_n - \tau \in (t_i, t_{i+1}]$. By solving a discrete set of algebraic equations for x_{n+1}, we can approximate $x(t_{n+1})$. This is called a temporal discretization of the initial value problem. Methods that compute x_{n+1} are called explicit if x_{n+1} can be solved explicitly. Otherwise, they are called implicit. A DDE is said to be stiff if for most explicit methods, the largest step size h_n guaranteeing

numerical stability and a small discretization error is excessively small [53]. This occurs when some components of solutions to the differential equation system decay much faster than others. In these cases, implicit methods usually perform much better than explicit methods.

Initial time-series simulations of the DDE model were performed with the Matlab function `dde23` [54]. Most of the code of `dde23` is based on explicit continuous Runge-Kutta methods, which are a family of methods used for temporal discretization of nonlinear differential equations [49]. However, due to the stiffness of the differential equation model in this thesis, some simulations were performed using `dde15s`, adapted from the Matlab stiff ODE solver `ode15s` by Dr Lawrence F. Shampine (Southern Methodist University) in Agrawal et al. [55]. The updated version of the software, `dde15s_updated`, was written by Michelle Przedborski [56]. The absolute and relative tolerances used were 10^{-9}.

1.7 THESIS OUTLINE

In Chapter 2, in Section 2.1, I will develop an 11-equation time-dependent delay differential equation model of the immune response during infection, including immune components responsible for the maintenance of immunological memory. Solutions of this model and the stability of steady states values will then be studied. First, solutions of a three-equation submodel of within-host viral dynamics without the immune response will be studied in Section 2.2.1. Then, solutions of a five-equation submodel of viral and innate immune dynamics will be studied in Section 2.2.2. Finally, solutions of the full 11-equation model of viral, innate immune, and adaptive immune dynamics will be studied in Section 2.2.3. Numerical simulations of these models will be performed and the effect of some parameters on model dynamics will be assessed in Section 2.3. Modeling these submodels, i.e. simplified systems, will allow us to study the influence of various immune compartments separately.

In Chapter 3, we will study the impact of the cell compartments which are responsible for maintaining immunological memory on reinfection time-courses. Specifically, in Section 3.1, a framework to model reinfections will be developed, taking into account the various factors which influence immunological memory. Numerical simulations will be performed in Section 3.2 and the impact of these factors will be discussed. A model of sex-biased difference in immune responses on infection and reinfection time courses will be developed and studied in Section 3.3. We will discuss the different sex-biased factors and their impact on the immune response as well as how to include them in the model previously developed.

CHAPTER 2

MATHEMATICAL MODELING OF THE IMMUNE RESPONSE TO INFLUENZA A

In this chapter, I will develop a time-dependent delay differential equation model of the immune response during infection, study its stability and perform numerical simulations representing various infection scenarios. The model will be derived in Section 2.1. First, a three-equation submodel of within-host viral dynamics without the immune response will be developed in Section 2.1.1. Then, a five-equation submodel of viral and innate immune dynamics will be developed in Section 2.1.2. Finally, the full 11-equation model of viral, innate immune, and adaptive immune dynamics will be developed in Section 2.1.3. The solutions and their stability will be studied in Section 2.2 with the three-, five-, and eleven-equation models studied in Sections 2.2.1, 2.2.2, and 2.2.3, respectively. Numerical simulations will be performed and presented in Section 2.3. Estimations of parameter values, model simulations for various infection scenarios, and sensitivity of the model to the parameters will be discussed in Sections 2.3.1, 2.3.2, and 2.3.3, respectively.

2.1 Derivation of the Delay Differential Equation Model

My goal is to model how innate and adaptive immune cell populations evolve during infection and reinfection with time-dependent delay differential equations. The model will be comprised of the following 11 time-dependent variables:

V : Free Virus Concentration ($\text{TCID}_{50} \cdot \text{mL}^{-1}$)

X : Uninfected, Susceptible (Target) Cell Population (cells)

Y : Infected Cell Population (cells)

R : Recovered and Resistant to Infection Cell Population (cells)

I : IFN Serum Concentration ($\text{pg} \cdot \text{mL}^{-1}$)

T_E : Effector CD8+ T-Cell Population (cells)

T_M : Memory T-Cell Population (cells)

T_H : Helper CD4+ T-Cell Population (cells)

B_{LL} : Long-lived B-Cell Concentration (cells $\cdot \mu\text{L}^{-1}$)

B_E : Effector B-cell Concentration (cells $\cdot \mu \mathrm{L}^{-1}$)

A : Antibody Concentration (pg $\cdot$ mL^{-1}).

The variables V, X, and Y constitute the basic viral dynamics. A three-equation submodel describing these dynamics will be derived in Section 2.1.1. The innate immune dynamics are comprised of the variables V, X, Y, R, and I. Building on the equations for viral dynamics derived in Section 2.1.1, the equations characterizing the innate immune response will be derived in Section 2.1.2. The full model, describing both the innate and the adaptive immune responses described by (2.1.1a)-(2.1.1k) will be derived in Section 2.1.3 by extending the innate immune response model developed in Section 2.1.2. The dynamics will be described by the following equations:

$$\dot{V} = k_V Y(t-\tau_V)\frac{\tilde{K}_1^n}{\tilde{K}_1^n + I^n(t-\tau_{IV})} - d_V V(t) - \rho_V A(t) V(t) \tag{2.1.1a}$$

$$\dot{X} = \mu - d_X X(t) - \beta X(t) V(t) - k_{IX} X(t) I(t) \tag{2.1.1b}$$

$$\dot{Y} = \beta X(t) V(t) - d_Y Y(t) - k_{T_E Y} T_E(t) Y(t) - k_{IY} I(t) Y(t) \tag{2.1.1c}$$

$$\dot{R} = k_{IX} X(t) I(t) + k_{IY} Y(t) I(t) - d_R R(t) \tag{2.1.1d}$$

$$\begin{aligned} \dot{I} = {} & k_I Y(t-\tau_I) + \frac{b_2 I(t-\tau_2)}{k_2 + I(t-\tau_2)} + k_{T_E I} T_E(t-\tau_{T_E I}) + k_{T_H I} T_H(t-\tau_{T_H I}) \\ & - d_I I(t) \end{aligned} \tag{2.1.1e}$$

$$\dot{T}_H = k_{T_H} \mathbb{1}_{V(t)>V_T} I(t) Y(t) - d_{T_H} T_H(t) \tag{2.1.1f}$$

$$\begin{aligned} \dot{T}_E = {} & k_{T_E} I(t-\tau_{T_E}) T_H(t-\tau_{T_E}) \mathbb{1}_{V(t-\tau_{T_E})>V_T} Y(t-\tau_{T_E}) \left(1 - \frac{T_E(t-\tau_{T_E})}{P(t-\tau_{T_E})}\right) \\ & + k_{T_M Y} \mathbb{1}_{V(t)>V_T} T_M(t) Y(t) - (1 - \mathbb{1}_{Y(t)}) T_E(t) \Big(d_{T_E pi} + k_{T_M} \Big) \\ & - d_{T_E} T_E(t) \end{aligned} \tag{2.1.1g}$$

$$\dot{T}_M = (1 - \mathbb{1}_{Y(t)}) k_{T_M} T_E(t) - k_{T_M Y} \mathbb{1}_{V(t)>V_T} T_M(t) Y(t) \tag{2.1.1h}$$

$$\begin{aligned} \dot{B}_{LL} = {} & k_{B_{LL}} \mathbb{1}_{V(t-\tau_{B_{LL}})>V_T} V(t-\tau_{B_{LL}}) T_H(t-\tau_{B_{LL}}) \\ & - k_{B_{LL}V} \mathbb{1}_{V(t-\tau_{B_{LL}V})>V_T} V(t-\tau_{B_{LL}V}) B_{LL}(t-\tau_{B_{LL}V}) \end{aligned} \tag{2.1.1i}$$

$$\begin{aligned} \dot{B}_E = {} & k_{B_E} \mathbb{1}_{V(t-\tau_{B_E})>V_T} V(t-\tau_{B_E}) T_H(t-\tau_{B_E}) \\ & + k_{B_{LL}V} \mathbb{1}_{V(t-\tau_{B_{LL}V})>V_T} V(t-\tau_{B_{LL}V}) B_{LL}(t-\tau_{B_{LL}V}) - d_{B_E} B_E(t) \end{aligned} \tag{2.1.1j}$$

$$\dot{A} = k_{B_{LL}A}B_{LL}(t) + k_{B_EA}B_E(t) - \rho_A A(t)V(t) - d_A A(t). \tag{2.1.1k}$$

The full model described by (2.1.1a)-(2.1.1k) is a system of 11 delay differential equations describing different phases of a within-host influenza infection. The constants k with a single variable subscript describe the primary production rate of that variable. The constants k with a double variable subscript indicate either (1) a contact rate between two cell types (in which case it multiplies a product of two variables) or (2) a production rate of a variable which is produced by different cell types, such as I and A (in which cases it multiplies a single variable). The delays have the same subscript as the constants, except when the variable with the delay is not multiplied by a constant. The constants d with a single variable subscript describe the decay rate of that variable.

The terms denoted

$$\mathbb{1}_{V>V_T}$$

are indicator functions, which turn certain components of the adaptive immune system on and off as different thresholds are crossed. Broadly, there are three phases to the immune response: initially, the innate immune response is induced, then the short-lived adaptive immune response is activated, and finally, the short-lived adaptive immune response is turned off post-infection and immunity levels are boosted. The indictor functions that generate these behaviors introduce discontinuities in the DDEs which will be discussed in Section 2.2.3.1.

The dynamics and interactions between all the model variables are shown in Figure 2.1. The compartments in blue (the free virus, susceptible cells, and infected cells), represent V, X, and Y, the basic viral dynamics. The compartments in green, i.e. the recovered cells and IFNs represent R and I, respectively. Together, the blue and green compartments describe the viral dynamics with innate immune response components. The adaptive immune response components are activated once viral antigen is above a certain threshold. The T-cell and B-cell compartments represent a simplification of the T-cell and B-cell dynamics, which make up the adaptive immune response. The T-cell and B-cell dynamics are shown in full in Figure 2.2 and Figure 2.3, respectively. The black arrows indicate stimulatory effect and the red repression arrows indicate inhibitory effect.

2.1.1 *Viral Dynamics*

Equations (1.4.1)-(1.4.3) in Section 1.4 form the basis of the viral dynamics in my model, described by (2.1.1a) to (2.1.1c). In fact, when there is no immune response whatsoever

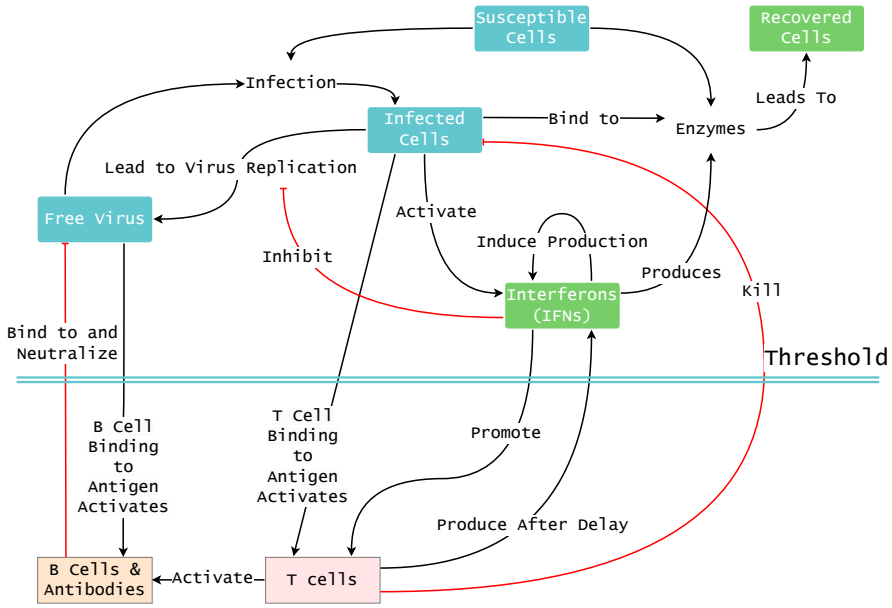

Figure 2.1: *Simplified Diagram of Viral and Immune Response Dynamics.*

(2.1.1a)-(2.1.1c) reduce to

$$\dot{V}(t) = k_V Y(t - \tau_V) - d_V V(t) \tag{2.1.2a}$$

$$\dot{X}(t) = \mu - d_X X(t) - \beta X(t) V(t) \tag{2.1.2b}$$

$$\dot{Y}(t) = \beta X(t) V(t) - d_Y Y(t). \tag{2.1.2c}$$

The first term in (2.1.2a) differs from (1.4.1) as it takes into account the duration of viral replication, i.e. the latent phase before an infected cell starts producing new virus, discussed in Section 1.5. Except for this delay, (2.1.2a)-(2.1.2c) are identical to (1.4.1)-(1.4.3). The inclusion of the production of healthy cells μ to the model allows us to model post-infection cell regeneration, which target-cell limited models cannot do. This has been done in previous models, which then allowed for distinguishing lethal from sublethal infections [57].

2.1.2 *Innate Immune Response Dynamics*

The innate immune response is made up of more than 7 different cell types, including different types of macrophages and NK cells [4]. This response is induced by different types of IFNs as well as IL action. Modeling each of these components separately would result in a 16 equation model with additional variables describing macrophages, NK cells, type I IFNs, type II IFNs, type III IFNs, and ILs. To reduce the number of equations that

make up the model (2.1.1), we consider that the entire innate immune response is included in the IFN compartment. This consolidation results from the idea that IFN action is an integral part of the innate immune response and that IFNs stimulate components of the innate immune system, such as NK cells and macrophages, at a rate that is assumed to be proportional to the amount of IFNs present [1, 13]. Certain IFN types have a similar role to ILs in effector and memory cell regulation, making the impact of ILs hard to quantify and to distinguish from that of IFNs [25, 31]. Most mathematical models of infection do not usually differentiate between the different types of IFNs and multiple previous models have made the assumption that the IFN compartment encompasses a wide range of innate immune response components with biologically sound results [13, 19, 40]. This assumption allows for considerable simplification of the model and which will allow for more specificity in the modeling of the adaptive immune response which is responsible for long-term memory.

Thus, we model the innate immune response with a single IFN compartment, I, whose dynamics are described by (2.1.1e). Moreover, the compartment R represents cells that have become resistant to infection due to IFN action, as described in (2.1.1d).

Low virus loads may be controlled by the innate immune response without inducing a short-lived adaptive immune response [4, 5]. In that case, the innate immune response to viral infections is described by the following five equations:

$$\dot{V} = k_V Y(t-\tau_V)\frac{\tilde{K}_1^n}{\tilde{K}_1^n + I^n(t-\tau_{IV})} - d_V V(t) \tag{2.1.3a}$$

$$\dot{X} = \mu - d_X X(t) - \beta X(t)V(t) - k_{IX} X(t)I(t) \tag{2.1.3b}$$

$$\dot{Y} = \beta X(t)V(t) - d_Y Y(t) - k_{IY} I(t)Y(t) \tag{2.1.3c}$$

$$\dot{R} = k_{IX} X(t)I(t) + k_{IY} Y(t)I(t) - d_R R(t) \tag{2.1.3d}$$

$$\dot{I} = k_I Y(t-\tau_I) + \frac{b_2 I(t-\tau_2)}{k_2 + I(t-\tau_2)} - d_I I(t). \tag{2.1.3e}$$

In (2.1.3a)-(2.1.3d), the terms highlighted in green represent the effect of the innate immune response, described by (2.1.3e), on the basic viral dynamics.

The innate immune response components were adapted from the model in Tan et al. [40] which considers virus-triggered innate immune signaling pathways and is made up of three compartments: V, the viral mRNA; I, the IFNs; and A, the antiviral proteins (AVPs) and seeks to characterize five reactions:

1. the replication of viral mRNAs;
2. the virus-activated IFN expression;
3. the expression of AVPs activated by IFNs;
4. the positive feedback of IFNs; and
5. the inhibition of virus replication by AVPs.

Each of these reactions occurs with a delay which we denote τ_V, τ_I, τ_3, τ_2, and τ_5, respectively. The model of [40] consists of three delay differential equations representing each compartment

$$\frac{dV}{dt} = k_1 V(t-\tau_V)\frac{b_1 K_1^n}{K_1^n + A^n(t-\tau_5)} - d_V V(t) \tag{2.1.4a}$$

$$\frac{dI}{dt} = k_I V(t-\tau_I) + \frac{b_2 I^{n_2}(t-\tau_2)}{k_2^{n_2} + I^{n_2}(t-\tau_2)} - d_I I(t) \tag{2.1.4b}$$

$$\frac{dA}{dt} = k_3 I(t-\tau_3) - d_3 A(t). \tag{2.1.4c}$$

AVP concentration values are much smaller than virus and IFN concentration values and we thus assume AVP concentration values return to steady state on a faster time scale than virus and IFN [40]. To simplify the model (2.1.4a)-(2.1.4c), we assume A is at quasi-steady state, that is

$$0 \approx \frac{dA}{dt} = k_3 I(t-\tau_3) - d_3 A(t) \tag{2.1.5}$$

$$\implies A(t) \approx \frac{k_3}{d_3} I(t-\tau_3) \tag{2.1.6}$$

$$A(t-\tau_5) \approx \frac{k_3}{d_3} I(t-(\tau_3+\tau_5)). \tag{2.1.7}$$

Assuming equality in (2.1.7), equation (2.1.4a) becomes

$$\frac{dV}{dt} = k_V V(t-\tau_V)\frac{b_1 \tilde{K}_1^n}{\tilde{K}_1^n + I^n(t-\tau_{IV})} - d_V V(t) \tag{2.1.8}$$

where

$$\tilde{K}_1 = \left(\frac{d_3}{k_3}\right)^{1/n} K_1$$

and with the parameter name change $\tau_3 + \tau_5 \to \tau_{IV}$.

The focus of the model (2.1.4) of [40] is the virus-mediated innate immune response. It does not explicitly model the basic viral dynamics presented in Nowak and May [27] and described in (1.4.1)-(1.4.3). In fact, the single compartment V representing viral mRNA produced from infection is a combination of two viral mRNA populations: (1) the viral mRNA that exists in free virions and (2) the viral mRNA that exists within infected cells. Free virus needs to enter host cells for viral replication and virus-activated IFN expression to occur (see Figure 2.1), which represents reactions 1 and 2, respectively. Because they cannot occur outside infected cells, we say these two reactions are driven by the infected cell population, Y.

In (2.1.1a), the infected cell compartment Y drives the production of viral mRNA, which results in free virus, as described in Section 2.1.1. As such, the factor $V(t - \tau_V)$ in 2.1.4a becomes $Y(t - \tau_V)$ in (2.1.3a). The inhibitory effect of the innate immune response is described by the term highlighted in green in (2.1.3a). In (2.1.4a), k_V is considered to be the production rate of viral mRNA and b_1, the maximal growth rate of viral mRNA. These two parameters were estimated and are thus not uniquely identifiable. Considering this, in (2.1.3a), we assume the production of free virus is described by a Hill function and its maximum growth rate is defined by $k_V Y(t - \tau_V)$. By putting (2.1.8) and (2.1.2a) together, we get (2.1.3a), which completely describes free virus dynamics in the presence of an innate immune response with the parameter name change $k_V b_1 \to k_V$.

Similarly, the viral mRNA which triggers IFN production comes from infected cells. As such, we can say the term $V(t - \tau_2)$ in (2.1.4b) is described by $Y(t - \tau_I)$ in (2.1.3e). The model [40] estimated $n_2 = 1$, which means there is no synergistic effect in IFN positive feedback. We choose to set $n_2 = 1$ which allows for simplification of the model. Thus, (2.1.3e) is obtained from (2.1.4b). In [40], the IFN levels represent normalized concentration values, that is the ratio of IFN concentration at a specific time to its initial concentration. In 2.1.1, $I(t)$ represent the difference between IFN levels at time t and basal concentrations.

The innate immune response also results in the production of recovered and resistant cells, described by (2.1.3d), which are not susceptible to infection. These cells are produced at rates k_{IX}, the production of resistant cells from susceptible cells, and k_{IY}, the recovery rate of infected cells. We consider that healthy cells that become resistant to infection are cells who are never directly in contact with the antigen but are near cells in contact with antigen. In this case, the spatial dimension of the model is not considered and 100% of healthy cells in contact with free virus become infected, as described in (2.1.3b) by the term βXV. This has been done in a previous model [58]. It could have been interesting to consider a more direct antiviral effect of IFN, i.e. a subset of healthy cells in contact with

virus become infected and the rest become resistant. In this scenario, IFN would reduce the total size of the infection through "resistance" to infection.

2.1.3 *Adaptive Immune Response*

Studies have suggested that the short-lived, effector adaptive immune response to infection, which includes T-cell, B-cell, and antibody responses, kicks in once the amount of antigen present is above a certain threshold [3, 6, 7]. Others have shown that the adaptive immune response, including memory T cell, is minor in individuals who are asymptotic or infected with low antigen doses [59, 60]. For this reason, we will consider that the adaptive immune response is activated when antigen levels cross a certain threshold. The only mechanism in the model (2.1.1) not subject to the threshold is antibody action on free virus. Once this threshold is crossed, the innate immune response is strong enough and the infection becomes symptomatic. Previous models have defined this threshold as being 1% of peak viral titers [13]. Thus, we can write the threshold condition as

$$V(t) > V_T.$$

The threshold crossing is time-dependent and because of the delays present in (2.1.1f)-(2.1.1j), the compartments described by these equations are not all activated at the same time. In fact, the mechanisms that occur after no delay will be activated first, which allows for modeling of immunological memory components being activated faster upon reinfection. The dynamics pertaining to these different threshold-crossing times are modeled by indicator functions and are explained in more detail in Section 2.2.3.1.

More generally, when $V \leq V_T$, only the innate immune response, described by (2.1.1e) and derived in Section 2.1.2, is activated. When $V > V_T$, the T-cell and B-cell compartments are activated. Helper, effector, and memory T-cell dynamics are described by (2.1.1f)-(2.1.1h), which will be derived in Section 2.1.3.1. Long-lived and effector B cells are described by (2.1.1i)-(2.1.1j) and antibody is described by (2.1.1k), which will be derived in Section 2.1.3.2. Some of these adaptive immune response components act directly on the innate immune response subsystem (2.1.3a)-2.1.3e. These components are highlighted in green in (2.1.9a) to (2.1.9e):

$$\dot{V} = k_V Y(t-\tau_V) \cdot \frac{\tilde{K}_1^n}{\tilde{K}_1^n + I^n(t-\tau_{IV})} - d_V V(t) - \rho_V A(t) V(t) \tag{2.1.9a}$$

$$\dot{X} = \mu - d_X X(t) - \beta X(t) V(t) - k_{IX} X(t) I(t) \tag{2.1.9b}$$

$$\dot{Y} = \beta X(t) V(t) - d_Y Y(t) - k_{T_E Y} T_E(t) Y(t) - k_{IY} I(t) Y(t) \tag{2.1.9c}$$

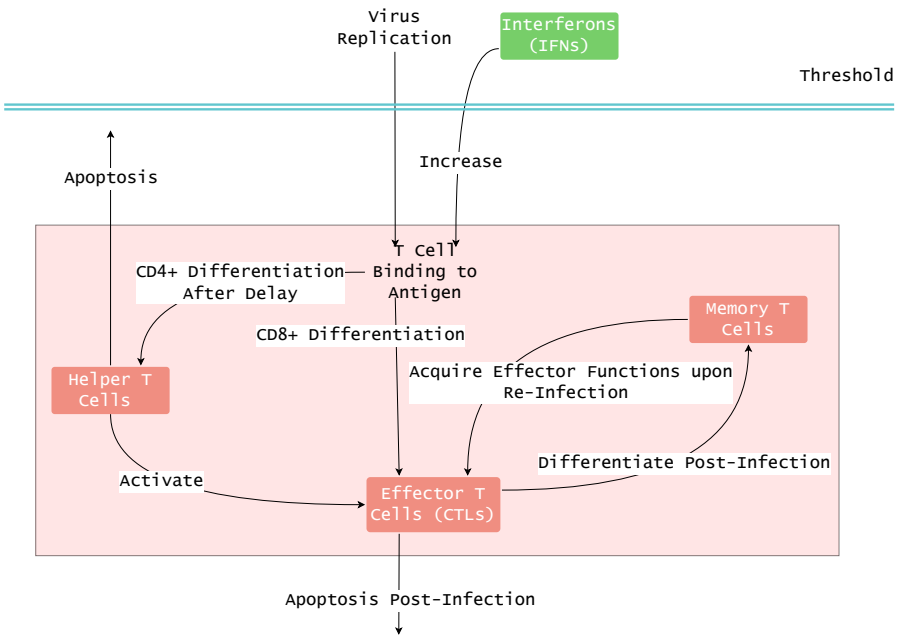

Figure 2.2: *Diagram of Complete T-cell Dynamics.*

$$\dot{R} = k_{IX}X(t)I(t) + k_{IY}Y(t)I(t) - d_R R(t) \tag{2.1.9d}$$

$$\dot{I} = k_I Y(t-\tau_I) + \frac{b_2 I(t-\tau_2)}{k_2 + I(t-\tau_2)} + k_{T_EI}T_E(t-\tau_{T_EI}) + k_{T_HI}T_H(t-\tau_{T_HI}) - d_I I(t). \tag{2.1.9e}$$

In (2.1.9a), the term highlighted in green represents free virus removal due to binding with antibody, where ρ_V represents the binding rate between antibody and free virus. In (2.1.9c), the highlighted term represents CTL killing of infected cells, where k_{T_EY} represents the killing rate of CTLs. In (2.1.9e), the two highlighted terms represent IFN production by effector CD8+ T cells and helper T cells, respectively. k_{T_EI} and k_{T_HI} are the production rates of IFN by effector and helper T cells, respectively [19, 61].

2.1.3.1 *T-cell Compartment*

In my model (2.1.1), when $V > V_T$, differentiation and activation of different types of naive T cells occurs. The interactions and dynamics between different T-cell types after T-cell activation are illustrated in Figure 2.2 and will be described below.

In the absence of disease, the naive CD4+ T-cell population is maintained through homeostatic proliferation which regulates naive CD4+ T cell turnover and keeps the cell population relatively constant [62]. Differentiation of naive CD4+ cells into helper T

cells T_H and their subsequent activation depends on antigen presentation. Before they are activated, CD4+ T cells do not have any effector functions, which are described in Section 1.3. For these reasons, to have a simpler model, there is no naive CD4+ T-cell compartment in my model (2.1.1). The production of helper cells, T_H, is modeled with the assumption that there are always enough naive CD4+ T cells, which is the case in healthy non-elderly adults [62].

In this case, T_H production is proportional to viral antigen, which in my model, in (2.1.1f), is ascribed to the infected cell population Y. This process is further promoted by IFN action, I, which increases binding of naive T cells to antigen. The production of T_H is thus modeled by

$$k_{T_H} \mathbb{1}_{V(t)>V_T} I(t) Y(t). \tag{2.1.10}$$

The removal of helper T cells is proportional to the number of helper T cells and is described by

$$-d_{T_H} T_H(t). \tag{2.1.11}$$

Combining (2.1.10) and (2.1.11), we obtain the two term equation (2.1.1f).

Similarly to naive CD4+ T cells, the population of naive CD8+ T cells is maintained through homeostatic proliferation. For the same reasons, to have a simpler model, there is no naive CD8+ T-cell compartment in my model (2.1.1). The production of CTLs, T_E, is modeled with the assumption that there are always enough naive CD8+ T cells, which is the case in healthy non-elderly adults [62]. The production of CTLs takes into account the delay between CD8+ T-cell differentiation and their activation and migration to infection sites [25]. This delay is denoted τ_{T_E}.

When the infection generates a threshold level of antigen, experimental results have shown that exposure to antigen for as little as 24 hours is enough to induce programmed naive CD8+ T-cell proliferation and differentiation into CTLs or effector CD8+ T cells [25, 28]. However, viral infections occurring in humans, including influenza A infections, are not cleared within 24 hours so T-cell exposure to antigen most likely continues after their initial activation and how further antigen exposure impacts this antigen-independent CD8 T-cell development is unclear [28]. Moreover, experimental results on antigen-independent T-cell development are performed in isolation and do not accurately reproduce the context of an infection, e.g. they do not take into account other components of the immune response [61, 63]. For these reasons, most mathematical models that consider CD8+ T cells dynamics during infection assume that CD8+ T-cell proliferation and differentiation depend continuously on the presence of viral antigen [29, 30, 64]. It is also assumed that the proliferation of CTLs is proportional to the amount of antigen or antigen presenting

cells [13]. Like T_H, my model (2.1.1) assumes CD8+ T-cell proliferation and differentiation depends continuously on the presence of antigen, ascribed to the population of infected cells Y.

The production of CTLs T_E is limited by the total population capacity of memory and effector T cells and so the maximum population of effector CD8+ T cells $P(t)$ is

$$T_E(t) + T_M(t) \leq T_{TOT} \implies T_E(t) \leq P(t) = T_{TOT} - T_M(t). \tag{2.1.12}$$

Models that exclude this density-dependence have been show to result in statistically poor fits to available data [16].

Moreover, the CTL proliferation rate is also proportional to the population of helper T cells T_H, which activate CTLs, as well as innate immune components I, which increase binding to viral antigen [13]. The production of CTLs is then modeled by the first term of (2.1.1g):

$$\dot{T_E} = k_{T_E} I(t - \tau_{T_E}) T_H(t - \tau_{T_E}) \cdot \mathbb{1}_{V(t-\tau_{T_E})>V_T} Y(t - \tau_{T_E}) \left(1 - \frac{T_E(t - \tau_{T_E})}{P(t - \tau_{T_E})}\right) \tag{2.1.13}$$

where k_{T_E} is the production rate of T_E and the last term in (2.1.13) ensures that (2.1.12) is satisfied.

The removal of CTLs is proportional to the number of CTLs and represents the cell disappearance rate, which includes death and long-term exit from blood [65]. It is described in (2.1.1g) by

$$-d_{T_E} T_E(t). \tag{2.1.14}$$

The other mechanisms that govern CTL production and decay depend on memory T cells. Memory T cells are split into 2 different subtypes: central memory T cells (T_{CM} cells) and effector memory T cells (T_{EM} cells). It is unclear whether both populations arise and are sustained independently or whether T_{CM} cells can become T_{EM} cells and vice versa [28, 29]. T_{EM} cells can kill targeted infected cells, similarly to CTLs. Moreover, they can carry out other effector functions more rapidly than CTLs activated as a result of the initial immune response [30]. To simplify this model and because the mechanisms that regulate memory T-cell subtypes are not well understood, only one memory T cell compartment will be considered, denoted T_M. These cells reacquire effector functions upon reinfection. To simplify the model further, we will consider that T_M become T_E, i.e. regain effector functions, at a rate $k_{T_M Y}$, with no delay. This process is modeled by the second term in (2.1.1g),

$$k_{T_M Y} \mathbb{1}_{V(t)>V_T} T_M(t) Y(t). \tag{2.1.15}$$

During the post-infection period, denoted $(1 - \mathbb{1}_Y)$, the population of CTLs declines very quickly, at a much faster rate than the normal death rate of T_E, described in (2.1.14). Indeed, Post-infection, 90 to 95% of CTLs are cleared and 5 to 10% differentiate into memory T cells. This is modeled in (2.1.1g) by the term

$$-(1 - \mathbb{1}_{Y(t)})T_E(t)\left(d_{T_E pi} + k_{T_M}\right) \tag{2.1.16}$$

where $d_{T_E pi}$ is the decay rate of CTLs post-infection and $k_{T_M}T_E(t)$ is the rate at which effector T cells differentiate into memory T cells post-infection. This term is non-zero if Y, the population of infected cells is zero, i.e. the infection has been cleared or no infection has occurred yet. Another way to model the production of memory T cells post-infection would be to consider that effector T cell become memory T cells at rate k_{T_M} after a delay τ_{T_M}, as was done in a previous model [16].

Putting (2.1.13), (2.1.14), (2.1.15), and (2.1.16) together, we obtain (2.1.1g).

As opposed to helper CD4+ and effector CD8+ T cells, memory T-cell populations are maintained over long periods of time, independent of infection. It is assumed the population of memory T cells is kept relatively constant over time, i.e.

$$(\text{production rate})(T_M(t)) = (\text{death rate})(T_M(t))$$

holds [66]. For this reason, in (2.1.1h), there are no terms representing independent production or removal of memory T cells.

Memory T cells are produced post-infection as described in (2.1.16). Memory T cells regain effector functions as described in (2.1.15), with opposite sign. Putting these two terms together, we obtain that the memory T-cell population varies according to (2.1.1h). Thus, (2.1.1f)-(2.1.1h) completely describe T-cell dynamics.

2.1.3.2 *B-cell and Antibody Compartment*

In their complete form, B-cell dynamics, including differentiation and effector function, are characterized by the schematics in Figure 2.3 and will be described below.

Minimal antigen doses may be controlled subclinically by innate defenses and may be insufficient to induce adaptive immune responses, such as B-cell differentiation [5]. As such, long-lived B cells and plasmablasts are only produced if the amount of viral antigen is greater than the threshold amount, i.e. $V > V_T$. This is the same threshold amount as required for T-cell activation, as explained in Section 2.1.3.

There are three distinct types of B cells: short-lived effector cells, long-lived memory cells, and long-lived plasma cells. Short-lived effector cells, also called plasmablasts, and

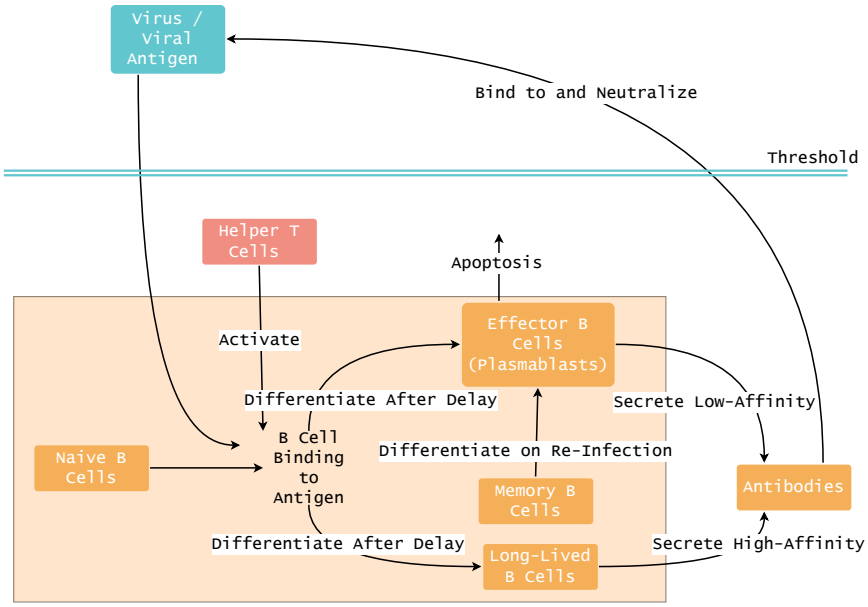

Figure 2.3: *Diagram of Complete B-cell Dynamics.*

long-lived plasma cells can secrete antibody but memory B cells cannot. These cells re-differentiate into plasmablasts upon reinfection. In my model, memory and plasma cells will be combined into one compartment, B_{LL}, representing long-lived cells to reduce the number of compartments and simplify the model. There are thus two B-cell compartments in (2.1.1): B_{LL}, described by (2.1.1i), and B_E representing short-lived effector B cells, whose dynamics are described by (2.1.1j). Both these compartments are made up of ASCs.

Both these types of cells result from naive B cells binding to viral antigen, differentiating, and being activated, as shown in Figure 2.3. Similarly as for T cells, to have a simpler model, there are no naive B-cell compartments in my model (2.1.1). The production of long-lived B cells B_{LL} and short-lived B cells B_E are modeled with the assumption that there are always enough naive B cells. The production of B_{LL} and B_E takes into account the the delay between B-cell differentiation and their activation and migration to infection sites after they are activated [18]. These delays are denoted $\tau_{B_{LL}}$ and τ_{B_E}, for the production of B_{LL} and B_E, respectively.

The production of both long-lived B cells B_{LL} and short-lived plasmablasts B_E is proportional to viral antigen, ascribed to the free virus population V, and to helper T cells T_H, which activate B cells. The production of these cells is represented by

$$k_{B_{LL}} \mathbb{1}_{V(t-\tau_{B_{LL}})>V_T} V(t-\tau_{B_{LL}}) T_H(t-\tau_{B_{LL}}) \tag{2.1.17}$$

$$k_{B_E} \mathbb{1}_{V(t-\tau_{B_E})>V_T} V(t-\tau_{B_E}) T_H(t-\tau_{B_E}) \tag{2.1.18}$$

where $k_{B_{LL}}$ is the production rate of B_{LL} and k_{B_E} is the production rate of B_E.

Upon reinfection, long-lived (memory) B cells can differentiate and become effector B cells B_E. This is triggered by long-lived B cells B_{LL} binding to viral antigen V at a rate $k_{B_{LL}V}$. This process occurs after a delay $\tau_{B_{LL}V}$ but is quicker than the differentiation of naive B cells into B_E after a primary infection [10]. This process is described by term

$$-k_{B_{LL}V}\mathbb{1}_{V(t-\tau_{B_{LL}V})>V_T}V(t-\tau_{B_{LL}V})B_{LL}(t-\tau_{B_{LL}V}) \tag{2.1.19}$$

Because long-lived B-cell populations are maintained for years, even in the absence of antigen, it is assumed the population of long-lived B cells is constant over time, so there is no antigen-independent removal term for [10].

Putting together (2.1.17) and (2.1.19), we obtain (2.1.1i).

Plasmablasts B_E are removed at a rate proportional to their population,

$$-d_{B_E}B_E(t). \tag{2.1.20}$$

Putting (2.1.18), (2.1.19) (as a production term, i.e. with positive sign), and (2.1.20), we obtain (2.1.1j).

We consider that antibody is produced by both long-lived B cells B_{LL} and plasmablasts B_E. This is modeled in (2.1.1k) by

$$k_{B_{LL}A}B_{LL}(t)+k_{B_EA}B_E(t) \tag{2.1.21}$$

where $k_{B_{LL}A}$ is the production rate of antibody A by long-lived B cells and k_{B_EA} is the production rate of antibody A by plasmablasts.

The model does not take into account antibody affinity. Indeed, antibody produced by long-lived B cells have a higher affinity to virus, i.e. higher binding rate to virus, than plasmablasts that are produced during a primary infection. Antibody binding to virus results in the neutralization (elimination) of virus and the elimination of antibody. In (2.1.1k), this is described by the term

$$-\rho_A A(t)V(t) \tag{2.1.22}$$

where the constant ρ_A is the binding rate of antibody A and free virus V. In (2.1.1a) the binding rate between antibody A and free virus V is denoted ρ_V. Considering A and V are not expressed in the same units, we have implicitly defined ρ_A as

$$\rho_A = k\rho_V \tag{2.1.23}$$

where k a unit normalization constant. So, in my model (2.1.1a)-(2.1.1k), there is a unique binding rate between antibody and virus but the parameters ρ_V and ρ_A express this binding rate in different units (see Table 2.7 in Section 2.3.1.2).

Removal of antibody also results from natural antibody clearance, represented by

$$-d_A A(t). \tag{2.1.24}$$

Putting (2.1.21), (2.1.22), and (2.1.24) together, we obtain (2.1.1k), which completely describes antibody dynamics.

2.2 Analysis of Solutions and Stability

2.2.1 *Viral Dynamics*

Because all variables represent biological quantities, it is important to establish positivity of the solutions. The viral dynamics presented in (2.1.2a)-(2.1.2c) can be rewritten as

$$\dot{x} = \begin{pmatrix} \dot{V}(t) \\ \dot{X}(t) \\ \dot{Y}(t) \end{pmatrix} = \begin{pmatrix} k_V Y(t-\tau_V) - d_V V(t) \\ \mu - d_X X(t) - \beta X(t) V(t) \\ \beta X(t) V(t) - d_Y Y(t) \end{pmatrix} = f(x,y) \tag{2.2.1}$$

where

$$x = \begin{pmatrix} V(t) \\ X(t) \\ Y(t) \end{pmatrix} \quad \text{and} \quad y = \begin{pmatrix} V(t-\tau_V) \\ X(t-\tau_V) \\ Y(t-\tau_V) \end{pmatrix} \in \mathbb{R}^3.$$

Theorem 3.1 from [48], presented in Section 1.5, establishes uniqueness of the solution for the initial-value problems and continuous initial conditions ϕ, provided f and f_x are continuous. For the system defined in (2.2.1), we have that f is a vector of polynomial functions, so it is smooth and thus, both f and f_x are continuous. Thus, for any continuous initial conditions ϕ, this system has a unique solution for a given set of parameters. Moreover, from Theorem 4.3 of [48], presented in Section 1.5, if the solution is unique, we have positivity of the solution if

$$\forall\, x, y \in \mathbb{R}^3_+ \quad x_i = 0 \implies f_i \geq 0$$

for any nonnegative initial conditions ϕ. For the system defined in (2.2.1), for nonnegative parameter values, we have

$$x_1 = 0 \implies f_1 = \bar{k}\tilde{K_1}^{-n} y_1 \geq 0, \tag{2.2.2}$$

$$x_2 = 0 \implies f_2 = \mu \geq 0, \tag{2.2.3}$$

$$x_3 = 0 \implies f_3 = \beta x_2 x_1 \geq 0. \tag{2.2.4}$$

Thus, by Theorem 3.4 of [48], for any nonnegative initial conditions ϕ, the model of basic viral dynamics, defined by the system (2.2.1), has a nonnegative solution.

Let $x^* = (V^*, X^*, Y^*)$ denote a steady state solution of the model (2.1.2a)-(2.1.2c), as defined in Section 1.5. This solution satisfies

$$0 = k_V Y^* - d_V V^* \tag{2.2.5}$$

$$0 = \mu - \beta X^* V^* - d_X X^* \tag{2.2.6}$$

$$0 = \beta X^* V^* - d_Y Y^*. \tag{2.2.7}$$

We can solve for explicit forms of x^*. When $V^* = Y^* = 0$, (2.2.5) and (2.2.7) hold. In this case, it is easy to see from (2.2.6) that

$$X^* = \frac{\mu}{d_X}.$$

This gives us a first steady state

$$(V^*, X^*, Y^*)_{\text{DF}} = \left(0, \frac{\mu}{d_X}, 0\right). \tag{2.2.8}$$

This steady state represents a disease-free (DF) equilibrium, that is the system is at equilibrium when an individual has no infection. We can also solve for V^*, X^*, Y^*, for $V^* \neq 0$, $Y^* \neq 0$. We have

$$(2.2.5) \implies Y^* = \frac{d_V V^*}{k_V} \tag{2.2.9}$$

$$(2.2.7) \implies Y^* = \frac{\beta X^* V^*}{d_Y}. \tag{2.2.10}$$

Equating (2.2.9) and (2.2.10), we get

$$\frac{d_V V^*}{k_V} = \frac{\beta X^* V^*}{d_Y}$$

$$\begin{aligned} &\iff \frac{d_V}{k_V} = \frac{\beta X^*}{d_Y} && \text{because } V^* \neq 0 \\ &\implies X^* = \frac{d_V d_Y}{k_V \beta}. \end{aligned} \tag{2.2.11}$$

Subbing in the value of X^* obtained in (2.2.11) in (2.2.6), we get

$$0 = \mu - \beta \left(\frac{d_V d_Y}{k_V \beta} \right) V^* - d_X \left(\frac{d_V d_Y}{k_V \beta} \right).$$

We can solve for V^* and we obtain

$$V^* = \frac{\mu k_V}{d_V d_Y} - \frac{d_X}{\beta}. \tag{2.2.12}$$

Putting this value back in (2.2.9), we get

$$Y^* = \frac{\mu}{d_Y} - \frac{d_V d_X}{k_V \beta}. \tag{2.2.13}$$

The values of (2.2.12), (2.2.11), and (2.2.13) form the second steady state, the endemic (E) equilibrium:

$$(V^*, X^*, Y^*)_{\mathrm{E}} = \left(\frac{k_V \mu}{d_V d_Y} - \frac{d_X}{\beta}, \frac{d_V d_Y}{k_V \beta}, \frac{\mu}{d_Y} - \frac{d_X d_V}{k_V \beta} \right). \tag{2.2.14}$$

This steady state represents an infection that will not die out but the number of infected cells will not increase exponentially and kill the individual, that is the disease becomes chronic. This system thus has two steady states: a unique disease-free equilibrium and a unique endemic equilibrium.

To ensure we have positive steady steady state values $Y^* > 0$ and $V^* > 0$ in (2.2.14), we need

$$k_V \beta \mu - d_X d_V d_Y \geq 0. \tag{2.2.15}$$

The first term in (2.2.15) is a product of the production rates of free virus (k_V), target cells (μ), and infected cells (β). The second term is a product of the decay rates of these variables This is equivalent to requiring that production rates be greater than decay rates. This is also equivalent to the condition:

$$R_0 := \frac{\beta k_V \mu}{d_V d_X d_Y} \geq 1. \tag{2.2.16}$$

We should note that when $R_0 = 1$, the steady state defined in (2.2.14) is the same as (2.2.8). In this case, there is only one steady state. We can also note that R_0 is the product of production rates divided by the product of decay rates.

In epidemiology, R_0 denotes the basic reproduction number of an infection, that is the expected number of cases expected to arise from a single infected individual in a population of susceptible individuals. If $R_0 > 1$, the infection will spread in the population; if $R_0 < 1$, the infection will die out. If $R_0 = 1$, the infection stays stable but will not cause an epidemic. We will study the stability of the two steady states defined in (2.2.8) and (2.2.14) for different values of R_0 to prove R_0 in my model is analogous to the epidemiological R_0, that is it represents the expected number of infected cells stemming from a single infected cell in a population of target cells.

Linearizing around the disease-free steady state (2.2.8) and following the general principles outlined in Section 1.5, we obtain the following characteristic polynomial

$$\Delta_{\text{DF}}(\lambda) = (d_X + \lambda)\left((d_V + \lambda)(d_Y + \lambda) - \frac{k_V \beta \mu}{d_X} e^{-\lambda \tau_V}\right). \tag{2.2.17}$$

The complete derivation of the characteristic polynomial is omitted here as it is a specific case of the linearization about the disease-free steady state of the innate immune system model derived in Section 2.2.2. We have that $\lambda = -d_X < 0$ is always a root of the characteristic polynomial (2.2.17). Because this root is negative, we need to study the other roots to determine stability.

If $\lambda = 0$ is a root of the characteristic polynomial (2.2.17), we get

$$0 = d_V d_Y - \frac{k_V \beta \mu}{d_X} \iff R_0 = 1$$

for R_0 defined in (2.2.16). This also means that

$$\Delta_{\text{DF}}(0) < 0 \iff R_0 > 1. \tag{2.2.18}$$

For $\lambda > 0$, $\Delta_{\text{DF}}(\lambda)$ defined in (2.2.17) is increasing and we can evaluate

$$\lim_{\lambda \to \infty} \Delta_{\text{DF}}(\lambda) = \lim_{\lambda \to \infty} (d_X + \lambda)\left((d_V + \lambda)(d_Y + \lambda) - \frac{k_V \beta \mu}{d_X} e^{-\lambda \tau_V}\right) = \infty. \tag{2.2.19}$$

In the case where $R_0 > 1$, because (2.2.18) and (2.2.19) hold, by the intermediate value theorem [67], we have that $\Delta_{\text{DF}}(\lambda) = 0$ on $(0, \infty)$, i.e. there is a positive real root of the characteristic polynomial (2.2.17). In this case, when $R_0 > 1$, the disease-free steady state

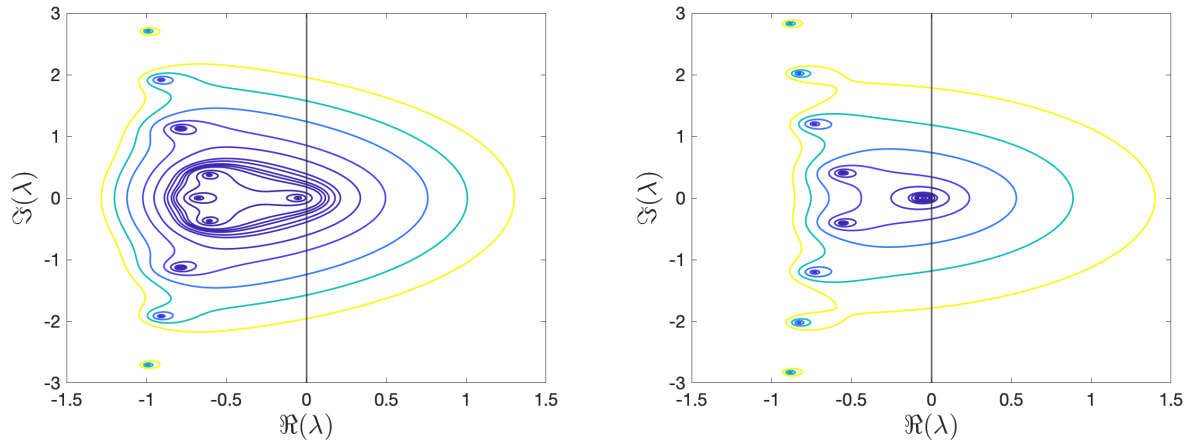

Figure 2.4: *Contour plots of $|\Delta(\lambda)|$ in the complex plane. The characteristic roots are at the center of the islands. (a) Contour plot for characteristic polynomial $\Delta_{\mathrm{DF}}(\lambda)$ of the system (2.1.2a)-(2.1.2c) linearized about the disease-free steady state (2.2.8) for $R_0 < 1$. (b) Contour plot for characteristic polynomial $\Delta_{\mathrm{E}}(\lambda)$ of the system (2.1.2a)-(2.1.2c) linearized about the disease-free steady state (2.2.14) for $R_0 > 1$.*

(2.2.8) is unstable.

We can follow a similar approach for the endemic disease steady state defined in (2.2.14). Linearizing about (2.2.14) and following the general principles outlined in Section 1.5, we obtain the following characteristic polynomial

$$\Delta_{\mathrm{E}}(\lambda) = (d_V + \lambda)\left(\frac{\beta k_V \mu}{d_V d_Y} + \lambda\right)(d_Y + \lambda) - (d_X + \lambda) d_V d_Y e^{-\lambda \tau_V}. \tag{2.2.20}$$

We can study the characteristic polynomial (2.2.20) as we did (2.2.17). We have that $\lambda = 0$ is a root of (2.2.17) if we get the following characteristic equation

$$0 = d_V d_X d_Y - k_V \beta \mu \iff R_0 = 1.$$

If $R_0 < 1$, then the endemic equilibrium (2.2.14) is negative, i.e. it does not occur biologically. For this reason, the analytical study of stability of this steady state is irrelevant for $R_0 < 1$.

Moreover, from Figure 2.4a, we find that the characteristic polynomial Δ_{DF} defined in (2.2.17) has no complex roots with nonnegative real part when $R_0 < 1$. This means that when $R_0 < 1$, the disease-free steady state defined in (2.2.8) is asymptotically stable. Similarly, from Figure 2.4b, we find that the characteristic polynomial Δ_{E} defined in (2.2.20) has no complex roots with nonnegative real part when $R_0 > 1$. This means that when $R_0 > 1$, the disease-free steady state defined in (2.2.14) is asymptotically stable.

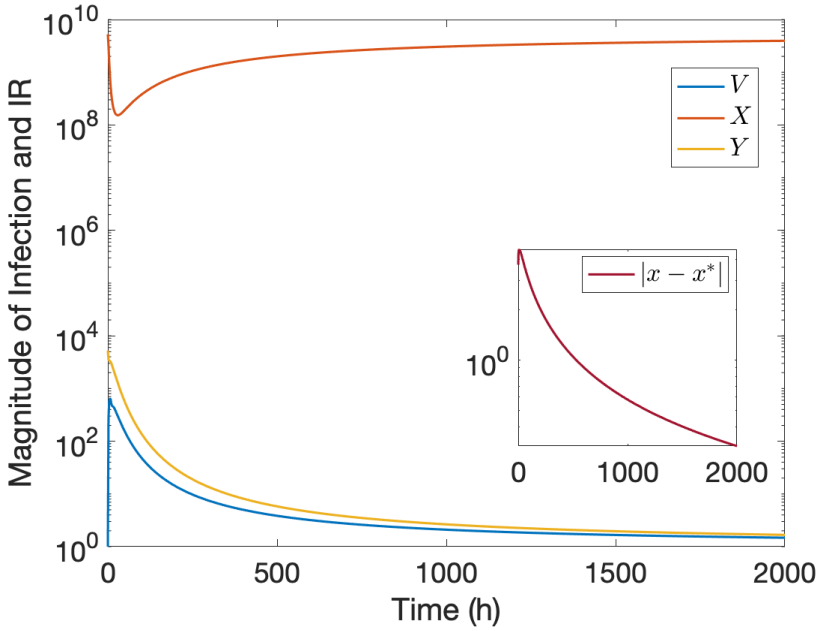

Figure 2.5: *Simulation of the viral dynamics defined in* (2.1.2a)-(2.1.2c) *for* $R_0 = 1$ *for initial conditions representing a small perturbation from the disease-free steady state* (2.2.8). *Initial conditions are* $[V^0, X^0, Y^0] = [V^*, X^*, \log_{10}(5250)]$. *The inset represents* $\|x(t) - x^*\|$ *where x(t) is the solution to* (2.1.2a)-(2.1.2c) *and* x^* *is the disease-free steady state defined in* (2.2.8).

Hence, we have that when $R_0 < 1$, the disease-free steady state (2.2.8) is stable and the endemic steady state (2.2.14) is negative and non-physical (and unstable); when $R_0 > 1$, the disease-free steady state is unstable and the endemic steady state is stable. This means that if $R_0 < 1$, the infection will die out and if $R_0 > 1$, the infection will spread in the body. Thus, there is a transcritical bifurcation at the point where $R_0 = 1$ because the two steady states collide and interchange stability. This is analogous to the definition of R_0 for infections at a population level.

The only difference occurs when $R_0 = 1$. In this case, in my model, as shown in Figure 2.5, small perturbations around the unique disease-free steady state (2.2.8), result in the system returning to this steady state, while in epidemiological models, when $R_0 = 1$, the infection remains stable. This is because my model takes into account cell proliferation and death, meaning that the infected cells will die out and healthy cells regenerate (see Section 2.3.1 for parameter values), whereas epidemiological population models assume the population is constant and do not consider birth and death of individuals.

2.2.2 *Innate Immune Response Dynamics*

Consider the submodel describing viral and innate immune response dynamics without adaptive immune components, described by equations (2.1.3a) to (2.1.3e). At steady state, this submodel must satisfy

$$0 = k_V Y^* \frac{\tilde{K}_1^n}{\tilde{K}_1^n + I^{*n}} - d_V V^* \tag{2.2.21a}$$

$$0 = \mu - d_X X^* - \beta X^* V^* - k_{IX} X^* I^* \tag{2.2.21b}$$

$$0 = \beta X^* V^* - d_Y Y^* - k_{IY} I^* Y^* \tag{2.2.21c}$$

$$0 = k_{IX} X^* I^* + k_{IY} Y^* I^* - d_R R^* \tag{2.2.21d}$$

$$0 = k_I Y^* + \frac{b_2 I^*}{k_2 + I^*} - d_I I^*. \tag{2.2.21e}$$

When $V^*, Y^* \neq 0$, solving (2.2.21a)-(2.2.21e), we obtain positive endemic equilibria denoting chronic infection. We can obtain an expression for Y^* as a function of I^* from (2.2.21e). We can use (2.2.21a) to define V^* as a function of Y^* and I^*. Then, from (2.2.21c), we can express X^* as a function of V^*, Y^*, and I^*. From (2.2.21d), we can express R^* as a function of X^*, Y^*, and I^*. Hence, we could express all of the variables as a function of I^*. Putting these expressions in (2.2.21b) will result in a single equation that I^* satisfies.

This results in a scalar equation in a single variable, I^*, and from the value(s) of I^*, we could obtain the corresponding values of V^*, X^*, Y^*, and R^*. However, because n is not necessarily an integer, the resulting expression might not be polynomial. For these reasons, there is no easily obtainable closed-form expression for each of the variables at steady state. We could plot this function of I^* to determine for which value(s) of I^* is (2.2.21b) satisfied but these values would depend on the specific parameter choice. For these reasons, this expression will not be studied analytically or numerically.

When $V = Y = 0$, the equalities in (2.2.21a) and (2.2.21c) hold. We then obtain

$$X^* = \frac{\mu}{d_X + k_{IX} I^*} \qquad \text{from Equation (2.2.21b)} \tag{2.2.22}$$

$$R^* = \frac{\mu k_{IX} I^*}{d_R (d_X + k_{IX} I^*)} \qquad \text{from Equation (2.2.21d).} \tag{2.2.23}$$

Equation (2.2.21e) holds if (1) $I^* = 0$ or if (2) $-d_I I^* + b_2 - d_I k_2 = 0$ and $I^* \neq 0$.

The first case results in the first disease-free steady state, which represents healthy

individuals:

$$(V^*, X^*, Y^*, R^*, I^*)_{\mathrm{DF}} = (0, \frac{\mu}{d_X}, 0, 0, 0). \tag{2.2.24}$$

The second type of disease-free steady state, $(V^*, X^*, Y^*, R^*, I^*)_{\mathrm{DF}^*}$ occurs when $I^* \neq 0$ and the condition

$$d_I I^* - b_2 + d_I k_2 = 0 \tag{2.2.25}$$

is satisfied. Equation (2.2.25) is a polynomial of degree one with the root

$$I^* = \frac{b_2}{d_I} - k_2 \geq 0. \tag{2.2.26}$$

In this case, the steady state, which represents individuals with no disease but with chronic inflammation, is

$$(V^*, X^*, Y^*, R^*, I^*)_{\mathrm{DF}^*} = \left(0, \frac{\mu}{d_X + k_{IX} I^*}, 0, \frac{\mu k_{IX} I^*}{d_R(d_X + k_{IX} I^*)}, I^*\right). \tag{2.2.27}$$

The system (2.1.4) defined by Tan et al. [40] can also reach these types of steady states.

If $b_2 d_I < k_2$, (2.2.26) is never satisfied. In this case, the only disease-free steady state is the steady state with no chronic inflammation, defined in (2.2.24). In particular, this occurs when $b_2 = 0$, which indicates that the IFN positive feedback loop, denoted by the term

$$\frac{b_2 I(t - \tau_2)}{k_2 + I(t - \tau_2)}$$

is a necessary condition for chronic inflammation.

To study the stability of the system, we can linearize (2.1.3a)-(2.1.3e) about any disease-free steady state. To do so, we linearize about the steady state defined in (2.2.27). In this case, we introduce the new variables $\xi(t) = X(t) - X^*$, $\varphi(t) = R(t) - R^*$, and $\zeta(t) = I(t) - I^*$, with $|\xi(t)|, |\varphi(t)|, |\zeta(t)| \ll 1$. The variables V and Y are implicitly defined about the steady state 0 and are assumed to be very small. To linearize about this steady state, we define $\varepsilon_* = (\varepsilon_V, \varepsilon_\xi, \varepsilon_Y, \varepsilon_\varphi, \varepsilon_\zeta)^T$, a small perturbation around the steady state, with $|\varepsilon_*| \ll 1$ such that the linearized dynamics are

$$(V(t), \xi(t), Y(t), \varphi(t), \zeta(t))^T = e^{\lambda t} \varepsilon_* \qquad \lambda \in \mathbb{C}. \tag{2.2.28}$$

Substituting this ansatz (2.2.28) into the model, for $n > 1$, (2.1.3a), becomes

$$\dot{V} = k_V Y(t - \tau_V) \tilde{K}_1^n (\tilde{K}_1^n + (\zeta + I^*)^n (t - \tau_{IV}))^{-1} - d_V V(t)$$

$$= k_V \frac{\tilde{K}_1^n}{\tilde{K}_1^n + I^{*n}} Y(t - \tau_V) - d_V V(t) + \mathcal{O}(Y\zeta^n)$$

with $Y\zeta^n \ll 1$. Hence, when linearized (2.1.3a) becomes

$$\dot{V} = \lambda e^{\lambda t}\varepsilon_V = k_V \frac{\tilde{K}_1^n}{\tilde{K}_1^n + I^{*n}} e^{\lambda(t-\tau_V)}\varepsilon_Y - d_V e^{\lambda t}\varepsilon_V$$

$$\iff \quad \lambda\varepsilon_V = k_V \frac{\tilde{K}_1^n}{\tilde{K}_1^n + I^{*n}} e^{-\tau_V}\varepsilon_Y - d_V\varepsilon_V.$$

Similarly, linearizing (2.1.3b) and we obtain

$$\dot{\xi}(t) = \dot{X}(t) = \mu - d_X\left(\xi(t) + \frac{\mu}{d_X + k_{IX}I^*}\right) - \beta\left(\xi(t) + \frac{\mu}{d_X + k_{IX}I^*}\right)V(t)$$
$$- k_{IX}\left(\xi(t) + \frac{\mu}{d_X + k_{IX}I^*}\right)(\zeta(t) + I^*)$$
$$= -(d_X + k_{IX})\xi(t) - \frac{\beta\mu}{d_X + k_{IX}I^*}V(t) - \frac{k_{IX}\mu}{d_X + k_{IX}I^*}I(t) + \mathcal{O}(\xi(V + \zeta))$$

with $\xi V \ll 1$ and $\xi\zeta \ll 1$. So we have the following linearized dynamics:

$$\dot{\xi} = \lambda e^{\lambda t}\varepsilon_\xi = -(d_X + k_{IX}I^*)e^{\lambda t}\varepsilon_\xi - \frac{\beta\mu}{d_X + k_{IX}I^*}e^{\lambda t}\varepsilon_V - \frac{k_{IX}\mu}{d_X + k_{IX}I^*}e^{\lambda t}\varepsilon_\zeta$$

$$\iff \quad \lambda\varepsilon_\xi = -(d_X + k_{IX}I^*)\varepsilon_\xi - \frac{\mu}{d_X + k_{IX}I^*}(\beta\varepsilon_V - k_{IX}\varepsilon_I).$$

For Y defined in (2.1.3c), the steady state is 0 and there are no delays, so the linearization about the steady state yields

$$\dot{Y}(t) = \beta\left(\xi(t) + \frac{\mu}{d_X + k_{IX}I^*}\right)V(t) - k_{IY}Y(t)(\zeta(t) + I^*) - (d_Y + k_{IY}I^*)Y(t)$$
$$= \frac{\beta\mu}{d_X + k_{IX}I^*}V(t) - (d_Y + k_{IY}I^*)Y(t) + \mathcal{O}(\xi V + Y\zeta).$$

The linearized dynamics of (2.1.3c) are

$$\dot{Y} = \lambda e^{\lambda t}\varepsilon_Y = \frac{\beta\mu}{d_X + k_{IX}I^*}e^{\lambda t}\varepsilon_V - (d_Y + k_{IY}I^*)e^{\lambda t}\varepsilon_Y$$

$$\iff \quad \lambda\varepsilon_Y = \frac{\beta\mu}{d_X + k_{IX}I^*}\varepsilon_V - (d_Y + k_{IY}I^*)\varepsilon_Y.$$

We can similarly linearize R defined in(2.1.3d) about its steady state

$$\begin{aligned}\dot{\varphi}(t) &= k_{IX}\left(\xi(t) + \frac{\mu}{d_X + k_{IX}I^*}\right)(\zeta(t) + I^*) + k_{IY}Y(t)(\zeta(t) + I^*) \\ &\quad - d_R\left(\varphi(t) + \frac{\mu k_{IX}I^*}{d_R(d_X + k_{IX}I^*)}\right) \\ &= k_{IX}I^*\xi(t) + k_{IY}I^*Y(t) - \frac{k_{IX}\mu}{d_X + k_{IX}I^*}\zeta(t) - d_R\varphi(t) + \mathcal{O}(\xi\zeta + Y\zeta^n).\end{aligned}$$

Thus, the linearized dynamics of (2.1.3d) are

$$\begin{aligned}\dot{R} = \lambda e^{\lambda t}\varepsilon_\varphi &= k_{IX}I^*e^{\lambda t}\varepsilon_\xi + k_{IY}I^*e^{\lambda t}\varepsilon_Y + \frac{k_{IX}\mu}{d_X + k_{IX}I^*}e^{\lambda t}\varepsilon_\zeta - d_R e^{\lambda t}\varepsilon_\varphi \\ \iff \quad \lambda\varepsilon_\varphi &= k_{IX}I^*\varepsilon_\xi + k_{IY}I^*\varepsilon_Y + \frac{k_{IX}\mu}{d_X + k_{IX}I^*}\varepsilon_\zeta - d_R\varepsilon_\varphi.\end{aligned}$$

The linearization of (2.1.3e) yields

$$\begin{aligned}\dot{\zeta} &= k_I Y(t - \tau_I) + b_2(\zeta(t - \tau_2) + I^*)(k_2 + (\zeta(t - \tau_2) + I^*)^{-1} - d_I(\zeta(t) + I^*) \\ &= k_I Y(t - \tau_I) + \frac{b_2 k_2}{(k_2 + I^*)^2}\zeta(t - \tau_2) - d_I\zeta(t) + \mathcal{O}(\zeta^2).\end{aligned}$$

In this case, the linearization of (2.1.3e) results in

$$\begin{aligned}\dot{\zeta} = \lambda e^{\lambda t}\varepsilon_I &= k_I e^{\lambda(t-\tau_I)}\varepsilon_Y + \frac{b_2 k_2}{(k_2 + I^*)^2}e^{\lambda(t-\tau_2)}\varepsilon_I - d_I e^{\lambda t}\varepsilon_I \\ \iff \quad \lambda\varepsilon_I &= k_I e^{-\lambda\tau_I}\varepsilon_Y + \frac{b_2 k_2}{(k_2 + I^*)^2}e^{-\lambda\tau_2}\varepsilon_I - d_I\varepsilon_I.\end{aligned}$$

The full linearized system of (2.1.3a)-(2.1.3e) about any disease-free steady state (of which there are at most two) is thus

$$\dot{V} = k_V\frac{\tilde{K}_1^n}{\tilde{K}_1^n + I^{*n}}Y(t - \tau_V) - d_V V(t) \tag{2.2.29a}$$

$$\dot{\xi} = -(d_X + k_{IX})\xi(t) - \frac{\beta\mu}{d_X + k_{IX}I^*}V(t) - \frac{k_{IX}\mu}{d_X + k_{IX}I^*}I(t) \tag{2.2.29b}$$

$$\dot{Y} = \frac{\beta\mu}{d_X + k_{IX}I^*}V(t) - (d_Y + k_{IY}I^*)Y(t) \tag{2.2.29c}$$

$$\dot{\varphi} = k_{IX}I^*\xi(t) + k_{IY}I^*Y(t) - \frac{k_{IX}\mu}{d_X + k_{IX}I^*}\zeta(t) - d_R\varphi(t) \tag{2.2.29d}$$

$$\dot{\zeta} = k_I Y(t-\tau_I) + \frac{b_2 k_2}{(k_2+I^*)^2}\zeta(t-\tau_2) - d_I\zeta(t) \tag{2.2.29e}$$

Hence, the linear system of equations that needs to be satisfied for (2.2.28) to be the solution of (2.2.29) is

$$A\varepsilon =: \begin{pmatrix} -d_V & 0 & k_V\frac{\tilde{K}_1^n}{\tilde{K}_1^n+I^{*n}}e^{-\lambda\tau_V} & 0 & 0 \\ \frac{-\beta\mu}{d_X+k_{IX}I^*} & -d_X-k_{IX}I^* & 0 & 0 & \frac{-k_{IX}\mu}{d_X+k_{IX}I^*} \\ \frac{\beta\mu}{d_X+k_{IX}I^*} & 0 & -d_Y-k_{IY}I^* & 0 & 0 \\ 0 & k_{IX}I^* & k_{IY}I^* & -d_R & \frac{k_{IX}\mu}{d_X+k_{IX}I^*} \\ 0 & 0 & k_Ie^{-\lambda\tau_I} & 0 & I_{\text{lin}}-d_I \end{pmatrix} \begin{pmatrix} \varepsilon_V \\ \varepsilon_\xi \\ \varepsilon_Y \\ \varepsilon_\varphi \\ \varepsilon_\zeta \end{pmatrix} = \lambda \begin{pmatrix} \varepsilon_V \\ \varepsilon_\xi \\ \varepsilon_Y \\ \varepsilon_\varphi \\ \varepsilon_\zeta \end{pmatrix} \tag{2.2.30}$$

where

$$I_{\text{lin}} = \frac{b_2k_2}{(k_2+I^*)^2}e^{-\lambda\tau_2}.$$

For A defined in (2.2.30), $\det(A-\lambda I)$, computed by co-factor expansion, leads to the following characteristic polynomial

$$\Delta(\lambda) = (d_X+k_{IX}I^*+\lambda)(d_R+\lambda)\left(d_I-\frac{b_2k_2}{(k_2+I^*)^2}e^{-\lambda\tau_2}+\lambda\right)\left(-(d_V+\lambda)(d_Y+k_{IY}I^*+\lambda)\right.$$
$$\left.+\frac{k_V\tilde{K}_1^n\beta\mu}{(\tilde{K}_1^n+I^{*n})(d_X+k_{IX}I^*)}e^{-\lambda\tau_V}\right). \tag{2.2.31}$$

For the disease-free steady state which has $I^*=0$, as defined in (2.2.24), the system defined in (2.2.30) simplifies to

$$A\varepsilon = \begin{pmatrix} -d_V & 0 & k_Ve^{-\lambda\tau_V} & 0 & 0 \\ \frac{-\beta\mu}{d_X} & -d_X & 0 & 0 & \frac{-k_{IX}\mu}{d_X} \\ \frac{\beta\mu}{d_X} & 0 & -d_Y & 0 & 0 \\ 0 & 0 & 0 & -d_R & \frac{k_{IX}\mu}{d_X} \\ 0 & 0 & k_Ie^{-\lambda\tau_I} & 0 & \frac{b_2}{k_2}e^{-\lambda\tau_2}-d_I \end{pmatrix} \begin{pmatrix} \varepsilon_V \\ \varepsilon_\xi \\ \varepsilon_Y \\ \varepsilon_R \\ \varepsilon_I \end{pmatrix} = \lambda \begin{pmatrix} \varepsilon_V \\ \varepsilon_\xi \\ \varepsilon_Y \\ \varepsilon_R \\ \varepsilon_I \end{pmatrix}. \tag{2.2.32}$$

Consequently, for $I^*=0$, $\det(A-\lambda I)$ defined in (2.2.31) simplifies to

$$\Delta(\lambda) = (d_X+\lambda)(d_R+\lambda)(d_I-\frac{b_2}{k_2}e^{-\lambda\tau_2}+\lambda)\left(-(d_V+\lambda)(d_Y+\lambda)+\frac{k_V\beta\mu}{d_X}e^{-\lambda\tau_V}\right). \tag{2.2.33}$$

In the corresponding characteristic equation of (2.2.31), $\Delta(\lambda) = 0$, the first two terms of the product will result in negative real eigenvalues for positive parameter values d_X, d_R, and k_{IX} and $I^* \geq 0$. The other terms could result in positive or negative real-part eigenvalues.

Studying the linearizations about both disease-free steady states (2.2.24) and (2.2.27), when both of these steady states exist, there are four possibilities to consider: (1) they are both unstable, (2) (2.2.24) is stable and (2.2.27) is unstable, (3) (2.2.24) is unstable and (2.2.27) is stable, or (4) they are both stable. Examples of each of the first three cases are shown in Figures 2.6-2.8, and they will be discussed in detail below. We will then show that the fourth case can never occur.

Figures 2.6-2.8 were obtained by varying two parameters: β, the contact rate between uninfected cells X and free virus V, and b_2, the maximal production rate of the IFN positive feedback. We have chosen to vary these parameters for two main reasons: (1) these parameters have biological significance and (2) the impact of variations in these parameters on the characteristic equation is easy to study. In fact, we can think of β as a way to represent the strength of the infection, i.e. a measure of infectiousness and b_2 as a way to represent the strength of the IFN feedback loop or more generally of the innate immune response. This is reflected in the form of the characteristic polynomial defined in (2.2.33). Positive real-part eigenvalues will arise from one of two factors in the product:

$$d_I - \frac{b_2 k_2}{(k_2 + I^*)^2} e^{-\lambda \tau_2} + \lambda \tag{2.2.34}$$

or

$$-(d_V + \lambda)(d_Y + \lambda) + \frac{k_V \beta \mu}{d_X} e^{-\lambda \tau_V}. \tag{2.2.35}$$

This makes testing hypotheses regarding convergence to steady state easier. Indeed, we expect a strong infection to result in an unstable disease-free equilibrium and a strong IFN positive feedback to result in a stable chronic inflammation steady state as defined in (2.2.27). A weak infection should result in a stable disease-free equilibrium and a weak IFN positive feedback should result in a stable disease-free steady state with no chronic inflammation as defined in (2.2.24). Varying exclusively these two parameters does not, however, provide a comprehensive illustration of the dynamics regarding the innate immune response that influence convergence to the various steady states. For example, k_V, which represents the virion rate production could have also been used to symbolize the strength of the infection. The respective impact and combined effects of β and k_V will be discussed in Section 2.3.3. Moreover, as discussed in Section 1.5, sufficiently large delays

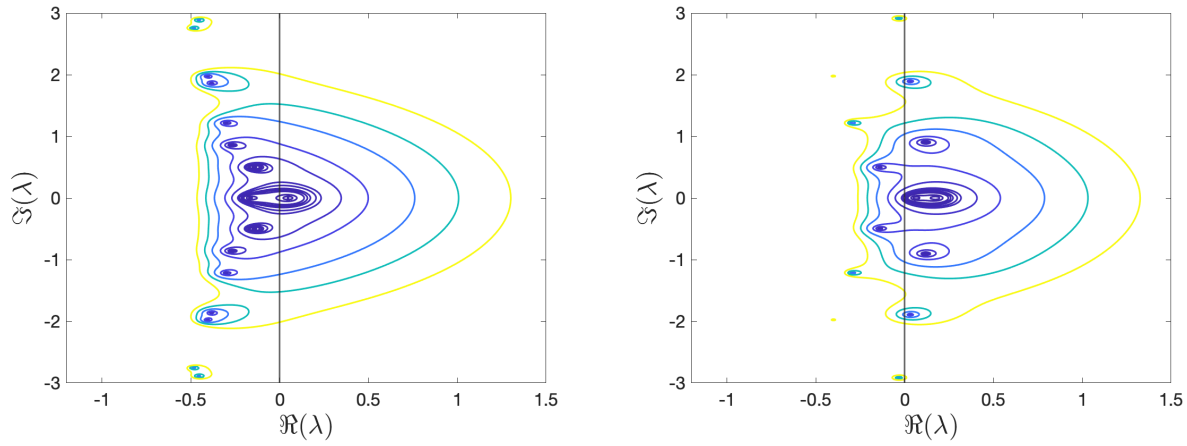

Figure 2.6: *Plots for the characteristic polynomial $\Delta(\lambda)$ of the system (2.1.3a)-(2.1.3e) linearized about the disease-free steady states for parameter values defined in Section 2.3.1.2. (a) Contour plot of $|\Delta(\lambda)|$ in the complex plane for the linearization about the first disease-free steady state ($I^* = 0$). (b) Contour plot of $|\Delta(\lambda)|$ in the complex plane for the linearization about the second disease-free steady state ($I^* \neq 0$). The characteristic roots are at the center of the islands.*

result in delay-induced instability and result in more complicated dynamics. However, in this case, the delays represent the duration of viral replication or cell production and, due to biological constraints, large delays will not occur. For this reason, we will not study the impact of increasing the delays on the stability of the equilibria of the model (2.1.3a)-(2.1.3e).

In Figure 2.6, obtained when using the parameter values of the full model, defined in Section 2.3.1, both disease-free steady states (2.2.24) and (2.2.27) have positive real eigenvalues, meaning that they are both unstable. In this case, the numerical simulations of the model converge to the endemic steady state as shown in Figure 2.11b, in Section 2.3.2.

Figure 2.7 was obtained by decreasing β, i.e. decreasing the infectiousness of the disease, when compared to Figure 2.6. Figure 2.7a has no eigenvalues with positive real part. This illustrates that a weak infection leads to control of the infection by the innate immune system, resulting in a disease-free steady state which is stable, the healthy disease-free steady state (2.2.24). Figure 2.7b has eigenvalues with positive real parts which means the chronic inflammation disease-free steady state (2.2.27) is unstable, due to the relative weakness of the IFN positive feedback.

Figure 2.8 was obtained by increasing b_2, i.e. increasing the IFN positive feedback, when compared to Figure 2.6. Figure 2.8b has no eigenvalues with positive real part. This illustrates that a strong IFN feedback loop is able to control the infection, resulting in a disease-free steady state which is stable, the chronic inflammation disease-free steady state

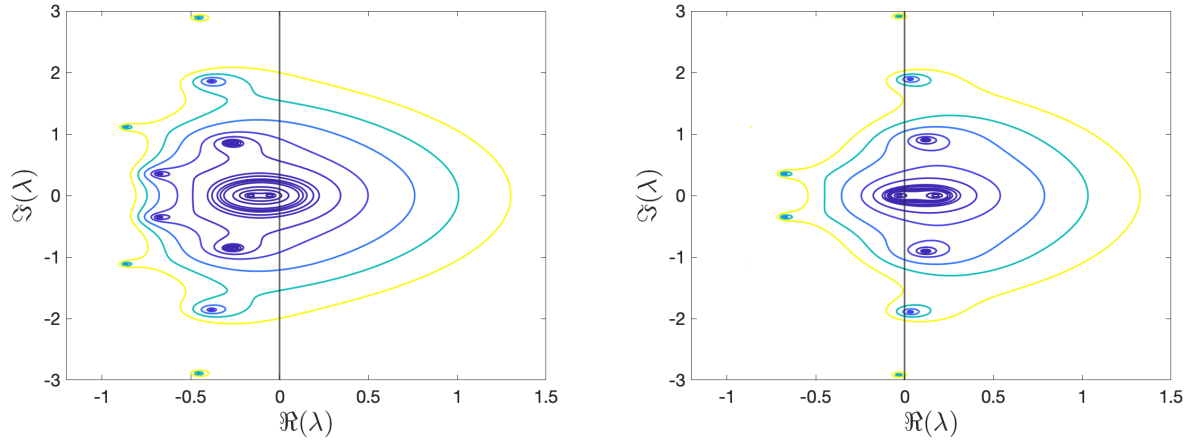

Figure 2.7: *Plots for the characteristic polynomial $\Delta(\lambda)$ of the system (2.1.3a)-(2.1.3e) linearized about the disease-free steady states for parameter values defined in Section 2.3.1, except for $\beta = 2.05 \cdot 10^{-4}$. (a) Contour plot of $|\Delta(\lambda)|$ in the complex plane for the linearization about the first disease-free steady state ($I^* = 0$). (b) Contour plot of $|\Delta(\lambda)|$ in the complex plane for the linearization about the second disease-free steady state ($I^* \neq 0$). The characteristic roots are at the center of the islands.*

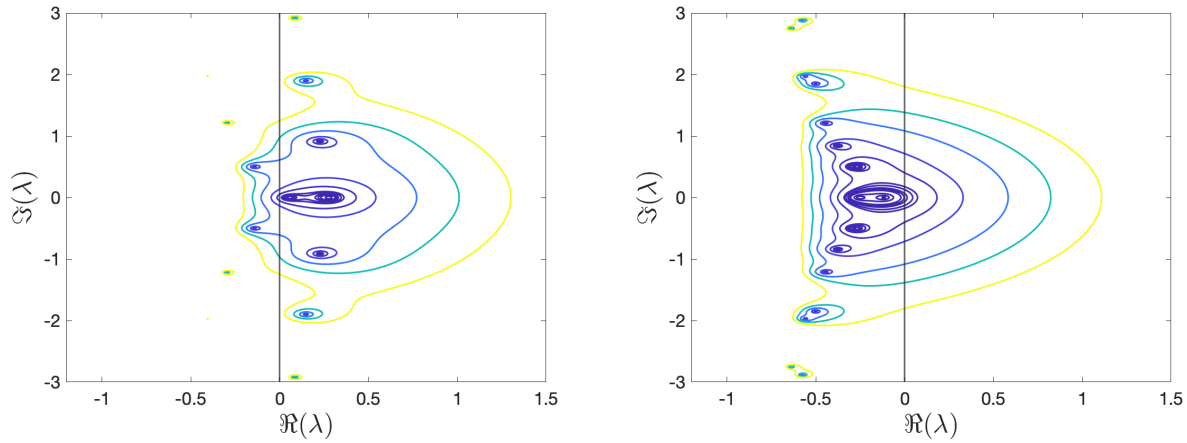

Figure 2.8: *Plots for the characteristic polynomial $\Delta(\lambda)$ of the system (2.1.3a)-(2.1.3e) linearized about the disease-free steady states for parameter values defined in Section 2.3.1, except for $b_2 = 4$. (a) Contour plot of $|\Delta(\lambda)|$ in the complex plane for the linearization about the first disease-free steady state ($I^* = 0$). (b) Contour plot of $|\Delta(\lambda)|$ in the complex plane for the linearization about the second disease-free steady state ($I^* \neq 0$). The characteristic roots are at the center of the islands.*

(2.2.27). Figure 2.8a has positive real eigenvalues which means the healthy disease-free steady state (2.2.24) is unstable, due to the strength of the IFN positive feedback. This result can also be obtained by decreasing β, i.e. decreasing the strength of the infection, in which case the innate immune response over powers the infection, leading to stability of (2.2.27).

We will prove that both disease-free steady states (2.2.24) and (2.2.27) cannot be stable for the same parameter values. Decreasing infectiousness β can lead to stability of either one of the disease-free equilibria (2.2.24) and (2.2.27). In this case, the strength of the IFN positive feedback b_2 will determine which of the two steady states, (2.2.24) or (2.2.27), is stable, based on the eigenvalues that arise from the term (2.2.34) of the characteristic polynomial $\Delta(\lambda)$, defined in (2.2.31). When $I^* = 0$, (2.2.34) satisfies the characteristic equation $\Delta(\lambda) = 0$ if

$$d_I - \frac{b_2}{k_2} e^{-\lambda \tau_2} + \lambda = 0$$

$$\implies d_I - \frac{b_2}{k_2} e^{-\lambda \tau_2} = -\lambda > 0.$$

Thus, we must have

$$d_I > \frac{b_2}{k_2} e^{-\lambda \tau_2} > \frac{b_2}{k_2} \tag{2.2.36}$$

because for negative λ and positive τ_2, $e^{-\lambda \tau_2} > 1$.

Similarly, when I^* is defined by (2.2.26), (2.2.34) satisfies the characteristic equation $\Delta(\lambda) = 0$ if

$$d_I - \frac{b_2 k_2}{k_2 + \left(\frac{b_2}{d_I} - k_2 \right)} e^{-\lambda \tau_2} + \lambda = 0$$

$$d_I - \frac{k_2 d_I^2}{b_2} e^{-\lambda \tau_2} + \lambda = 0$$

$$\implies d_I - \frac{k_2 d_I^2}{b_2} e^{-\lambda \tau_2} = -\lambda > 0.$$

Thus, we must have

$$d_I > \frac{k_2 d_I^2}{b_2} e^{-\lambda \tau_2}$$

$$\implies \frac{b_2}{k_2} > d_I e^{-\lambda\tau_2} > d_I \tag{2.2.37}$$

because for negative λ and positive τ_2, $e^{-\lambda\tau_2} > 1$.

Equations (2.2.36) and (2.2.37) cannot hold concurrently. For this reason, (2.2.24) and (2.2.27) cannot both be stable. Interestingly, (2.2.37) is equivalent to having I^*, defined in (2.2.26), strictly positive. In other words, (2.2.27) is stable when it is defined for biologically real values of I^*.

When there is equality in (2.2.26), there is a unique disease-free steady state, with $I^* = 0$, defined by (2.2.24), with a zero eigenvalue, resulting from the term (2.2.34). Thus, there is a transcritical bifurcation at this point. In this case, we have

$$b_2 = d_I k_2. \tag{2.2.38}$$

For small enough β, numerical simulations representing a small perturbation from the healthy disease-free steady state (2.2.24) result in the model converging to the healthy disease-free steady state (2.2.24), which is shown in Figure 2.9a. For β large enough, a small perturbation from the healthy disease-free steady state (2.2.24) result in the model converging to the endemic disease steady state, which is shown in Figure 2.9b. In this case, stability of the unique disease-free steady state is entirely determined by the infectiousness of the infection, as the strength of IFN positive feedback is fixed.

2.2.3 *Full Model Dynamics*

A steady state $(V^*, X^*, Y^*, R^*, I^*, B^*_{LL}, B^*_E, A^*, T^*_E, T^*_M, T^*_H)$ of the full model defined in (2.1.1) satisfies

$$0 = k_V Y^* \frac{\tilde{K}_1^n}{\tilde{K}_1^n + I^{*n}} - d_V V^* - \rho A^* V^* \tag{2.2.39a}$$

$$0 = \mu - d_X X^* - \beta X^* V^* - k_{IX} X^* I^* \tag{2.2.39b}$$

$$0 = \beta X^* V^* - d_Y Y^* - k_{IY} I^* Y^* \tag{2.2.39c}$$

$$0 = k_{IX} X^* I^* + k_{IY} Y^* I^* - d_R R^* \tag{2.2.39d}$$

$$0 = k_I Y^* + \frac{b_2 I^*}{k_2 + I^*} + k_{T_E I} T^*_E + k_{T_H I} T^*_H - d_I I^* \tag{2.2.39e}$$

$$0 = k_{T_H} \mathbb{1}_{V^* > V_T} I^* Y^* - d_{T_H} T^*_H \tag{2.2.39f}$$

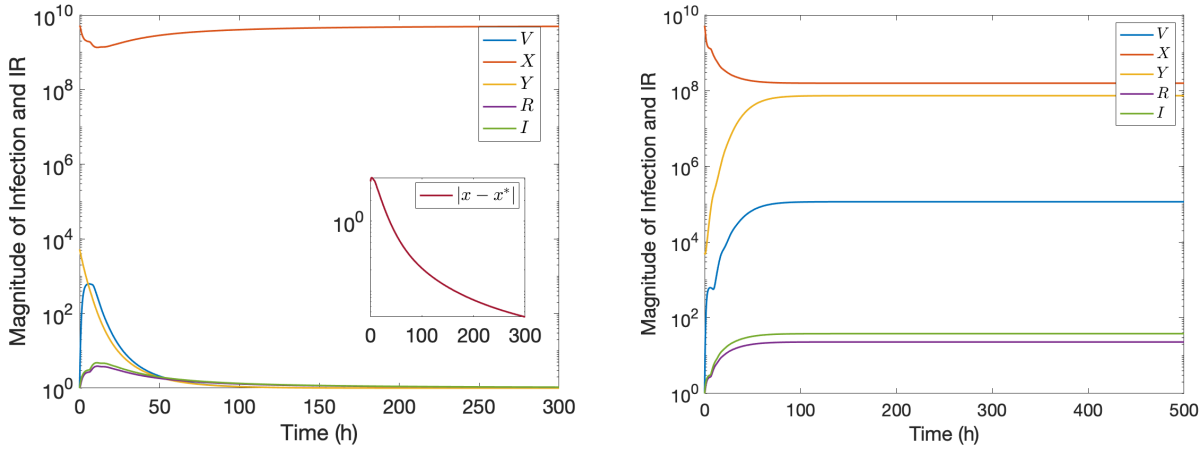

Figure 2.9: *Simulation of the viral dynamics defined in (2.1.3a)-(2.1.3e) for initial conditions representing a small perturbation from the disease-free steady state (2.2.24). Initial conditions are* $[V^0, X^0, Y^0, R^0, I^0] = [V^*, X^*, \log_{10}(5250), 0, 0]$. *(a) Simulation for parameter values defined in Section (2.3.1.2), except for* $\beta = 2.175 \cdot 10^{-3}$ *and* b_2 *defined in (2.2.38). The inset represents* $\|x(t) - x^*\|$ *where x(t) is the solution to (2.1.3a)-(2.1.3e) and* x^* *is the disease-free steady state defined in (2.2.27). (b) Simulation for parameter values defined in Section (2.3.1.2), except for* b_2 *defined in (2.2.38).*

$$0 = k_{T_E} \cdot \mathbb{1}_{V^*>V_T} Y^* \left(1 - \frac{T_E^*}{P^*}\right) \cdot I^* \cdot T_H^* + k_{T_M Y} \mathbb{1}_{V^*>V_T} T_M^* Y^* - (1 - \mathbb{1}_{Y^*}) \left(d_{T_E pi} T_E^* + k_{T_M} T_E^*\right) - d_{T_E} T_E^* \tag{2.2.39g}$$

$$0 = (1 - \mathbb{1}_{Y^*}) k_{T_M} T_E^* - k_{T_M Y} \mathbb{1}_{V^*>V_T} T_M^* Y^* \tag{2.2.39h}$$

$$0 = k_{B_{LL}} \mathbb{1}_{V^*>V_T} V^* T_H^* - k_{B_{LL}V} \mathbb{1}_{V^*>V_T} V^* B_{LL}^* \tag{2.2.39i}$$

$$0 = k_{B_E} \mathbb{1}_{V^*>V_T} V^* T_H^* + k_{B_{LL}V} \mathbb{1}_{V^*>V_T} V^* B_{LL}^* - d_{B_E} B_E^* \tag{2.2.39j}$$

$$0 = k_{B_{LL}A} B_{LL}^* + k_{B_E A} B_E^* - \rho A^* V^* - d_A A^*. \tag{2.2.39k}$$

If $V^* = Y^* = 0$, then (2.2.39a) and (2.2.39c) hold. Then, for a non-zero threshold V_T, (2.2.39j), (2.2.39g), and (2.2.39f) become

$$0 = -d_{T_H} T_H^* \implies T_H^* = 0 \tag{2.2.40}$$

$$0 = d_{T_E pi} T_E^* + k_{T_M} T_E^* - d_{T_E} T_E^* \implies T_E^* = 0 \tag{2.2.41}$$

$$0 = -d_{B_E} B_E^* \implies B_E^* = 0. \tag{2.2.42}$$

Moreover, from (2.2.39k), we get

$$A^* = \frac{k_{B_{LL}A} B^*_{LL}}{d_A} \tag{2.2.43}$$

Equations (2.2.39i) and (2.2.39h) both reduce to $0 = 0$ when $V_T > 0$ so the steady states B^*_{LL} and T^*_M are not uniquely defined for disease-free steady equilibria. This allows for the modeling of different immunological memory levels. Given (2.2.40)-(2.2.42), the disease-free steady state expressions X^*, R^*, and I^* are the same as in the disease-free steady state expression for the innate immune system model (2.2.27), with I^* defined in (2.2.26), in Section 2.2.2. In this case, I^* is not uniquely defined. Hence, disease-free steady states for the full immune system model are

$$\left(0, \frac{\mu}{d_X + k_{IX} I^*}, 0, \frac{\mu k_{IX} I^*}{d_R (d_X + k_{IX} I^*)}, I^*, 0, 0, T^*_M, B^*_{LL}, 0, \frac{k_{B_{LL}A} B^*_{LL}}{d_A}\right). \tag{2.2.44}$$

The steady state (2.2.44) is not unique because I^*, B^*_{LL}, and T^*_M are not uniquely defined. When there is no chronic inflammation, i.e. $I^* = 0$, the innate immune component steady states are described by (2.2.24), and (2.2.44) simplifies to

$$\left(0, \frac{\mu}{d_X}, 0, 0, 0, 0, 0, T^*_M, B^*_{LL}, 0, \frac{k_{B_{LL}A} B^*_{LL}}{d_A}\right). \tag{2.2.45}$$

Equation (2.2.45) represents a healthy individual whose immune system functions normally. In fact, post-infection no immune cell populations should remain, besides T_M, B_{LL}, and A, the components that make up immunological memory.

There are multiple different forms of endemic disease steady states. In fact, it is possible that (1) $V^* \neq 0$ but $V^* \leq V_T$ or that (2) $V^* \neq 0$ and $V^* > V_T$.

In the first case, X^*, Y^*, R^*, and I^* can be obtained by following a similar process as can be used to obtain endemic disease steady state of the innate immune system (2.1.3a)-(2.1.3e), which was detailed in Section 2.2.2. T_H, T_E, and B_E can be defined as they were in (2.2.40), (2.2.41), and (2.2.42), respectively. Similarly, (2.2.39h) and (2.2.39i) reduce to $0 = 0$, so B^*_{LL} and T^*_M are not uniquely defined. From (2.2.39k), we can define A^* as function of B^*_{LL} and V^* and from (2.2.39a), we can define A^* as a function of V^* and Y^*. By equating these two definitions of A^*, we can define V^* as a function of B^*_{LL} and Y^*. Thus, all steady state values can be expressed as a function of I^* and B^*_{LL}.

For the second case, when $V^* > V_T$, (2.2.39a)-(2.2.39k) are satisfied when infected and recovered cells, and most immune components are non-zero. It is not evident how to algebraically determine a closed-form expression for most steady state values, with the

exception of T_M^*. We could determine the other steady state values satisfying (2.2.39a)-(2.2.39k) numerically.

To determine T_M^*, considering $Y^* \neq 0$, we have that (2.2.39h) reduces to

$$-k_{T_M Y} T_M^* Y^* = 0 \implies T_M^* = 0. \tag{2.2.46}$$

This proves that the absence of memory T cells is a necessary condition for the persistence of elevated viral titers. Equivalently the presence of memory T cells, i.e. $T_M \neq 0$, keeps viral titers relatively low ($V \leq V_T$). Indeed, if $T_M \neq 0$, for (2.2.39h) to be satisfied, either (1) $Y^* = 0$, in which case $V^* = 0$, from (2.2.39b) and (2.2.39c), and $T_E = 0$, from (2.2.39g) or (2) $Y^* \neq 0$, in which case (2.2.39h) reduces to

$$-k_{T_M Y} \mathbb{1}_{V^* > V_T} T_M^* Y^* = 0. \tag{2.2.47}$$

In this case, for $T_M^*, Y^* \neq 0$, we have $V^* \leq V_T$.

In Sections 2.3 and 3.2, we will consider scenarios where the infection is cleared before the memory T cells are depleted, which does not give rise to high virus levels. In Section 3.2 we will use the model (2.1.1) to study reinfection scenarios and their impact on long-term immunity, in which case we will consider that each infection is cleared before the next one begins. Thus, we will be interested in studying disease-free steady states after each infection and endemic disease steady states of (2.1.1) will not be studied in detail.

2.2.3.1 *Piecewise-smooth Dynamics*

The full model describes the dynamics of the immune system during an infection and post-infection. Post-infection the population of CD8+ T cells T_E contracts and they differentiate into memory T cells T_M. We can define a piecewise-smooth (PWS) function to represent these two phases. If we define $x(t)$ to be an 11-dimensional vector representing the variables of the full model at time t, with x_i, the i-th component of the vector. Equations (2.1.1g) and (2.1.1h) describe two distinct phases: the infection phase (when $Y(t) > 0$) and the post-infection phase (when $Y(t) = 0$). Then, from the definitions presented in Section 1.5.1, we can define

$$S_1 = \{x(t) : x_3(t) = 0\}$$
$$S_2 = \{x(t) : x_3(t) > 0\}$$

with $x_3(t) = Y(t)$. Then, we have the switching manifold

$$\sum_{12} = \{x(t) : \ x_3(t) = 0\}.$$

We want to define a function H such that when $x(t) \in S_1$, $H \leq 0$ and when $x(t) \in S_2$, $H > 0$. From the switching manifold, we can explicitly define the function H to be

$$H(x(t), x(t - \tau_V), \ldots) = x_3(t) = Y(t).$$

We can define the vector fields F_1, describing the infection phase, and F_2, describing the post-infection phase, where $F_{1,i}$ and $F_{2,i}$ represent the i-th component of each vector field. The full model presented in (2.1.1a)-(2.1.1k) describes both the infection and post-infection phases for all variables, except for T_E and T_M. During the infection phase, these variables described by (2.1.1g) and (2.1.1h), respectively, can be written as

$$\begin{aligned} \dot{T_E}(t) = k_{T_E} I(t - \tau_{T_E}) T_H(t - \tau_{T_E}) \cdot \mathbb{1}_{V(t-\tau_{T_E})>V_T} Y(t - \tau_{T_E}) \left(1 - \frac{T_E(t - \tau_{T_E})}{P(t - \tau_{T_E})}\right) \\ + k_{T_M Y} \mathbb{1}_{V(t)>V_T} T_M(t) Y(t) - d_{T_E} T_E(t). \end{aligned} \tag{2.2.48}$$

$$\dot{T_M}(t) = -k_{T_M Y} \mathbb{1}_{V(t)>V_T} T_M(t) Y(t) \tag{2.2.49}$$

During the post-infection phase, we have

$$\begin{aligned} \dot{T_E} = k_{T_E} I(t - \tau_{T_E}) T_H(t - \tau_{T_E}) \cdot \mathbb{1}_{V(t-\tau_{T_E})>V_T} Y(t - \tau_{T_E}) \left(1 - \frac{T_E(t - \tau_{T_E})}{P(t - \tau_{T_E})}\right) \\ + k_{T_M Y} \mathbb{1}_{V(t)>V_T} T_M(t) Y(t) - \left(d_{T_E pi} + k_{T_M} + d_{T_E}\right) T_E(t). \end{aligned} \tag{2.2.50}$$

$$\dot{T_M} = -k_{T_M Y} \mathbb{1}_{V(t)>V_T} T_M(t) Y(t) + k_{T_M} T_E(t) \tag{2.2.51}$$

We have $x_7(t) = T_E(t)$ so we have $F_{1,7} = \dot{T_E}$, as defined in (2.2.48) and $F_{2,7} = \dot{T_E}$, as defined in (2.2.50). Similarly, we have $x_8(t) = T_M(t)$ so we have $F_{1,8} = \dot{T_M}$, as defined in (2.2.49) and $F_{2,8} = \dot{T_E}$, as defined in (2.2.51). For all other components, i.e. for all $i \neq 7, 8$, we can define $F_{1,i} = F_{2,i}$, where the vector field is described by equations (2.1.1a)-(2.1.1f) and (2.1.1i)-(2.1.1k). Then the model can be be described in the following way

$$\dot{x} = \begin{cases} F_1(x(t), x(t - \tau_V), \ldots) & \text{if } H \leq 0 \\ F_2(x(t), x(t - \tau_V), \ldots) & \text{if } H > 0 \end{cases} \tag{2.2.52}$$

In this case, there are equilibria which lie on the switching manifold: the disease-free steady states described in (2.2.44). The numerical simulations (see Section 2.3.3) did not

reveal any qualitative differences in behavior for different parameter values indicating that there are no discontinuity-induced bifurcations occurring for positive parameter values at this steady state.

Within the infection phase, there are also two distinct phases: when $V \leq V_T$, only the innate immune system is activated and when $V > V_T$, the adaptive immune system is also activated. However, the adaptive immune system components, described by (2.1.1f)-(2.1.1j) are not all activated at the same time. Some components cross the threshold after no delay, i.e when $V(t) > V_T$. Other components cross the boundary after a delay. In the model defined in (2.1.1a)-(2.1.1k), there are four delays that have an impact on the threshold condition: τ_{T_E} in (2.1.1g), $\tau_{B_{LL}}$ in (2.1.1i), $\tau_{B_{LLV}}$ in (2.1.1i) and (2.1.1j), and τ_{B_E} in (2.1.1j). Each of these delays is distinct, i.e. for each delay we can write the threshold condition as $V(t-\tau_i) > V_T$, for $i = 1, 2, 3, 4$. Without loss of generality, we suppose

$$0 < \tau_1 < \tau_2 < \tau_3 < \tau_4.$$

For a finite number of discrete delays, we can define each delayed variable $V(t-\tau_i)$ as a distinct threshold [50]. Initially, viral titers are low, i.e $V(t),\ V(t-\tau_i) \leq V_T$ but V is increasing. After the infection, peaks V is decreasing. In this case, the intersection manifolds are

$$\begin{aligned}
\sum_{01} &= \{x(t) : x_1(t) = V_T,\ x_1(t-\tau_i) \leq V_T\} \qquad \text{for } i = 1, 2, 3, 4 \\
\sum_{12} &= \{x(t) : x_1(t) > V_T,\ x_1(t-\tau_1) = V_T,\ x_1(t-\tau_i) \leq V_T\} \qquad \text{for } i = 2, 3, 4 \\
&\vdots \\
\sum_{45} &= \{x(t) : x_1(t),\ x_1(t-\tau_i) > V_T,\ x_1(t-\tau_4) = V_T\} \qquad \text{for } i = 1, 2, 3 \\
\sum_{56} &= \{x(t) : x_1(t) = V_T,\ x_1(t-\tau_i) > V_T,\ \} \qquad \text{for } i = 1, 2, 3, 4 \\
&\vdots \\
\sum_{90} &= \{x(t) : x_1(t),\ x_1(t-\tau_i) \leq V_T,\ x_1(t-\tau_4) = V_T\} \qquad \text{for } i = 1, 2, 3
\end{aligned}$$

with $x_1(t) = V(t)$.

There are thus 10 distinct vector fields which define $\dot{x}(t)$. The explicit definition and analysis of these vector fields will be omitted because there are no steady states or limit cycles in any of the switching manifolds so there are no discontinuity-induced bifurcations. In fact, when the vector field cross the switching manifolds, the infection is either increasing or decreasing. Moreover, the numerical simulations (see Section 2.3.3) did not reveal any

qualitative differences in behavior for different parameter values with regards to these switching manifolds.

2.3 NUMERICAL SIMULATIONS

The numerical simulations of (2.1.1) presented in this section will model acute infections, i.e. infections that are cleared by the immune response. In other words, we will simulate scenarios where a healthy individual contracts an infection. This induces an immune response which results in infection clearance, after which an individual is considered healthy again. In this case, we are considering a case where there is initially no chronic inflammation in the absence of infection.

As presented in Table 1.2, the variables of interest in the model (2.1.1) are measured in different units and because of this and inherent differences in the measured quantities, peak values are of different magnitudes, ranging from the order of 10 (concentrations in mL) to 10^9 (number of cells in the lungs). Specifically, in a very short time span (<100 hours), the number of infected cells grows to peak at $\sim 10^9$ and then decreases to 0 within 200 hours. We need to account for these different scales explicitly to perform numerical simulations and analyze model dynamics of (2.1.1). To do so, all variables will be measure in $\log_{10}(\text{unit})$ of their respective units, presented in Table 1.2. This choice is the result of certain variables usually being presented in these units (viral titers, IFN levels, and antibody levels) [1, 8, 14]. This allows us to view all variable time courses on a single graph to better visualize the different phases of the infection, which in turn allows us to analyze the relationship between different cell compartments and the dynamics that occur. Moreover, modeling variables in $\log_{10}(\text{unit})$, instead of the original units found in Table 1.2, avoids having parameters values that are smaller or of equal magnitude as the tolerance 10^{-9}, defined in Section 1.6, which can occur in this type of model [68]. In this case, the log transformation results in stabilization of the computational algorithm. One main issue arises from this choice: most immune compartments are 0 at the disease-free steady state defined in (2.2.44), which in a log scale results in $\log_{10}(\text{unit}) = 0 \iff \text{unit} = 10^0 = 1$. For example, this means that the disease-free steady state value of infected cells defined in (2.2.44) is 1 and the number of infected cells never actually reaches 0. If we wanted the number of infected cells to be 0, we would need $\log_{10}(0) = -\infty$, which can't be reached numerically. However, we suppose that this is negligible because a single infected cell would not result in an infection and this is within the tolerance of experimental measures for the different immune components.

Variable	Value	Unit	Reference
X^0	$\log_{10}(5.25 \cdot 10^9)$	$\log_{10}$(cells)	[12, 14, 41]
Y^0	$\log_{10}(5.25 \cdot 10^3)$	$\log_{10}$(cells)	(2.3.4)
T_M^0	$\log_{10}(10^4)$	$\log_{10}$(cells)	(2.3.5)
B_{LL}^0	$\log_{10}(90.5)$	$\log_{10}$(cells) $\cdot \mu L^{-1}$	(2.3.14)
A^0	$\log_{10}(3 \cdot 10)$	$\log_{10}(\text{pg} \cdot \text{ml}^{-1})$	(2.3.12)

Table 2.1: *Non-Zero History Functions for Numerical Simulations of* (2.1.1)*, for* $-\tau \leq t \leq 0$

2.3.1 *Estimation and Computation of Parameter and Steady State Values*

2.3.1.1 *Estimation and Computation of Steady State Values*

The contraction of an infection represents a perturbation of the disease-free steady state (2.2.45), which represents a healthy individual, with no chronic inflammation, i.e. $I^* = 0$. For this reason, numerical simulations of (2.1.1) presented in Section 2.3.2 begin at a disease-free steady state, for all variables except for a small perturbation, which represents the exposure to virus and contraction of the infection. In this case, the perturbation of the steady state results from assuming that the initial number of infected cells is positive, i.e. $Y^0 > 0$. This does not represent a biologically realistic scenario, because infections are contracted after exposure to free virions V, modeled by $V^0 > 0$, as detailed in Section 1.1. However, assuming that $Y^0 > 0$ and that the initial free virus population is $V^0 = 0$ leads to more reliable estimations of viral kinetics than perturbing the steady state by having $V^0 > 0$ [11].

The perturbation of the disease-free equilibrium occurs at time $t = 0$, before which the system (2.1.1) is at a disease-free steady state defined in (2.2.45). For this reason, the history functions of all variables are constant for $-\tau \leq t < 0$, where $-\tau := -\max\{\tau_V, ..., \tau_{T_E}\}$. Specifically, all variables are zero at the disease-free steady state (2.2.45) except for healthy, target cells X; memory T cells T_M; long-lived B cells B_{LL}; and antibody A. Indeed, in the absence of infection, the number of healthy, target cells is the number of epithelial cells in the lung, so it is non-zero. We can define $X(t) = X^0$ for $-\tau \leq t0$ as the initial number of target cells. Moreover, due to natural infections occurring early in life, most adults have some immunity against influenza A, i.e. they have non-zero antibody levels [10, 18, 69]. We can define $A(t) = A^0$ for $-\tau \leq t0$ as the initial antibody levels. Because this is a steady state value, as defined in (2.2.44), we must also have $B_{LL}^0 \neq 0$ where $B_{LL}(t) = B_{LL}^0$ for $-\tau \leq t \leq 0$. Similarly, due to previously existing immunity, we assume $T_M^0 \neq 0$ where $T_M(t) = T_M^0$ for $-\tau \leq t \leq 0$. The non-zero constant history functions are found in Table 2.1.

Post-infection, the system is once again in a disease-free steady state, defined in (2.2.44),

Variable	Value	Unit	Reference
X^*	$\log_{10}(5.25 \cdot 10^9)$	$\log_{10}(\text{cells})$	(2.3.1)
T_M^*	$\log_{10}(1.52 \cdot 10^4)$	$\log_{10}(\text{cells})$	(2.3.11)
B_{LL}^*	$\log_{10}(3.56 \cdot 10^3)$	$\log_{10}(\text{cells} \cdot \text{mL}^{-1})$	(2.3.17)
A^*	$\log_{10}(4.8 \cdot 10^2)$	$\log_{10}(\text{pg} \cdot \text{mL}^{-1})$	(2.3.13)

Table 2.2: *Non-Zero Disease-Free (Without Inflammation) Steady State Values for Numerical Simulations of* (2.1.1).

which means all variables are zero except for X, T_M, B_{LL}, and A. The post-infection steady state values for variables which are non-zero are found in Table 2.2.

The estimated number of healthy susceptible cells pre-infection X^0 is taken directly from the literature. The steady state value of X is unique which means there is complete regeneration of epithelial cells post-infection. The steady state of X post-infection can thus be defined:

$$X^* = X^0, \quad -\tau \leq t \leq 0. \tag{2.3.1}$$

This is consistent with experimental observations [70].

As mentioned previously, the initial number of infected cells Y^0 does not represent a biologically realistic quantity because infections are transmitted between individuals by inhaling free virions. This number was chosen to be

$$Y^0 = \log_{10}(5.25 \cdot 10^3). \tag{2.3.2}$$

or 0.0001% of cells in the lung to obtain realistic viral time-courses. Discussion on the impact of this choice is presented in Section 2.3.3. This would give us the history function of $Y(t)$

$$Y(t) = \begin{cases} 0 & -\tau \leq t < 0 \\ Y^0 & t = 0 \end{cases} \tag{2.3.3}$$

for $-\tau \leq t \leq 0$, with Y^0 defined in (2.3.2). Because of the delay in viral replication τ_V in (2.1.1a), (2.3.3) results in delayed virion production, i.e. $V(t) = 0$ for all $t < \tau_V$. This means that, for a time, infected cells exist in the absence of free virions. However, this does not occur in reality. Instead, by choosing

$$Y(t) = Y^0 \tag{2.3.4}$$

for $-\tau \leq t \leq 0$, with Y^0 defined in (2.3.2), virion production will start immediately, reflecting a more realistic scenario where infected cells drive virion production and virions

drive infection of cells.

We assume the number of memory T cells before the infection occurs T_M^0 is 10^4 cells, which is the same order of magnitude as the peak number of CD8+ T cells (see Table 1.2).

$$T_M^0 = \log_{10}(10^4) = 4. \tag{2.3.5}$$

In this case, we do not consider antigenic similarity between strains. The impact of similarity between influenza strains on the immune response will be discussed in Chapter 3.

Post-infection, 5 to 10% of CD8+ T cells become memory cells. Assuming the infection is cleared at time $t_C > 0$, we have $Y(t) > 0$ for $0 \leq t < t_C$ and $Y(t_C) = 0$. We can thus define

$$T_M^* = T_M^0 + p \cdot T_E(t_C) \tag{2.3.6}$$

where $p \in (0.05, 0.1)$ and $T_E(t_C)$ is the number of effector T cells when the infection is cleared. The effector T-cell population peaks at time t_{PEAK} and until the infection is cleared, i.e for $t \in (t_{PEAK}, t_C)$, the decrease in effector T cells is only attributable to natural cell death, which occurs at rate d_{T_E} (see (2.1.1g), detailed in Section 2.1.3.1). The decrease in effector T cells is

$$\dot{T_E}(s) = -d_{T_E} T_E(s). \tag{2.3.7}$$

Thus, we can define the solution of the ODE (2.3.7)

$$D(s) := T_E(s) = c \exp(-d_{T_E} s), \quad c \in \mathbb{R}.$$

If $s = 0$ when $t = t_{PEAK}$, we have

$$D(0) = T_E(t_{PEAK}) = c \implies D(s) = T_E(t_{PEAK}) \exp(-d_{T_E} s).$$

During the infection, effector T-cell production continues. Thus, at time t_C, the number of effector T cells is

$$T_E(t_C) > D(t_C - t_{PEAK}) = T_E(t_{PEAK}) \exp(-d_{T_E}(t_C - t_{PEAK})) \tag{2.3.8}$$

Considering the infection is cleared within a few weeks and d_{T_E}, which will be defined in (2.3.26) and derived in Section 2.3.1.2, is very small, we have

$$\exp(-d_{T_E}(t_C - t_{PEAK})) \approx (1 - \delta) \tag{2.3.9}$$

for $\delta > 0$, $\delta \ll 1$. Putting (2.3.9) in (2.3.8), we obtain

$$T_E(t_C) > T_E(t_{PEAK})(1 - \delta) \implies T_E(t_C) \approx T_E(t_{PEAK}). \tag{2.3.10}$$

Then, 10% of CD8+ T cells become memory cells, and putting (2.3.10) and (2.3.6) together, we obtain the number of memory T cells

$$T_M^* = \log_{10}(10^4 + 0.1 \cdot 5.2 \cdot 10^4) = \log_{10}(1.52 \cdot 10^4). \tag{2.3.11}$$

Antibody levels expand 20-fold during influenza A infections [13]. The peak of antibody levels is assumed to be the median of the range of experimental values, found in Table 1.2. As such, A^0, the value of $A(t)$ pre-simulation for all $-\tau \leq t \leq 0$ is

$$A^0 = \log_{10}\left(\frac{1}{20} \cdot 6 \cdot 10^2\right) = \log_{10}(3 \cdot 10)\ \log_{10}(\text{pg} \cdot \text{mL}^{-1}). \tag{2.3.12}$$

Post-infection, the antibody levels are boosted 16-fold [18]. Thus, we have

$$A^* = 16 \cdot A^0 = \log_{10}(16 \cdot 30) = \log_{10}(4.8 \cdot 10^2)\ = \log_{10}(\text{pg} \cdot \text{mL}^{-1}). \tag{2.3.13}$$

Moreover, the normal range for memory B cells in healthy subjects is $27 - 154$ cells per μL [46]. Taking the median value of this range for the initial steady state of the long-lived B-cell population, we have

$$B_{LL}(t) = \log_{10}(90.5) \quad -\tau \leq t \leq 0. \tag{2.3.14}$$

The initial production rate of antibody by long-lived B cells, $k_{B_{LL}A}$ can be determined by the initial values of A and B_{LL}. In fact, at the disease-free steady state, we have

$$A(t) = \frac{k_{B_{LL}A} B_{LL}(t)}{d_A} \quad -\tau \leq t \leq 0 \tag{2.3.15}$$

$$\implies k_{B_{LL}A} = \frac{A(t) d_A}{B_{LL}(t)} = \frac{\log_{10}(3 \cdot 10) \cdot 0.04}{24 \cdot \log_{10}(90.5)} \approx 1.26 \cdot 10^{-3}. \tag{2.3.16}$$

From the value of A^* computed in (2.3.13) and the steady state expression of A^* derived in (2.2.39k), we can compute the value of B_{LL}^*:

$$B_{LL}^* = \frac{A^* d_A}{k_{B_{LL}A}} \approx \frac{\log_{10}(4.8 \cdot 10^2) \cdot 0.04}{24 \cdot 1.26 \cdot 10^{-3}} \approx \log_{10}(3.56 \cdot 10^3). \tag{2.3.17}$$

2.3.1.2 *Estimation and Computation of Parameter Values*

Some parameter values were taken from experimental data found in the literature. The parameter values which were found in the literature all represent decay rates of certain variables or delays in certain biological processes. These processes are defined and their

Parameter	Range of Values	Unit	Reference
Delay for Viral Production (τ_V)	$8-12$	h	[1, 40, 71]
Virus Decay rate (d_V)	$1/3-2$	h^{-1}	[1]
Infected Cell Decay Rate (d_Y)	$1/48-0.2$	h^{-1}	[1, 12]
Delay for IFN Production (τ_I)	$4-8$	h	[40, 72]
Delay for IFN Production by CTLs (τ_{T_EI})	5	h	[61]
IFN Decay Rate (d_I)	$0.1-0.7$	h^{-1}	[40, 73]
Delay for T-Cell Production (τ_{T_E})	$72-120$	h	[1, 13, 25]
Effector B-Cell Decay Rate (d_{B_E})	$1/120-1/72$	h^{-1}	[35]
Ab Decay Rate (d_A)	$0.04/24$	h^{-1}	[74]

Table 2.3: *Ranges of Parameter Values Found in the Literature.*

values are stated in Table 2.3. Within these ranges the parameters were chosen to obtain the appropriate time-courses for all variables. The chosen parameter values are stated in Table 2.4. Other parameters were computed from known parameter values. These parameter values are found in Table 2.5. Some parameters were subject to constraints resulting from steady state values, linearization constraints, or from other parameter values. The parameters were estimated based on these constraints and the parameter values subject to constraints are found in Table 2.6. The remaining parameters are free and were chosen to best approximate infection time-courses for all variables. These parameter values are found in Table 2.7.

More generally, parameter values were determined in three phases, which are closely linked to the infection phases defined in the model (2.1.1) and detailed in Section 2.1: (1) infection occurs and the innate immune system is activated, (2) the adaptive immune system is activated, and (3) the infection is cleared (post-infection phase). This methodology capitalizes on the complementary action of the innate and adaptive immune responses. Indeed, as presented in Section 1.1, the innate immune response controls the initial growth of the infection, including when the adaptive immune system has not been activated yet, while the adaptive immune response governs the elimination of the infection. Thus, we can determine the parameters which pertain to the innate immune system, i.e. parameters which appear in (2.1.3a)-(2.1.3e), first, to have peak time and value of viral and innate immune system components V, X, Y, and I, as defined in Tables 1.1 and 1.2, respectively. The peak of R is determined by the peak of I (see (2.1.1d)). Once all parameters which appear in (2.1.3a)-(2.1.3e) have been fixed, we can determine parameters that regulate adaptive immune dynamics during the infection (excluding immunological memory components T_M and B_{LL}). The parameters included in this category are all of the parameters in

Parameter	Value	Unit
τ_V	8	h
d_V	1.0	h^{-1}
d_Y	$5.55 \cdot 10^{-2}$ *	h^{-1}
τ_I	6	h
$\tau_{T_E I}$	5	h
d_I	0.675	h^{-1}
τ_{T_E}	72	h
d_{B_E}	0.01	h^{-1}
d_A	$1.67 \cdot 10^{-3}$ *	h^{-1}

Table 2.4: *Chosen parameter values from ranges found in the literature for numerical simulations of (2.1.1). The values with a * are stated to three significant figures but the simulations use the values with full precision to obtain the correct steady state values.*

the full model (2.1.1) not already determined, with the exception of $k_{B_{LL}}$ and $k_{T_M Y}$. The last two parameter values, pertaining to immunological memory components, are determined in the last phase which relates to post-infection equilibria. Similar methodology was used in [8] to determine parameter values in two phases, representing the innate and adaptive immune responses, respectively.

Below, we present parameter value derivations, for the parameters which are subject to constraints or which are computed from other parameters. The parameters a presented in the order in which they appear in the full system (see (2.1.1a)-(2.1.1k)).

In Section 2.2.2, the linearization of the innate immune response model about the disease-free steady state supposes

$$n > 1. \tag{2.3.18}$$

This constraint was used to estimate n.

Moreover, it is assumed the regeneration of cells in the lungs occurs over a period of three to four weeks [70]. d_X, the decay rate of target cells was chosen so that X returns to steady state in that time period. From the estimated decay rate of healthy cells, we can estimate the proliferation rate of these cells. In fact, at steady state, we have

$$X^* = \frac{\mu}{d_X} \implies \mu = X^* d_X = \log_{10}(5.25 \cdot 10^9) \cdot 2.725 \approx 26.4. \tag{2.3.19}$$

We assume that the decay rate of recovered cells is the same as that of susceptible cells because we assume these cells are not impacted by the infection but they are still subject to

other biological factors that lead to decay, as are healthy cells. That is, we have

$$d_R = d_X. \tag{2.3.20}$$

From the range in Table 2.3, d_Y was estimated to be

$$d_Y = \frac{1}{18}. \tag{2.3.21}$$

To have positivity of the disease-free equilibrium defined in (2.2.44), specifically to have, $I^* > 0$, we need (2.2.26) to hold, i.e.

$$k_2 \leq \frac{b_2}{d_I}. \tag{2.3.22}$$

This constraint was used to estimate k_2.

Around 8 days after the beginning of the infection, a much higher proportion of CD8+ T cells produce IFN compared to than CD4+ T cells [31]. To model this, we have

$$k_{T_H I} \ll k_{T_E I} \implies k_{T_H I} \ll 0.05 \tag{2.3.23}$$

where $k_{T_E I} = 0.05$ was estimated.

T-cell and B-cell proliferation only begins once the infection has crossed a certain threshold which has previously been defined as 1% of the maximal viral titer [13]. So we have

$$V_T = \log_{10}(0.01 \cdot 10^6) = \log_{10}(10^4) = 4. \tag{2.3.24}$$

During the infection, the growth of CD8+ T cells T_E is limited by the number of memory cells T_M. We define the maximum T-cell population to be the peak of the T-cell response when an adult already has some levels of immunity which gives

$$T_{TOT} = T_E(t_{PEAK}) = \log_{10}(5.2 \cdot 10^4) \approx 4.71 \tag{2.3.25}$$

where $T_E(t_{PEAK})$ was chosen from the range in Table 1.2. As an individual is reinfected, the number of memory T cells will increase and the proliferation of CD8+ T cells will be constrained by (2.3.25). The average proliferation (p) rate of naive and effector CD8+ T cells is $p = 0.002$ d^{-1} [65]. At homeostasis, this the proliferation rate is the same as the death rate d_{T_E}. During an infection the proliferation rate increases greatly, as described in (2.1.1g) but it is assumed the decay rate representing natural cell death and exit from the

Parameter	Value	Unit	Reference
μ	$26.5*$	$\log_{10}(\text{cells})\cdot\text{h}^{-1}$	(2.3.19)
d_R	2.725	h^{-1}	(2.3.20)
V_T	$\log_{10}(10^4)$	$\log_{10}(\text{TCID}_{50})$	(2.3.24)
T_{TOT}	$4.71*$	$\log_{10}(cells)$	(2.3.25)
d_{T_E}	$8.33\cdot10^{-5}*$	h^{-1}	(2.3.26)
k_{T_M}	$1.40\cdot10^{-3}*$	h^{-1}	(2.3.29)
d_{T_Epi}	$1.26\cdot10^{-2}*$	h^{-1}	(2.3.30)
$k_{B_{LL}A}$	$1.26\cdot10^{-3}*$	$\log_{10}(\text{pg}\cdot\text{mL}^{-1})[\log_{10}(\text{cells}\cdot\mu\text{L}^{-1})\cdot\text{h}]^{-1}$	(2.3.16)
k_{B_EA}	$2.62\cdot10^{-3}*$	$\log_{10}(\text{pg}\cdot\text{mL}^{-1})[\text{h}]^{-1}$	(2.3.34)

Table 2.5: *Computed parameter values for numerical simulations of* (2.1.1)*. The values with a $*$ are stated to three significant figures but the simulations use the stated formulas to compute them to full precision to obtain the correct steady state values.*

blood does not. From this, we obtain

$$d_{T_E} = p \implies d_{T_E} = 8.33\cdot10^{-5}\,\text{h}^{-1}. \tag{2.3.26}$$

At their peak proliferation rates, CD8+ T cells proliferate and expand at a rate faster than CD4+ T cells [65, 66]. The production rates of CD8+ T cells and CD4+ T cells were estimated to produce this behavior, which results in

$$k_{T_H} = 3.765\cdot10^{-3}\,[\log_{10}(\text{pg}\cdot\text{mL}^{-1})\cdot\text{h}]^{-1}. \tag{2.3.27}$$

CD4 + T cells also decay faster than CD8+ T cells so from (2.3.26) have that

$$d_{T_H} > \frac{0.002}{24}\,\text{h}^{-1}. \tag{2.3.28}$$

Post-infection, the effector CD8+ T-cell population contracts and over the course of two to three weeks (336 to 504 hours), 5% to 10% of CTLs become memory T-cells. It is assumed the 90%-95% of T cells who die do so over the same period. From the peak value for CD8+ T cells in Table 1.2, the post-infection CTL disappearance rate is

$$\frac{\log_{10}(5.2\cdot10^4)}{504} \le k_{T_M} + d_{T_Epi} \le \frac{\log_{10}(5.2\cdot10^4)}{336}.$$

Assuming 10% of CTLs become memory T cells and 90% of CTLs die, we obtain

$$0.1\cdot\frac{\log_{10}(5.2\cdot10^4)}{504} \le k_{T_M} \le 0.1\cdot\frac{\log_{10}(5.2\cdot10^4)}{336}$$

Parameter	Value	Unit	Reference
n	1.775	Unitless	(2.3.18)
k_2	$8 \cdot 10^{-1}$	$\log_{10}(\text{pg} \cdot \text{mL}^{-1})$	(2.3.22)
$k_{T_H I}$	$3 \cdot 10^{-3}$	$[\log_{10}(\text{cells}) \cdot \text{h}]^{-1}$	(2.3.23)
k_{T_H}	$3.765 \cdot 10^{-3}$	$[\log_{10}(\text{pg} \cdot \text{mL}^{-1}) \cdot \text{h}]^{-1}$	(2.3.27)
d_{T_H}	$6 \cdot 10^{-3}$	h^{-1}	(2.3.28)
$k_{T_M Y}$	$6.580050090 \cdot 10^{-5}$	$[\log_{10}(\text{cells}) \cdot \text{h}]^{-1}$	(2.3.31)
$k_{B_{LL}}$	$1.758133200 \cdot 10^{-3}$	$[\log_{10}(\text{TCID}_{50} \cdot \text{mL}^{-1}) \cdot \text{h}]^{-1}$	(2.3.32)
$\tau_{B_{LL}}$	10	h	(2.3.35)
$\tau_{B_{LL}V}$	8	h	(2.3.36)

Table 2.6: *Estimated parameter values for numerical simulations of* (2.1.1) *subject to constraints stated to their precision*

$$0.90 \cdot \frac{\log_{10}(5.2 \cdot 10^4)}{504} \leq d_{T_E pi} \leq 0.90 \cdot \frac{\log_{10}(5.2 \cdot 10^4)}{336}.$$

The values used are

$$k_{T_M} = 0.1 \cdot \frac{\log_{10}(5.2 \cdot 10^4)}{336} \approx 1.40 \cdot 10^{-3}\,\text{h}^{-1} \tag{2.3.29}$$

$$d_{T_E pi} = 0.90 \cdot \frac{\log_{10}(5.2 \cdot 10^4)}{336} \approx 1.26 \cdot 10^{-2}\,\text{h}^{-1}. \tag{2.3.30}$$

T_M decreases slightly during the course of the infection as memory T cells regain effector functions, but is boosted post-infection until is reaches steady state.The steady state value T_M^* is not uniquely defined in the steady state expression (2.2.45), but we want numerical simulations to converge to the value defined in (2.3.11). The only remaining free parameter in (2.1.1h) is $k_{T_M Y}$. Thus, $k_{T_M Y}$ was chosen so that T_M^* reaches the steady state determined in (2.3.11), within the tolerance (10^{-9}). The value

$$k_{T_M Y} = 6.580050090 \cdot 10^{-5}\,[\log_{10}(\text{cells}) \cdot \text{h}]^{-1} \tag{2.3.31}$$

was tuned using a decision tree-based search.

Similarly, the steady state value B_{LL}^* is not uniquely defined in the steady state expression (2.2.45), but we want numerical simulations to converge to the value defined in (2.3.17). The value of the parameter $k_{B_{LL}}$ was estimated using the same method as for (2.3.31) to obtain the steady state value derived in (2.3.17):

$$k_{B_{LL}} = 1.758133200 \cdot 10^{-3}\,[\log_{10}(\text{TCID}_{50} \cdot \text{mL}^{-1}) \cdot \text{h}]^{-1}. \tag{2.3.32}$$

From this, we also obtain the correct steady state value A^*. The peak of $A(t)$ is determined by the production rates $k_{B_{LL}A}$ (defined in (2.3.16)) and k_{B_EA}. Long-lived B cells produce higher-affinity antibody than short-lived, effector B cells. Because this model only includes a single population of antibody A which binds to virus at a constant rate defined by ρ_A and ρ_V, we assume that the ratio of the production rates $k_{B_{LL}A}$ and k_{B_EA} is the same as that of the highest-affinity antibodies to the lowest-affinity antibodies. The antibody binding rates range from 25% to 52% [18].That means

$$\frac{k_{B_{LL}A}}{k_{B_EA}} = \frac{0.52}{0.25} \tag{2.3.33}$$

$$\implies k_{B_EA} = \frac{0.52}{0.25} \cdot k_{B_{LL}A} \approx 2.08 \cdot 1.26 \cdot 10^{-3} \approx 2.62 \cdot 10^{-3}. \tag{2.3.34}$$

Moreover, B-cell proliferation and differentiation processes do not occur at the same time. Upon infection, naive B cells differentiate into long-lived B cells slower than they differentiate into effector B cells. Upon reinfection, long-lived B cells re-differentiate into effector B cells much faster than naive B cells differentiate into effector B cells. This leads to the following constraints

$$\tau_{B_{LL}V} < \tau_{B_{LL}} < \tau_{B_E}.$$

τ_{B_E} was chosen to obtain the correct timing of the peak for B_E and was estimated to be 36 h. From this, $\tau_{B_{LL}}$ was estimated and finally from $\tau_{B_{LL}}$, $\tau_{B_{LL}V}$ was estimated, leading to

$$\tau_{B_{LL}} = 10 \text{ h} \tag{2.3.35}$$

$$\tau_{B_{LL}V} = 8 \text{ h}. \tag{2.3.36}$$

2.3.2 *Simulations of the Model*

Numerical simulations of (2.1.1a)-(2.1.1k), using the initial conditions defined in Table 2.1 and parameter values defined in Tables 2.4-2.7 in Section 2.3.1.2 result in the steady state values defined in Table 2.2 in Section 2.3.1.1 and the dynamics shown in Figure 2.10.

Figure 2.10 shows the model (2.1.1a)-(2.1.1k) returning to the disease-free steady state post-infection, from an infection infecting around 50% of the lungs. In this case, all components of the immune system are activated and work normally. This illustrates the case of a healthy individual clearing a relatively strong influenza A infection. If certain parts of the immune system are not activated, for example in the case of immuno-compromised patients, the dynamics can change drastically. Figure 2.11a and 2.11b illustrate the dynamics of the submodels defined in (2.1.2a)-(2.1.2c) and (2.1.3a)-(2.1.3e),

Parameter	Value	Unit
$\tilde{K_1}$	4.25	$\log_{10}(\text{pg} \cdot \text{mL}^{-1})$
k_V	0.755	$\log_{10}(\text{TCID}_{50} \cdot \text{mL}^{-1}) \cdot [\log_{10}(\text{cells}) \cdot \log_{10}(\text{pg} \cdot \text{mL}^{-1}) \cdot \text{h}]^{-1}$
τ_{IV}	5	h
ρ_V	$3 \cdot 10^{-2}$	$[\log_{10}(\text{pg} \cdot \text{mL}^{-1}) \cdot \text{h}]^{-1}$
d_X	2.725	h^{-1}
β	$2.175 \cdot 10^{-2}$	$[\log_{10}(\text{TCID}_{50} \cdot \text{mL}^{-1}) \cdot \text{h}]^{-1}$
k_{IX}	$2.5 \cdot 10^{-1}$	$[\log_{10}(\text{pg} \cdot \text{mL}^{-1}) \cdot \text{h}]^{-1}$
k_{IY}	$3.75 \cdot 10^{-2}$	$[\log_{10}(\text{pg} \cdot \text{mL}^{-1}) \cdot \text{h}]^{-1}$
k_{T_EY}	$5.5 \cdot 10^{-2}$	$[\log_{10}(\text{cells}) \cdot \text{h}]^{-1}$
k_I	$9 \cdot 10^{-2}$	$\log_{10}(\text{pg} \cdot \text{mL}^{-1}) \cdot [\log_{10}(\text{cells}) \cdot \text{h}]^{-1}$
b_2	$1.5 \cdot 10^{-1}$	$\log_{10}(\text{pg} \cdot \text{mL}^{-1}) \cdot \text{h}^{-1}$
τ_2	6	h
k_{T_EI}	$5 \cdot 10^{-2}$	$[\log_{10}(\text{cells}) \cdot \text{h}]^{-1}$
τ_{T_HI}	7	h
k_{T_E}	$1.485 \cdot 10^{-3}$	$[\log_{10}(\text{cells}) \cdot \log_{10}(\text{pg} \cdot \text{mL}^{-1}) \cdot \text{h}]^{-1}$
$k_{B_{LL}V}$	$7.5 \cdot 10^{-4}$	$[\log_{10}(\text{TCID}_{50} \cdot \text{mL}^{-1}) \cdot \text{h}]^{-1}$
k_{B_E}	$2.25 \cdot 10^{-3}$	$[\log_{10}(\text{TCID}_{50} \cdot \text{mL}^{-1}) \cdot \text{h}]^{-1}$
τ_{B_E}	36	h
ρ_A	$5 \cdot 10^{-6}$	$[\log_{10}(\text{TCID}_{50} \cdot \text{mL}^{-1}) \cdot \text{h}]^{-1}$

Table 2.7: *Free parameter values stated to their precision for numerical simulations of* (2.1.1).

respectively.

We can see in Figure 2.11a that without an immune response, the initial viral growth is unbounded and very quickly (in less than 24 hours) the number of infected cells is greater than the initial number of healthy cells, i.e. $Y > X^0$. In this case, with the parameter values defined in Section 2.3.1, R_0, as defined in (2.2.16), is $R_0 \approx 2.87 \gg 1$. This indicates that for these parameter values, an individual with no immune system would die in under 24 hours after infection. Figure 2.11b illustrates a case where only part of the immune system is working: only the innate immune response is activated. This is not sufficient to control the infection, as the number of infected cells still exceeds the initial number of target cells, but it illustrates how effective the innate immune system is, as the number of infected cells is drastically smaller. Moreover, the time it takes for the number of infected cells to exceed the the initial number of target cells is much longer. This is due to the innate immune system significantly inhibiting viral growth, as seen in Figure 2.14, which allows time for the adaptive immune response to kick in, which then controls infection clearance.

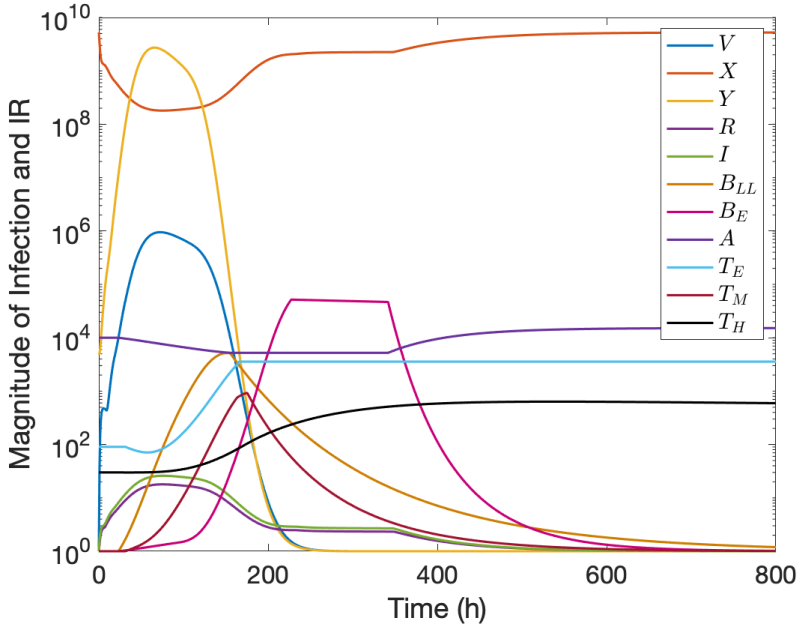

Figure 2.10: *Model simulation of* (2.1.1a)-(2.1.1k) *with default parameter values defined in Tables 2.4-2.7 and initial conditions defined in Table 2.1 in Section 2.3.1.2.*

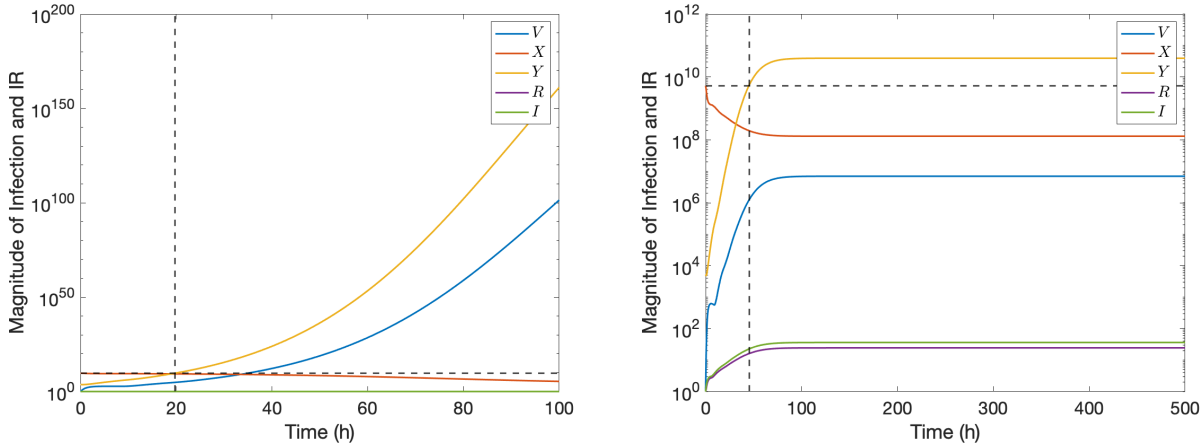

(a) **(b)**

Figure 2.11: *Submodel simulations of* (2.1.1a)-(2.1.1k) *with default parameter values defined in Tables 2.4-2.7 in Section 2.3.1.2, for relevant parameters. The horizontal dashed line indicates the initial number of target cells. If the number of infected cells is greater than the initial number of target cells, the individual has died from the infection. The time at which this occurs is denoted by the vertical dashed line. (a) Model simulation of* (2.1.2a)-(2.1.2c) *with initial conditions* $[V^0, X^0, Y^0] = [0, X^*, \log_{10}(5250)]$. *(b) Model simulation of* (2.1.3a)-(2.1.3e) *with initial conditions* $[V^0, X^0, Y^0, R^0, I^0] = [0, X^*, \log_{10}(5250), 0, 0]$.

Four different scenarios will be studied for the full model defined in (2.1.1a)-(2.1.1k): (1) there is no previous immunity; (2) there is no innate immune system; (3) there is no T-cell compartment; and (4) there is no B-cell compartment. These scenarios are shown in Figure 2.12.

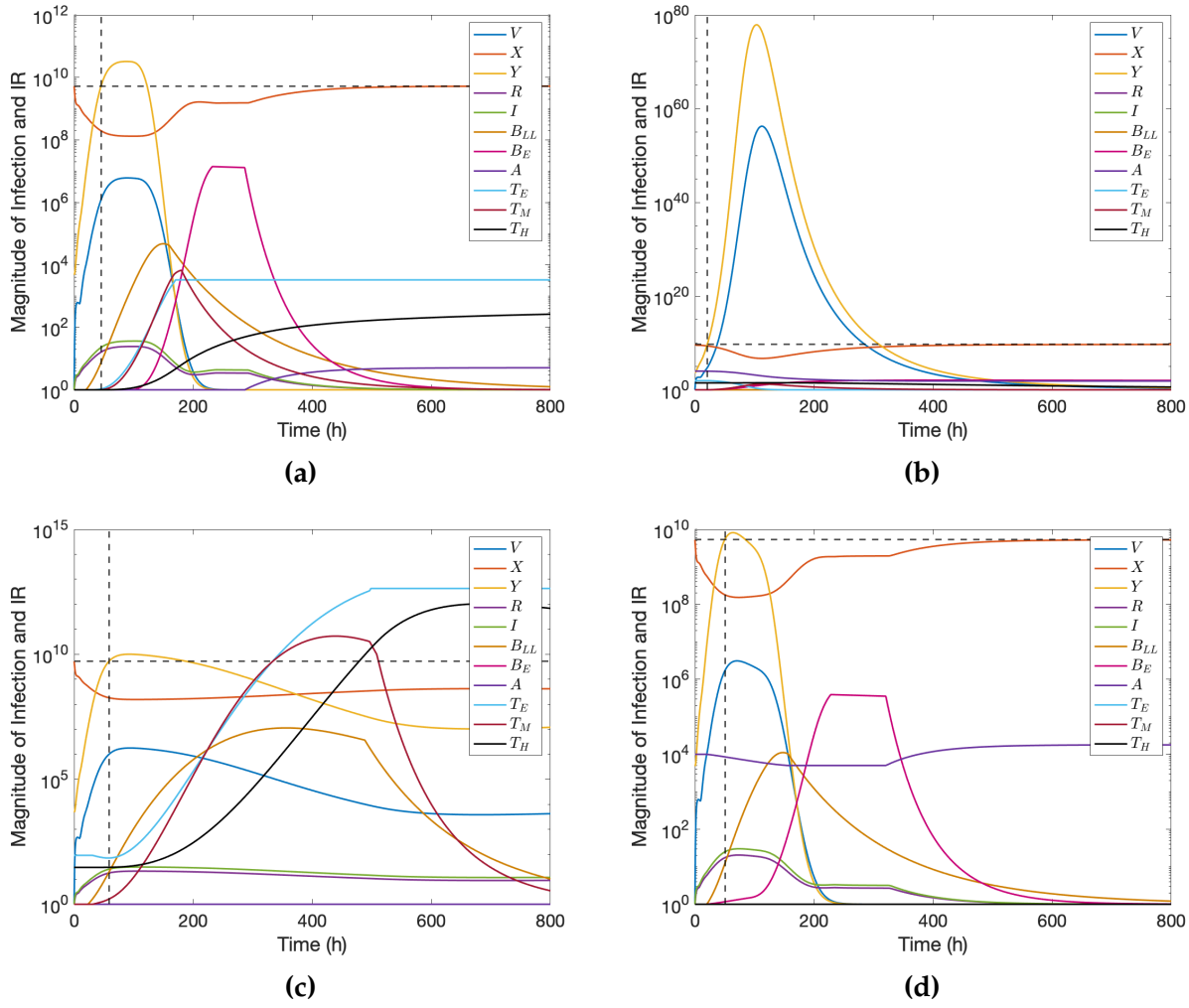

Figure 2.12: *Model Simulation of* (2.1.1a)-(2.1.1k) *with default parameter values defined in Tables 2.4-2.7 in Section 2.3.1.2. The horizontal dashed line indicates the initial number of target cells. If the number of infected cells is greater than the initial number of target cells, the individual has died from the infection. The time at which this occurs is denoted by the vertical dashed line. (a) Full model with no previous immunity. Initial conditions are* $[0; \log_{10}(5.25 \cdot 10^9); \log_{10}(5250); 0; 0; 0; 0; 0; 0; 0; 0;]$. *(b) Model with the adaptive immune response only* ($I = 0$). *Initial conditions defined in Table 2.1. (c) Full model without a T-cell response. Initial conditions defined in Table 2.1, except for* $T_M^0 = 0$. *(d) Full model without a T-cell response. Initial conditions defined in Table 2.1, except for* $B_{LL}^0 = 0$ *and* $A^0 = 0$.

All four panels of Figure 2.12 illustrate the same outcome. In fact in all cases, there is a point where the number of infected cells Y is greater than the initial number of cells in the lungs, i.e. $Y > X^0$. This represents a case where an individual who has

contracted influenza A has died from the disease. Because the model is not target cell limited, new healthy cells are produced at a high rate which makes it possible for there to be more infected cells than there are cells in the lungs. This issue is discussed further in Section 2.3.3. However, Figure 2.10 still illustrates an important fact: the absence of any one of the immune response components leads to an individual dying of the disease. The impacts of each of these components are varied and are discussed below.

As shown in Figure 2.12a, when there is no previous immunity, but all immune system components are activated, the dynamics of the model are quite similar to Figure 2.10 but all short-lived cell populations peak higher, to compensate for the lack of long-lived/memory cells.

As shown in Figure 2.12b, when there is no IFN, virus replication is uninhibited which leas to to extreme virus proliferation and growth in the early stages of the infection. In this case, an individual dies notably faster than in all other cases studied in Figures 2.12a, 2.12c, and 2.12d. The adaptive immune response is activated later on and thus cannot control the infection and prevent it from taking over. In Figure 2.10 as well as all other panels of Figure 2.12, where the IFN compartment is activated, the initial growth rates of the virus are similar. This underscores how crucial IFN and the innate immune system are to control the initial phase of the infection.

As shown in Figure 2.12c, when there are no T cells, B-cell production is increased to compensate for the lack of T cells. Even though, as mentioned previously, IFN allows for control of the early virus growth, the combination of IFN and B-cell action is not enough for the system to converge to a disease-free steady state. This indicates how essential T cells are for clearing a symptomatic infection.

As shown in Figure 2.12d, when there are no B cells or antibody, the dynamics of the model look quite similar to those of the full model shown in Figure 2.10. However, T-cell production is increased to compensate for the lack of B cells.

2.3.3 *Sensitivity Analysis*

The qualitative behavior of the model defined in (2.1.1a)-(2.1.1k) is the same for any constant history function for infected cells Y^0 in the range $[\log_{10} 5.25 \cdot 10^0, \log_{10} 5.25 \cdot 10^6]$. This represents an initial infected cell population ranging from five infected cells to 1% of the peak number of infected cells. As shown in Figure 2.13a, when the initial number of infected cells is lower, peak viral titers occur at around 115 hours post-infection (4.8 days post-infection) compared to around 72 hours post-infection (3 days post-infection) in the full model shown in Figure 2.10. Peak viral titers are the same for both the simulations shown in Figures 2.13a and 2.10. Similar time courses as those shown in Figure 2.13a

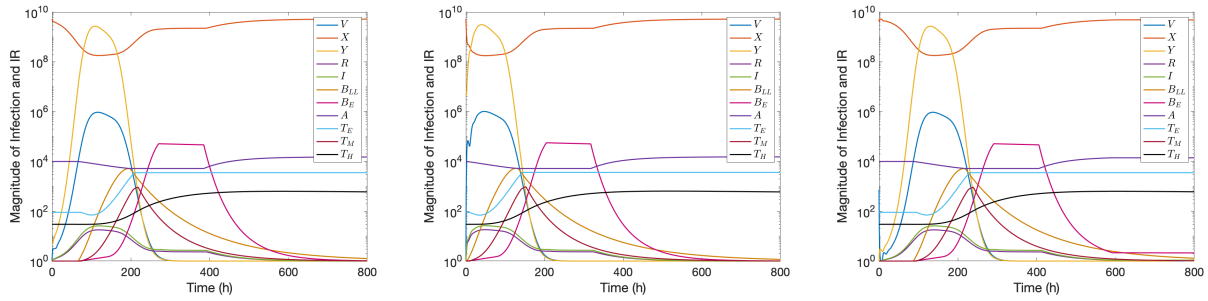

(a) **(b)** **(c)**

Figure 2.13: *Model Simulation of* (2.1.1a)-(2.1.1k) *with default parameter values defined in Tables 2.4-2.7 in Section 2.3.1.2. (a) Initial conditions are defined in Table 2.1, except for* $Y^0 = \log_{10}(5.25 \cdot 10^0)$*. (b) Initial conditions are defined in Table 2.1, except for* $Y^0 = \log_{10}(5.25 \cdot 10^6)$*. (c) Initial conditions are defined in Table 2.1, except for* $V^0 = \log_{10}(7.5 \cdot 10^2)$ *and* $Y^0 = 0$*.*

are obtained for $Y^0 = 1$. In Figure 2.13b, when the initial number of infected cells is greater, viral titers peak at around 46 hours post-infection (1.9 days post-infection) and the peak value of viral titers is around 8% greater. These peaks all occur within the physiologically realistic ranges given for viral titers (see Table 1.1 and 1.2) so this model does not discriminate between different initial quantities of infected cells. However, it probably would have been more realistic to model the system (2.1.1a)-(2.1.1k) with a non-constant number of infected cells for the history function. Moreover, Figure 2.13c illustrates model dynamics when the perturbation from steady state comes from having the initial number of infected cells $Y^0 = 0$ and having a non-zero V^0, i.e. the infection is introduced into the body through free virus instead of infected cells. The initial value used was $V^0 = \log_{10}(7.5 \cdot 10^2) < V_T$ [1]. This scenario is more realistic, because cells cannot become infected without healthy cells first coming into contact with virions. In this case, the viral titers peak at the same point as in Figure 2.10 but the peak occurs much later. Indeed, in Figure 2.13c viral titers peak at around 136 hours post-infection (5.6 days post-infection) which is outside the physiologically realistic ranges given for viral titers (see Table 1.1). The qualitative dynamics remain the same.

In all cases shown in Figures 2.11 and 2.10, the strength of the infection plays a huge role on what components are sufficient and necessary to control an infection. We can consider 2 parameters as defining the strength of the infection: β, the contact rate between healthy cells X and free virus V, which is a measure of infectiousness, and k_V the viral proliferation/replication rate. The infection is weaker for smaller values of β and k_V so very small values of β and k_V result in low-dose infections, which, as mentioned in Section 1.2, can be entirely controlled by the innate immune system. Similarly, greater values of β and k_V result in a stronger infection. Ideally, the combined action of the innate

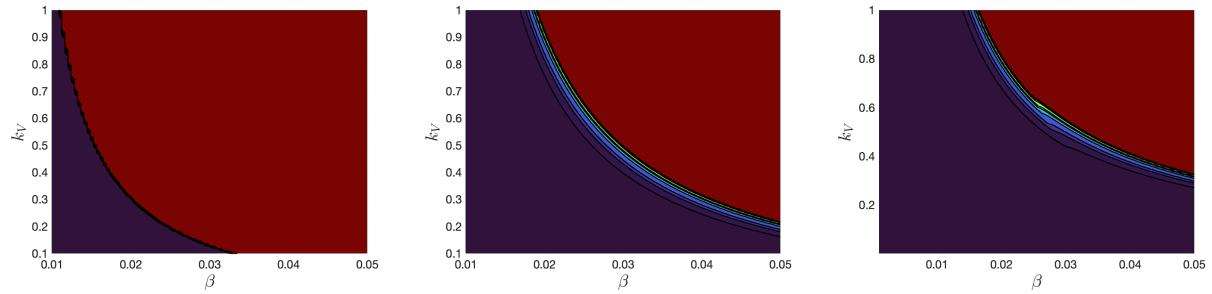

(a) **(b)** **(c)**

Figure 2.14: *Infection outcomes for various infection strengths with default parameter values defined in Tables 2.4-2.7 in Section 2.3.1.2, except for β and k_V. Purple indicates the maximum number of infected cells is <1% of total number of target cells X^0. Red indicates maximum number of infected cells is 100% of total number of target cells X^0. (a) Model (2.1.2a)-(2.1.2c) with initial conditions $[V^0, X^0, Y^0] = [0, X^*, \log_{10}(5250)]$. (b) Model (2.1.3a)-(2.1.3e) with initial conditions $[V^0, X^0, Y^0, R^0, I^0] = [0, X^*, \log_{10}(5250), 0, 0]$. (c) Model (2.1.1a)-(2.1.1k) with initial conditions defined in Table 2.1.*

and adaptive immune responses is able to fight off relatively strong infections. In this case, we are interested in how strong the infection can be, i.e. how big β and k_V can be, and still have the infection be controlled by the immune response. We consider that an infection is controlled by the immune response if less than 100% of the initial number of target cells are infected. Figure 2.14 and Figure 2.15 show the impact of different infection strengths on the ability of the immune response to control an infection. Figure 2.15 was generated using a 100x100 mesh of parameter values for β and k_V. Figure 2.15 was generated using a 20x20 mesh of parameter values for β and k_V, due to computational time. Increasing the number of mesh points would yield a figure with better resolution. Moreover, Figures 2.14 and 2.15 were generated using a relatively narrow range of β values because the model is especially sensitive to this parameter.

Figure 2.14a shows that when there is no immune system, the infection is either extremely small (<1% of cells are infected) or kills the individual (100% of initial target cells become infected). Figure 2.14b shows that the innate immune response has a massive impact on the outcome of the infection. Indeed, in this case, much stronger infections, i.e. infections with greater k_V and β, result in subclinical infections, that is infections that are entirely controlled by the innate immune system. Figure 2.14b illustrates that the inclusion of the adaptive immune response results in subclinical infections for even greater values of k_V and β. The combined action of innate and adaptive immune responses results in control of higher dose infections, though the acceptable increase in k_V and β is markedly smaller. Indeed, the contrast between Figures 2.14a and 2.14b is greater than that between Figures 2.14b and 2.14c. This indicates that the innate immune response is absolutely

crucial in controlling infection growth and while the addition of the adaptive immune response does have an impact, it does not allow for control of substantially greater dose infections, when compared to the innate immune response.

The maximum number of infected cells is not an adequate measure of the adaptive immune response's impact on the evolution of a flu infection, but the maximum number of infected cells provides a comprehensive view of adaptive immune dynamics, as shown in Figure 2.15.

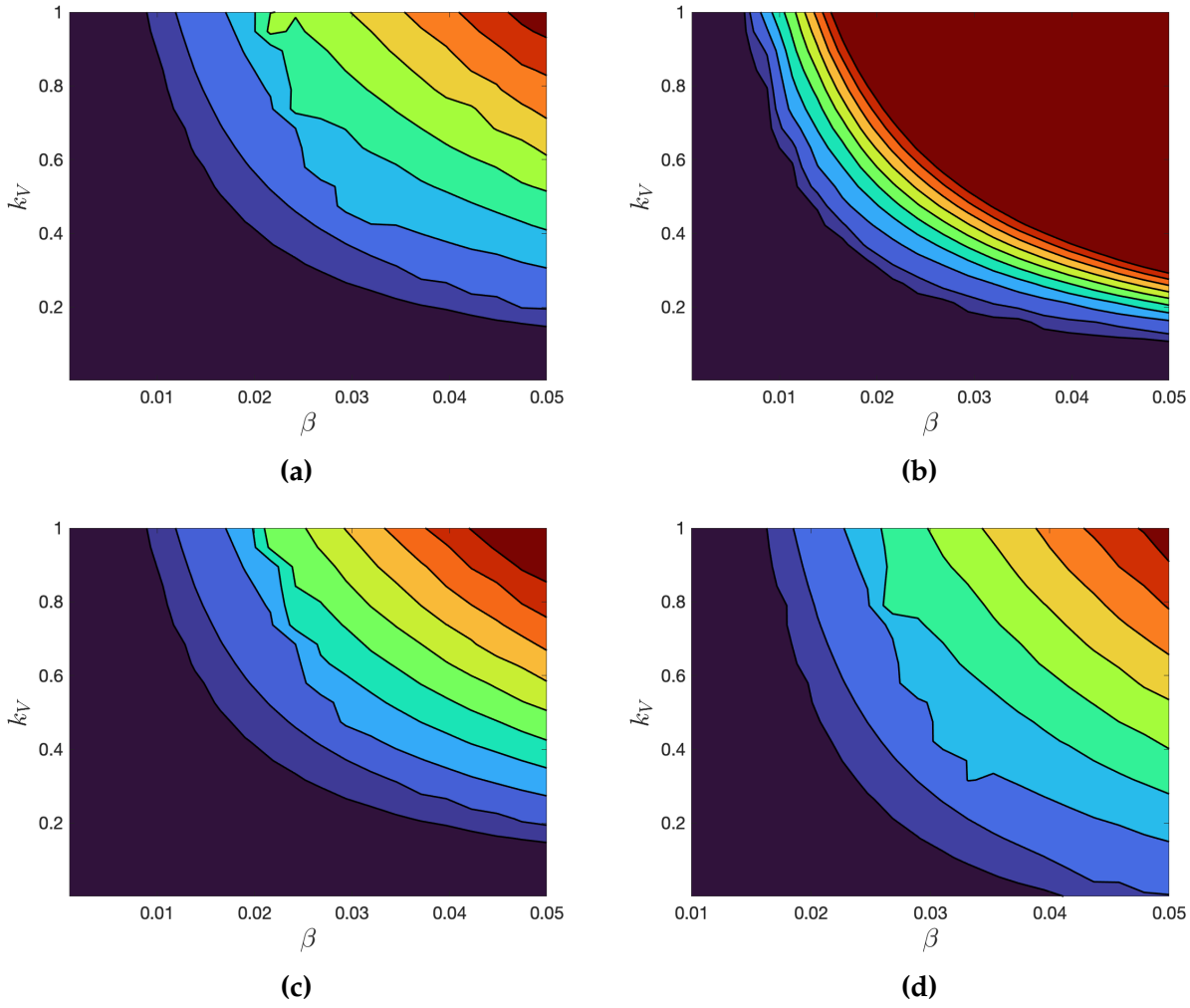

Figure 2.15: *Total number of cells infected for various infection strengths with default parameter values defined in Tables 2.4-2.7 in Section 2.3.1.2, except for β and k_V. (a) Full model. Initial conditions defined in Table 2.1. (b) Model with the adaptive immune response only ($I = 0$). Initial conditions defined in Table 2.1. (c) Full model without a T-cell response. Initial conditions defined in Table 2.1, except for $T_M^0 = 0$. (d) Full model without a B-cell response. Initial conditions defined in Table 2.1, except for $B_{LL}^0 = 0$ and $A^0 = 0$.*

In (2.1.1a), the decay of free virus is driven by

$$\dot{V}(t) = -d_V V(t) - \rho_V A(t) V(t) \tag{2.3.37}$$

and in (2.1.1c), the decay of infected cells is driven by

$$\dot{Y}(t) = -k_{IY} I(t) Y(t) - d_Y Y(t) - k_{T_E Y} Y(t) T_E(t). \tag{2.3.38}$$

In (2.3.37), for physiologically realistic parameter values, A is bounded, i.e. $A(t)$ reaches a maximum during the course of the infection. In this case, the decay of V is

$$\dot{V}(t) = -d_V V(t) - \rho_V A(t) V(t) \leq -d_V V(t) - \rho_V \max\{A(t)\} V(t). \tag{2.3.39}$$

Similarly, in (2.3.38), T_E bounded, as defined in (2.1.1g) and for physiologically realistic parameter values I is bounded, i.e. $I(t)$ reaches a maximum during the course of the infection. In this case, the decay of Y is

$$\dot{Y}(t) = -k_{IY} \max\{I(t)\} Y(t) - d_Y Y(t) - k_{T_E Y} Y(t) T_{TOT}. \tag{2.3.40}$$

From (2.3.39) and (2.3.40), we have that both the infected cells and the free virus population decay exponentially and do not reach 0, their disease-free steady state value, in finite time. This means that the infection is never completely resolved. Moreover, in some cases, a new infection arises from a very small number of infected cells. In reality, once the number of infected cells is low enough, the infection always die out in finite time because it is not possible to have a number of infected cells or free virions < 1. To circumvent this issue in my simulations, a tolerance value is used to manually set Y to zero if it is below a certain tolerance. Forcing $Y = 0$ for $Y <$ `tol` means that a new infection will never occur once the primary infection has been cleared, unless a new perturbation is introduced into the system.

The value of the tolerance used to determine when an infection has been cleared, for any value < 1 does not impact the infection time-course of any variable, except for T_E and T_M. Indeed, all other variables are very close to their steady state value defined in (2.2.45) before the infection is completely cleared (between 200 and 400 hours in Figure 2.10) and forcing $Y = 0$ when it is below a certain tolerance does not impact the dynamics for these variables. However, T_E clearance and T_M production occur post-infection, denoted $(1 - \mathbb{1}_{Y(t)})$ in (2.1.1g) and (2.1.1h). This is equivalent to saying these processes only occur when $Y = 0$. In this case, these processes are initiated at the precise time t at which $Y(t) = 0$. If we increase the tolerance, T_E cell clearance will start earlier; if we decrease the tolerance, T_E cell clearance will start later. The time it takes for T_E and T_M to reach

their steady state values, as defined in (2.2.45), does not visibly change because during the infection, the decay of T_E is entirely described by the term $-d_{T_E}T_E(t)$ in (2.1.1g), where d_{T_E} is very small (see Table 2.5) and there is no production of T_M.

The choice of tolerance allows us to precisely determine the timing of effector T-cell decay. Moreover, because the number of memory T-cell is dependent on the number of effector T cells present at the end of the infection, as described (2.3.6), the choice of tolerance determines precisely the value of the parameter k_{T_MY}, defined in (2.3.31), which uniquely determines the steady state value T_M^*. Current experimental data estimates the decay occurs two to three weeks post-infection, as presented in Section 1.3, but if additional experimental data was available, time courses for T_E and T_M post-infection could be tuned by adjusting the tolerance. In this case $5 \cdot 10^{-5}$ was chosen.

2.3.3.1 *Discussion on Parameter Values*

From a public health or medical perspective, one of the goals of mathematical modeling of within-host infections is to produce "transmissibility" or "virulence" as readouts of the model to quantify these phenomena and improve outcomes. One step we can make in this direction is having physiologically relevant parameters, both conceptually and numerically. The parameters presented in Section 2.3.1 have conceptual biological meanings but their values are often defined in units that cannot be expressed in biologically meaningful values. This does not allow for an easy intuitive understanding of these parameters and can impede understanding of their influence on immune dynamics. For example, many parameters, including β which represents the contact rate between target cells X and free virus V and is used as a measure disease "infectiousness", are in units of $[\log_{10}(\text{TCID}_{50} \cdot \text{mL}^{-1}) \cdot \text{h}]^{-1}$, which are not intuitively meaningful and thus do not provide an easily transferable measure of "infectiousness", which could be used to compare various strains across models. This problem has occurred in many other models [8, 37].

As mentioned when discussing Figure 2.12, the model is not target-cell limited and so when the infection is not controlled by the immune system, the number of infected cells can proliferate to a point where $Y > X^0$, i.e. the number of infected cells is greater than the number of cells in the lungs (the initial number of target cells at any disease-free steady state defined in (2.2.44)). In a target-cell limited model, if the number of infected cells is equal to the number of cells in the lungs, i.e. $Y = X^0$, then the individual has died. We can interpret $Y = X^0$ in the model defined in (2.1.1a)-(2.1.1k) in the same way and consider that the dynamics that occur after the threshold $Y > X^0$ is crossed do not represent physiologically realistic infection time courses. This still allows for the study of the impact of different components, compartments and parameters of the model and a measure of

their relative contribution to controlling the infection, as discussed in Section 2.3.2.

The issue arises because the healthy target cell compartment X has an artificially high cell turnover rate, which means there are constantly new cells produced and free to be infected. In fact, from d_X, we can estimate the half-life of lung epithelial cells which is time it would take for the cell population to halve in size if there were no proliferation [65]. We have

$$\text{half-life}_X = \frac{\ln(2)}{d_X} = \frac{\ln(2)}{2.725} \approx 0.25 \text{ h}.$$

Experimentally the half-life of epithelial cells in the lungs was found to be 17 months or approximately 12240 hours [75]. This extreme difference is due to the fact that d_X was estimated to have X return to the disease-free steady state (2.2.44) in 3 to 4 weeks, as is biologically the case. Moreover, the decay rate of infected cells d_Y, defined in (2.3.21), is much lower than that of healthy cells, which is unrealistic. Similar issues have arisen in previous models of influenza, including target-cell limited models. For example, in many target-cell limited models, the growth of infected cells and viral titers is correctly estimated because it is constrained by the number of target cells to model the rapid decrease of viral titers post-peak, the viral decay parameter is over-estimated [11].

The delays τ_{T_E} and τ_{B_E}, which determine delay before effector T-cell and effector B-cell production, respectively, determine the time at which these cell populations peak during an infection. As such, the model is very sensitive to these delays, and the values presented in Tables 2.3 and 2.7, respectively, were chosen to obtain the correct peaks.

It would be interesting to perform a more thorough sensitivity analysis, particularly with regards to global sensitivity of the model and the contributions of the non-linear terms.Aen

CHAPTER 3

MODELING OF REINFECTION AND VACCINATION

In Chapter 2, a within-host model of influenza A infections was developed. Equation (2.1.1) includes three variables responsible for long-term immunity: memory T cells T_M, long-lived B cells B_{LL}, and antibody A. As opposed to other immune components, these cell populations do not die out at the end of the primary infection but are maintained, even in the absence of viral antigen, and allow for a more rapid immune response in the event of reinfections (called secondary, tertiary, etc., infections) [3, 10, 18, 30]. In this chapter, we will study the impact of these cell compartments on reinfection time-courses. In Section 3.1, a framework to model reinfections will be developed, taking into account the various factors which influence immunological memory: the similarity between infections, the type of exposure to the virus, the time interval between exposures, and the season during which the exposure occurs. These factors will be discussed in Sections 3.1.1, 3.1.2, 3.1.3, and 3.1.4, respectively. Numerical simulations will be performed and presented in Section 3.2. The impact of sex on infections and reinfections will be discussed in Section 3.3.

3.1 REINFECTION MODELING

Influenza is an acute infection, with infection time-courses described by (2.1.1) occurring over a short period of time (a few weeks to a month), as shown in Figure 2.10. Months or even years might go by before an individual is re-exposed to an influenza virus, a time during which immune cell populations will evolve. There are thus multiple time scales to consider when developing a framework to model reinfections: infection dynamics are fast and inter-infection dynamics are slow. The model (2.1.1) does not describe the slow dynamics that govern the evolution of immune cell populations in between infections. In between infections, (2.1.1) is at the disease-free steady state defined in (2.2.45).

When an individual is re-exposed to influenza after a primary infection, recall of previously acquired immune memory induces a quick immune response dependent on memory T cells T_M, long-lived B cells B_{LL}, and antibody A, which are non-zero at the disease-free equilibrium defined in (2.2.45). After each infection, T_M, B_{LL}, and A levels are boosted. This is illustrated in Figure 3.1, for T_M specifically but is similar for antibody and long-lived B cells. In Chapter 2, the initial condition and steady state value of memory T cells are denoted T_M^0 and T_M^*, respectively. In this chapter, we will write $T_{M,i}^0$ to denote the

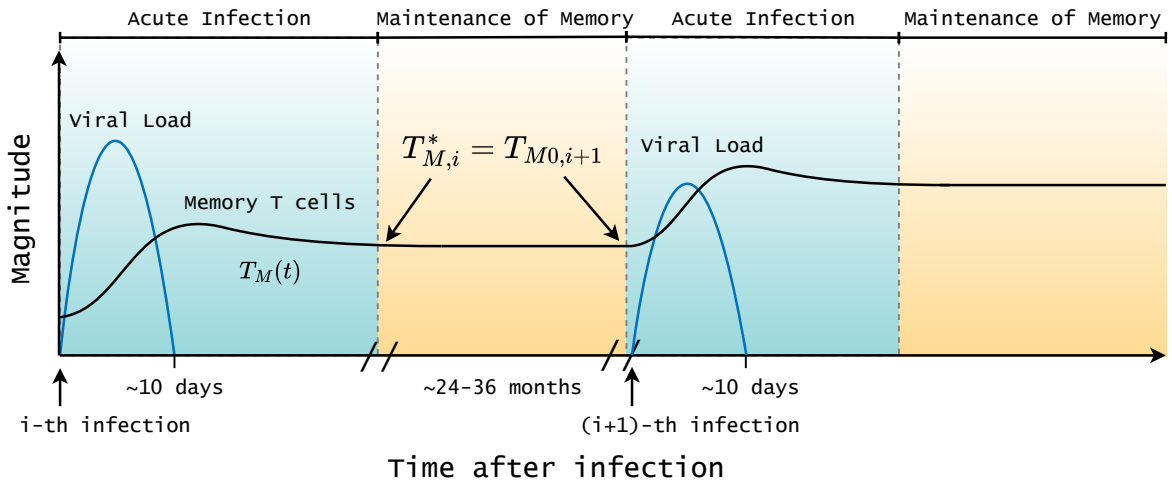

Figure 3.1: *Memory T-cell Evolution during and between Infections.*

initial population of memory T cells for the i-th infection and $T^*_{M,i}$ to denote the steady state value of memory T cells after the i-th infection, and similarly for other variables. We define the i-th infection as starting at time $t_i = 0$. Because the system (2.1.1) is at steady state in between infections, we would have

$$T^0_{M,i+1} = T^*_{M,i} \tag{3.1.1}$$

$$B^0_{LL,i+1} = B^*_{LL,i} \tag{3.1.2}$$

$$A^0_{i+1} = A^*_i, \tag{3.1.3}$$

as shown in Figure 3.1 for T_M. However, in between infections, there are variations in these cell populations, which are not explicitly modeled in (2.1.1). As such, for every reinfection $i+1$, the initial conditions will be calculated from the steady state values of infection i, i.e. $T^*_{M,i}$, $B^*_{LL,i}$, and A^*_i. The explicit expressions for these initial conditions will be derived in Sections 3.1.1-3.1.3 and stated in Section 3.2.

The number of healthy, target cells returns to its initial (unique) steady state value, so we have

$$X^0_{i+1} = X^*_i = X^0_i = \cdots = X^0_1 = X^0. \tag{3.1.4}$$

where X^0 denotes the initial condition of the primary infection, which is defined in Table 2.1. As shown in Figure 2.13 in Section 2.3.3, the initial number of infected cells Y^0 does not have a strong impact on the model dynamics. Consequently, this number will be

taken to be constant for every infection and reinfection, i.e.

$$Y_{i+1}^0 = Y_i^0 = \cdots = Y_1^0 = Y^0 \tag{3.1.5}$$

where Y^0 denotes the initial condition of the primary infection, which is defined in Table 2.1.

The mechanisms that explain how various factors impact memory T-cell and antibody populations have been studied, and will be described in the following sections, to develop a framework for modeling reinfections. Then, these processes and their impact on memory T cells and antibody levels will be quantified to obtain values to numerically simulate various reinfection scenarios. However, as mentioned in Section 1.3, the many mechanisms that influence the persistence long-lived B cells B_{LL} are not well understood [10, 18, 35]. As such, the impact of various factors on immunological memory resulting from B-cell populations is hard to quantify. To quantify B-cell concentrations, we will consider that every reinfection begins at a disease-free steady state (2.2.45). In this case, (2.2.43) must be satisfied and rewriting this expression as

$$B_{LL,i}^* = \frac{d_A A_i^*}{k_{B_{LL}A}}, \tag{3.1.6}$$

we can compute $B_{LL,i}^*$ from A_i^*.

Many questions relating to various immune cell populations are of interest when modeling reinfections. Studies have suggested that if preexisting antibody levels are high enough, a secondary infection will not trigger a short-lived adaptive immune response effector T cells and B cells because virus will be controlled and cleared by memory cell populations and innate defenses, which is known as sterilizing immunity [3, 30]. It has also been shown that immunological memory could reduce the magnitude and the severity of the infection by limiting pathogen replication such that the infection results only in mild disease, which is known as protective immunity [30, 76, 77]. For influenza, neither natural infections nor vaccination result in sterilizing or protective immunity, owing to virus mutations [78]. In this case, immunological memory components can lead to faster control of infection growth than the primary response, i.e. can memory and long-lived immune cells reduce peak viral loads and the duration of the infection, which is known as immunoattenuation [30, 78]. However, the effect of immunity in preventing influenza infection versus attenuating illness, and correlates of protection, i.e. measurable signs that a person is immune, are not well characterized [78]. To the best of my knowledge, these are still open questions in immunology and more specifically in mathematical modeling of immune responses.

The goal of the numerical simulations in Section 3.2 is to reproduce various scenarios over long periods of time (years) to study their impact on long-term immunity. Different vaccination strategies or how often an individual is infected, for example, can impact long-term immunity levels [79].

Many different factors influence the strength and the quality of the immune memory recall, one of the most important being the similarity between influenza strains. In fact, as mentioned in Section 1.1, the adaptive immune response is antigen-specific, meaning that adaptive immune cells target specific antigens or viruses. To evade this specific immune response, seasonal influenza viruses mutate very quickly and the gradual accumulation of genetic mutations periodically results in the emergence of a novel variant, or a novel strain [3, 10, 18, 80]. The emergence of new variants through this process, called antigenic drift, hinders the adaptive immune system's ability to recognize the virus and mount an immune response. If the novel strain is similar to a previously encountered strain, some antigen-specific immune cells, i.e. adaptive immune components, that have previously proliferated will activate and proliferate once again in response to the similar antigen. The immune response to similar strains, induced by recall of previously acquired immune memory, is called cross-reactive and, as mentioned in Section 1.1, is strongest when influenza strains are most similar [3, 10, 30]. Measures of cross-reactivity will be discussed in Section 3.1.1.

The rapidly mutating nature of influenza viruses has a huge impact on the development of vaccines and the implementation of vaccination strategies. Influenza A vaccines are developed bi-annually to target a specific influenza strain that is predicted to be the dominant one in the following winter (in both the Northern and Southern Hemispheres) [10]. For this reason, as mentioned in Section 1.1, the immune response resulting from vaccination is extremely targeted and does not confer broad immunity to different strains of influenza [18]. For this reason, previous vaccinations have a limited impact on the immune system's ability to control infections that arise from exposure to novel strains. On the contrary, the immune response induced by natural infection confers broader and longer-lived immunity. Differences in modeling natural infections and vaccination will be discussed in Section 3.1.2.

With time or after repeated exposures to influenza viruses, the strength of the immune response for a specific antigen increases [30]. This is illustrated in Figure 3.1 for memory T cells. My model (2.1.1) was developed to reproduce this feature within the course of a single infection, and the parameter values presented in Section 2.3.1.2 were chosen so that $T_M^* > T_M^0$, $B_{LL}^* > B_{LL}^0$, and $A^* > A^0$. Single infection time-courses, shown in Figure 2.10, demonstrate that T_M, B_{LL}, and A are boosted over the course of a single infection. However, some immunological memory compartments, such as antibody, wane slowly over time

and it has been suggested that repeated exposure of low-dose antigen could keep immune levels high over long periods of time (years) [10, 30]. Because antibody waning is not directly included in the model equations (2.1.1), the impact of inter-infection interval length on antibody waning and the immune response upon reinfection is discussed in Section 3.1.3.

The last factor that will be considered is the season during which the infection occurs. This will be discussed in Section 3.1.4.

This modeling does not account for cross-reactivity with different pathogens or the competition between different pathogens on the maintenance of immunological memory. Infection resulting from exposure to a new pathogen, such as an unrelated disease can lead to an increase in certain memory T-cell subtypes or lineages but a decline in others [30]. Because in (2.1.1) we only consider one memory T-cell compartment, we do not consider the impact of other infectious diseases on the immune response to reinfections. Moreover, this modeling assumes that the infectiousness of the infection and the viral replication rate, denoted by the parameters β and k_V respectively, are constant across all secondary infections. This might not be the case and the infectiousness and viral replication rate have an important impact on the immune system's ability to control an infection, as shown in Figure 2.14.

3.1.1 *Similarity Between Infections*

Similarity between flu strains is crucial in determining the strength of the immune response to a new infection. If a novel flu strain or flu variant is very similar to previously encountered ones, the immune response will be strong. If it is dissimilar, the immune response will be much weaker [10, 18]. A measure of similarity between different flu strains can be obtained by considering conserved viral epitopes. Epitopes are chemical groups found on the surface of molecules that are recognized by T cells, B cells, and antibody. Upon recognition, these cells can bind to epitopes and induce an immune response. As the virus mutates, some epitopes are conserved and some mutate [10]. Reinfections to different flu strains can boost responses to specific epitopes that are shared between two virus strains, i.e. that have not mutated [18]. As such, we can consider the percentage of conserved epitopes to represent a measure of similarity between two influenza strains. Previous models have implemented this [27, 42].

Memory T-cell action against the conserved epitopes can confer protection to various strains of influenza [76]. This is because T cells, as opposed to antibody, recognize more conserved parts of influenza viruses that are not as prone to mutations [81, 82]. Highly conserved T-cell epitopes, i.e. epitopes conserved in more than 70% of flu strains, are

enough to induce a protective CD8+ T-cell response [82, 83]. In this sense, memory T cells provide heterologous, broad protection to different influenza subtypes. In humans, influenza A-specific CD8+ T cells can persist for decades after infection or vaccination [30, 80].

Because memory T cells persist for decades, we consider that after an infection, memory T cells are conserved until the following infection occurs, no matter the amount of time between infections. We assume that memory T cells will be cross-reactive to virus strains with conserved epitopes of the primary infection. Conserved T-cell epitopes across a wide variety of influenza strains account for 30% to 50% of all T-cell epitopes [84]. For this reason, we will assume that higher levels of epitopes are conserved in strains that are very similar. We will assume that the percentage of conserved epitopes between flu strains, is a randomly distributed variable denoted C_{Unif} because mutations that lead to antigenic drift occur randomly. We will further assume that between 30% and 100% of T-cell epitopes are conserved, i.e there is always some level of similarity between flu infections (30% of conserved epitopes) and you can be reinfected by the same strain (100% of conserved epitopes), for natural infections. We will model this as $C_{Unif} \sim U(0.3, 1)$, where U is the uniform distribution with minimum 0.3 (30%) and maximum 1 (100%). Thus, we denote the initial number of memory T cells for a the i-th reinfection

$$T^0_{M,i+1} = C_{Unif} T^*_{M,i}. \tag{3.1.7}$$

The case of memory T-cell immunity arising from vaccination will be discussed in Section 3.1.2.

Antibody epitopes are generally conserved at a much lower rate than T-cell epitopes [84]. For this reason, the immunity mediated by antibody is constrained to the few viral strains which are very similar to the primary infection, i.e. have high epitope conservation [80]. Variants with substantial mutations, or fewer conserved epitopes, cannot be neutralized by existing host antibodies because there is less cross-reactivity [81, 84]. Antibody levels on reinfection also depend on the elapsed time since the previous infection. To account for the time-dependence, an expression for the initial amount of antibody on reinfection will be derived and explained in Section 3.1.3.

3.1.2 *Type of Exposure*

The model (2.1.1) was derived to describe within-host dynamics in natural influenza A infections. The increased immunity that results from natural infections also confers immunity to different or heterologous strains of influenza than that of the primary infection

[30, 82]. As described in the previous section, Section 3.1.1, this broad immunity is the result of CD8+ T-cell action which recognizes parts of the virus less prone to mutations [81, 82]. However, currently used influenza A vaccines induce an antibody response, but they do not induce an efficient CD8+ T-cell response [80]. The antibody-induced immunity and protection resulting from natural infections is broader and longer-lived than that resulting from vaccination, which is extremely targeted towards components more prone to mutations. Indeed, antibody titers can remain high for decades after a natural infection, but wane quickly after vaccination [18]. Thus, natural infections can protect an individual against a secondary infection with a different strain, whereas vaccination cannot. Increased antibody titers resulting from vaccination can only attenuate secondary infections caused by strains similar to those of the primary infection and offer little protection against dissimilar strains [82].

For modeling the type of exposure, we will consider that natural infections and vaccinations are equally likely, i.e. for each exposure, each type of exposure has a $50/50$ chance of occurring. This will be modeled with a Bernouilli distribution, which represents a single experiment with two outcomes i.e. yes or no. The mean of the Bernouilli distribution represents the probability of the "yes" event occuring. In this case, for each exposure, vaccination occurs with probability $p = 0.5$ and natural infection occurs with probability $p = 0.5$, which means the Bernouilli distribution has mean 0.5. Denote the type of each exposure E_{Bern}, we have $E_{Bern} \sim \text{Bernouilli}(0.5)$.

The model (2.1.1) derived in Chapter 2 describes immune dynamics during natural infections. The model (2.1.1) does not produce accurate time-courses for vaccinations because vaccinations do not result in healthy cells becoming infected. However, we assume that the steady state values of (2.1.1) defined in (2.2.45), accurately described the steady state values of antibody A and long-lived B cells B_{LL} after vaccination because the boost in antibody titers resulting from natural infections and vaccination are similar [85]. For this reason, simulating the model (2.1.1) will reproduce the antibody boost resulting from vaccination.

Because influenza vaccination does not induce a CD8+ T-cell response, we want the initial number of memory T cells of the next natural infection to be determined by the steady state value of memory T cells after the previous natural infection. Supposing exposures $i-1$ and $i+1$ are natural infections and exposure i is the result of vaccination, then

$$T^0_{M,i+1} = T^*_{M,i-1}. \tag{3.1.8}$$

This way, vaccination has no impact on T-cell immunological memory, but T-cell memory acquired from previous infections is not lost. Vaccination will only boost antibody titers

(and indirectly long-lived B cells who maintain these antibody levels) but not memory T cells.

The antibody boost induced by vaccination depends on two factors: time elapsed since the previous exposure and total number of previous vaccinations. An expression for the initial amount of antibody on reinfection following a vaccination will be derived and explained in Section 3.1.3. The impact of the number of previous infections will be described in Section 3.1.2.1.

3.1.2.1 *Number of previous infections*

Repeated exposures to antigen with low-dose natural infections can increase antibody levels and can contribute to long-term protection and immunity [30, 31]. However, the opposite is true for flu vaccinations: repeated vaccinations result in diminishing antibody titer boosting after each vaccination or diminishing antibody half-life after each vaccination [86, 87]. In either case, after a few months, post-vaccination antibody titers are lower in individuals having received multiple vaccinations. To model this phenomenon, initial antibody titers for reinfections will depend on the number of previous vaccinations. Because initial antibody levels on reinfection are time-dependent with regard to the time elapsed since the previous exposure, this will be discussed in Section 3.1.3.

The number of previous vaccinations for the first reinfection will be a random number in $\{1, \ldots, 7\}$, which is the number of previous vaccinations for which there is experimental data available in [87].

3.1.3 *Time Between Infections*

People generally get the flu once every few years [88]. Assuming the period of time between flu infections, which we denote T, is normally distributed with mean 36 months (3 years) and standard deviation 12 months (1 year), we have $T_{Norm} \sim \mathcal{N}(36, 12)$. In this case, approximately 68% of inter-infection time intervals are in $[24, 48]$, or between two and four years after the primary infection. Approximately 95% of reinfections occur after one to five years and approximately 99.7% of reinfections occur 0 to 6 years after the primary infection, i.e the inter-infection interval time is in $[0, 72]$. This seems to be a reasonable assumption. If the inter-infection time interval sampled from T_{Norm} is negative, it will be resampled.

As mentioned in Sections 3.1.1, we suppose the number of memory T cells is invariant over long periods of time (decades). As such, the number of memory T cells at the beginning of a secondary infection or vaccination $T^0_{M,i}$ is not impacted by the time elapsed

between infections. On the other hand, antibody resulting from natural infections provide relatively long-lasting protection but wane exponentially over time. As such, initial antibody titers of the $(i+1)$-th infection are described by

$$A^0_{i+1} = A^*_i e^{-aT_{Norm}} \tag{3.1.9}$$

where T_{Norm} is the time between infections, in months, and a is the rate of decrease, which is determined by the time at which antibody reach half-peaks. Indeed, we have

$$a = \frac{\ln(2)}{t_{1/2}} \tag{3.1.10}$$

where $t_{1/2}$ is the time at which antibody titers reach half-peaks. Experimentally, this has generally been estimated to be a few years, though there is a lot of variability and some studies estimate half-peaks to occur a few decades after the primary infection [10, 18, 85, 89, 90]. We will choose $t_{1/2} = 48$, i.e. half-peaks are reached after 2 years. From (3.1.10), this gives

$$a = \frac{\ln(2)}{48}.$$

The variability in estimates of antibody waning is explained in part by how similar the current infecting strain is to strains previously encountered by an individual. To model this phenomena, we will take into account the similarity between strains, defined by C_{Unif}, as we did for memory T cells in (3.1.7). Thus, (3.1.9) becomes

$$A^0_{i+1} = C_{Unif} A^*_i e^{-aT_{Norm}}. \tag{3.1.11}$$

The post-infection antibody waning rates are constrained by post-vaccination antibody waning rates, for which experimental values are presented in Table 3.1 and described further in this section. Indeed, post-infection antibody waning is slower than post-vaccination antibody waning so half-peak values must be reached later. Antibody titers boosted by vaccination generally wane much faster than that, with half-peak estimates ranging from less than a year to three years [85, 86].

When modeling post-vaccination antibody waning, we need to take into account the number of previous vaccinations. In fact, the initial antibody boost post-exposure is independent of the number of previous vaccinations but additional vaccinations provide antibody boosts that wane with increasing speed [86, 87]. Half-peaks are reached around 600 days after the first vaccination and are reached in less than a year after the seventh vaccination [85–87]. The monthly antibody waning rate a is estimated from [87], where

Cumulative Number of Vaccinations	Half-Life (in months)	a
1	32	0.022
2	28	0.025
3	24	0.029
4	20	0.035
5	17	0.041
6	13	0.053
7	9	0.077

Table 3.1: *Half-Life of antibody titers post-vaccination for influenza A, estimated from [87]. a is stated to two significant figures but the simulations use the values with full precision, computed using the formula defined in* (3.1.10).

monthly percentage decline of antibody titers were measured for up to 7 successive vaccinations. These values are shown in Table 3.1. We do not consider strain similarity for antibody boosts resulting from vaccination because vaccines are developed to target a specific strain, which can vary a lot from year to year. In this case, initial antibody levels are described simply by (3.1.9), with a defined in Table 3.1.

3.1.4 *Season*

In the Northern Hemisphere, the flu season occurs every year from October to April and usually peaks in January [70]. Individuals are much more likely to be exposed to the flu during these months. As such, we consider two seasons: winter, occurring from October to April, and summer, occurring from May to September. This can be described by a random variable $S_{Bern} \sim \text{Bernouilli}(0.8)$, for a Bernouilli distribution as described in Section 3.1.2. The probability of a flu infection in the winter is 0.8 and the probability of a flu infection in the summer is 0.2, which means it is four times as likely an individual will be exposed to influenza in the winter compared to the summer. These values were chosen somewhat arbitrarily because of lack of easily accessible data quantifying this disparity. To keep the reinfection framework relatively simple, we consider that the season and the time elapsed since the last infection are independent variables, even though in reality the number of months since the previous infection could be used to determine the season.

We can model the seasonality of influenza by considering the impact low temperatures have on immune defenses. A previous study has suggested that exposure to cold temperature during these months impairs IFN-induced antiviral responses [91]. In the model (2.1.1), IFNs inhibit viral replication inside infected cells, as described in (2.1.1a). The parameter n, found in Table 2.7, determines the effectiveness of the IFN inhibition: as

n increases, IFN inhibition increases; as n decreases, IFN inhibition decreases. The model (2.1.1) and the parameter values used for the numerical simulations in Section 2.3 describe a 'typical' infection with the flu. As such, we will consider that the parameter values presented in Section 2.3 describe a winter infection because it is more likely to occur. To model summer infections, when IFN responses are not inhibted by low temperatures, we need to increase n, i.e when $S_{Bern} = 0$

$$n > 1.775 \tag{3.1.12}$$

which is the value of n defined in Table 2.7. The parameter values for various reinfection scenarios will be presented in Section 3.2.

3.2 Numerical Simulations

The goal of our numerical simulations is to study the impact of different variables on the immune response to influenza on re-exposure as described in Section 3.1. Initially, we consider an unrealistic scenario where immunological memory is perfectly conserved between natural infections i.e. the infecting strain is exactly the same and no time has elapsed between infections, so antibody titers do not wane. For the purpose of this simulation, we use the same parameter values as in Section 2.3. The history functions for the i-th infection are defined for $-\tau \leq t_i < 0$. The history functions for the first infection are those presented in Table 2.1. For subsequent infections, we have X^0_{i+1} defined by (3.1.4), Y^0_{i+1} defined by (3.1.5), and $T^0_{M,i+1}$, $B^0_{LL,i+1}$, and A^0_{i+1}, defined by (3.1.1), (3.1.2), (3.1.3), respectively for the $(i+1)$-th infection. Put together, all the non-zero history functions are

$$\begin{aligned} X^0_{i+1} &= X^0 \\ Y^0_{i+1} &= Y^0 \\ T^0_{M,i+1} &= T^*_{M,i} \\ B^0_{LL,i+1} &= B^*_{LL,i} \\ A^0_{i+1} &= A^*_i. \end{aligned} \tag{3.2.1}$$

All other variables are zero for $-\tau \leq t_{i+1} < 0$, which is their steady state value defined in (2.2.45), as for simulations of a single infection presented in Section 2.3.1.1.

The system defined in (2.1.1) is at steady state between infections and the inter-infection period occurs on a different time scale than the acute infection period (years vs. days). For these reasons, reinfection time courses for each variable are plotted over each other such that time is measured from the onset of the i-th infection at time t_i. Using the

initial conditions defined in (3.2.1) and parameter values defined in Tables 2.4-2.7, time courses for viral and innate immune components, described by (2.1.1a)-(2.1.1e), are shown in Figure 3.2 and time courses for adaptive immune components, described by (2.1.1f)-(2.1.1k), are shown in Figure 3.3.

As seen in Figures 3.2a-3.2e, 3.3a-3.3b, and 3.3e, the dynamics of all components, except those responsible for immunological memory, are similar across infections. The levels of T_M, B_{LL}, and A increase substantially from one infection to the other, as shown in Figures 3.3c-3.3d, and 3.3f, which is the result of the model's design. All variable peaks are in the same order of magnitude as shown in Figure 2.10, except for effector CD8+ T cells (Figure 3.3b), long-lived B cells (Figure 3.3d), and antibody (Figure 3.3f). The resulting differences between these reinfections and the initial model simulation, presented in Figure 2.10 are shown in Figure 3.4.

As we can see in Figure 3.4a, viral and innate immune components peak within 2 hours of the original model simulation but, as shown in Figure 3.4b, adaptive immune components present a lot more variability. Indeed, short-lived adaptive immune components (helper and effector T cells, and effector B cells) peak around the same time as during the original simulation. However, antibody and long-lived B cells peak up to more than 150 hours earlier as an individual is reinfected, which is consistent with immunological memory inducing proliferation early on in secondary infections, as described in Section 3.1. As we can see in Figure 3.3c, the memory T-cell peak is reached when memory T cells attain their post-infection steady state values, as defined in (2.2.45). Figure 3.4b shows this occurs later and later as the number of infections increases. Because the production of memory T cells begins when the infection is cleared, this does not support the hypothesis that increased immunological memory reduces the duration of the infection, as described in Section 3.1.

Figure 3.4c shows a monotonic decrease in peak values for free virus V and infected cells Y as the number of infections increases, which supports the assertion that repeated infections can reduce the magnitude of subsequent infections. Moreover, this decrease seems to approach a limit as the number of infections increases. This does not however have an influence on the IFN and recovered cell compartments, for which the peak values do not vary much. In Figure 3.4d, we can see short-lived adaptive immune component peaks, i.e. T_H, T_E, and B_E peaks, decrease as the number of infections increases. In contrast, immunological memory component peaks, i.e. T_M, B_{LL}, and A peaks, increase as the number of infections increases. This occurs in part because by design of the model (2.1.1), $T_E + T_M$ is bounded to account for limits in anatomical space, as described in Section 2.1.3.1.

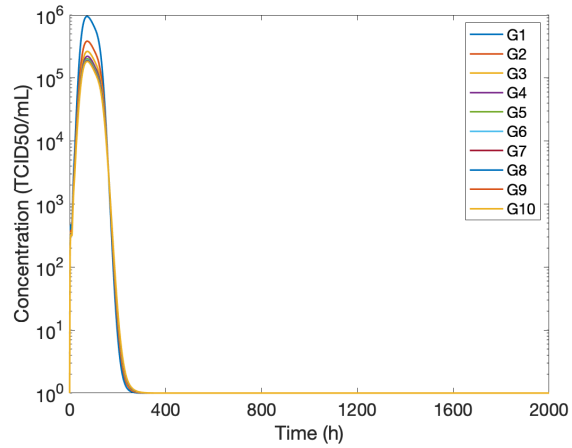

(a) *Free Virus*

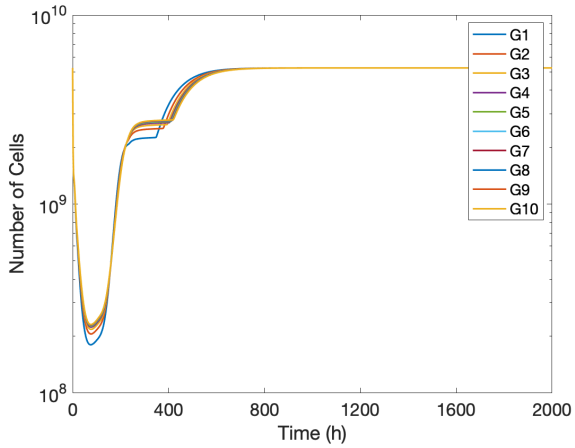

(b) *Healthy Cells*

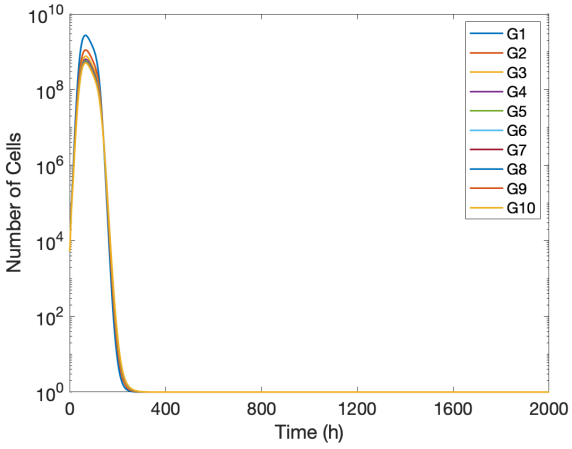

(c) *Infected Cells*

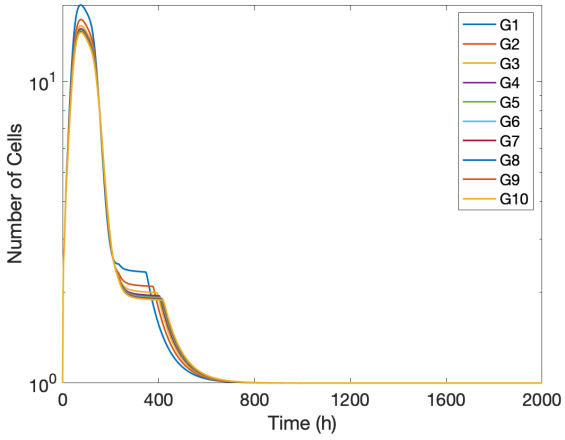

(d) *Recovered Cells*

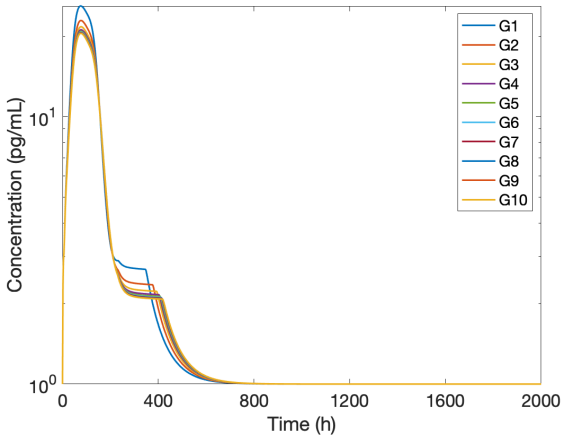

(e) *IFN*

Figure 3.2: *Time courses of 10 successive natural infections with history functions defined in* (3.2.1) *and parameter values defined in Tables* 2.4-2.7. *Time is measured from the onset of the i-th infection. (a) Free virus V. (b) Target cells X. (c) Infected cells Y. (d) Recovered cells R. (e) IFN I.*

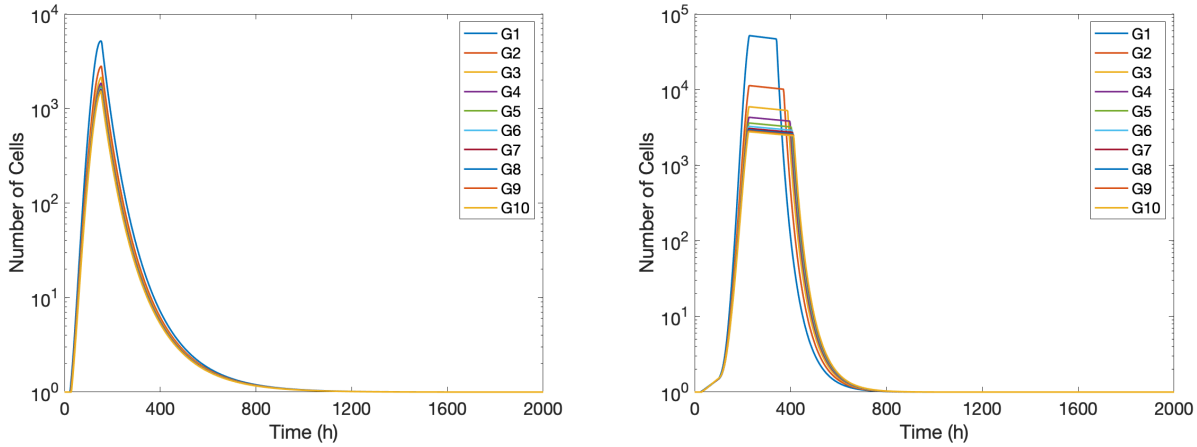

(a) *Helper T cells*

(b) *Effector T cells*

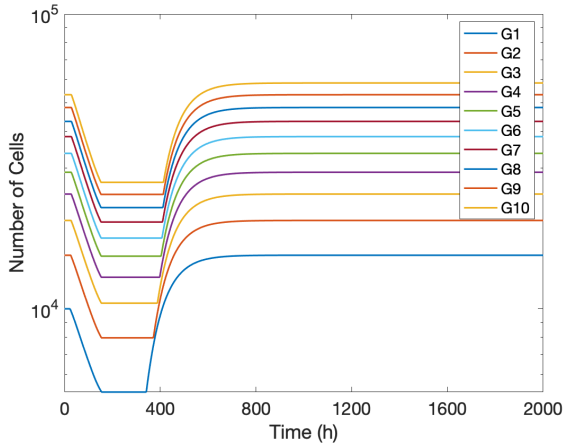

(c) *Memory T cells*

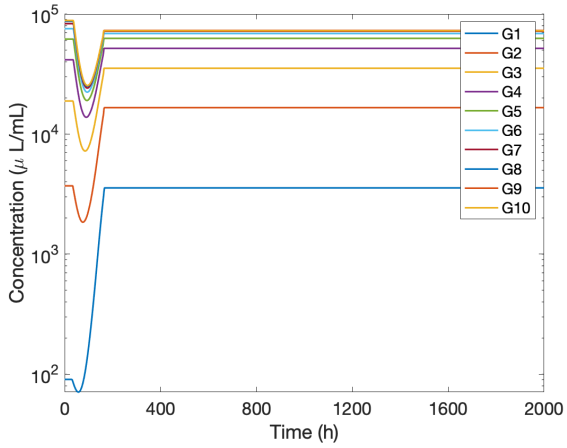

(d) *Memory B cells*

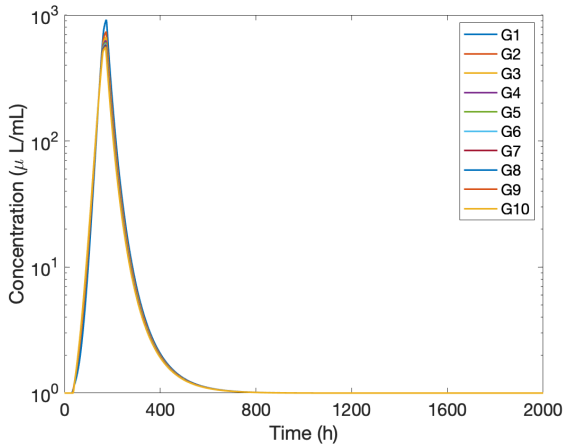

(e) *Effector B cells*

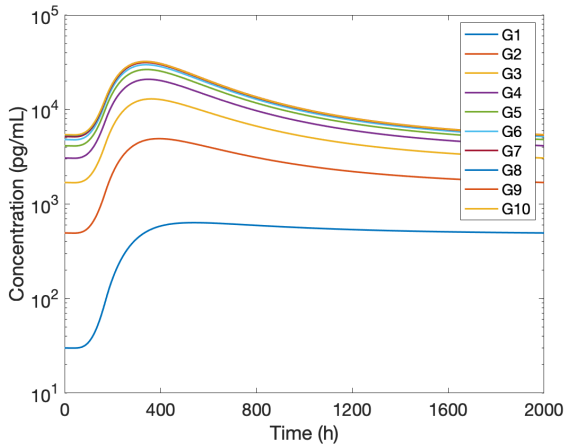

(f) *Antibody*

Figure 3.3: *Time courses of 10 successive natural infections with history functions defined in* (3.2.1) *and parameter values defined in Tables* 2.4-2.7. *Time is measured from the onset of the i-th infection. (a) Helper T cells T_H. (b) Effector CD8+ T cells T_E. (c) Memory T cells T_M. (d) Long-lived B cells B_{LL}. (e) Short-lived B cells B_E. (f) Antibody A.*

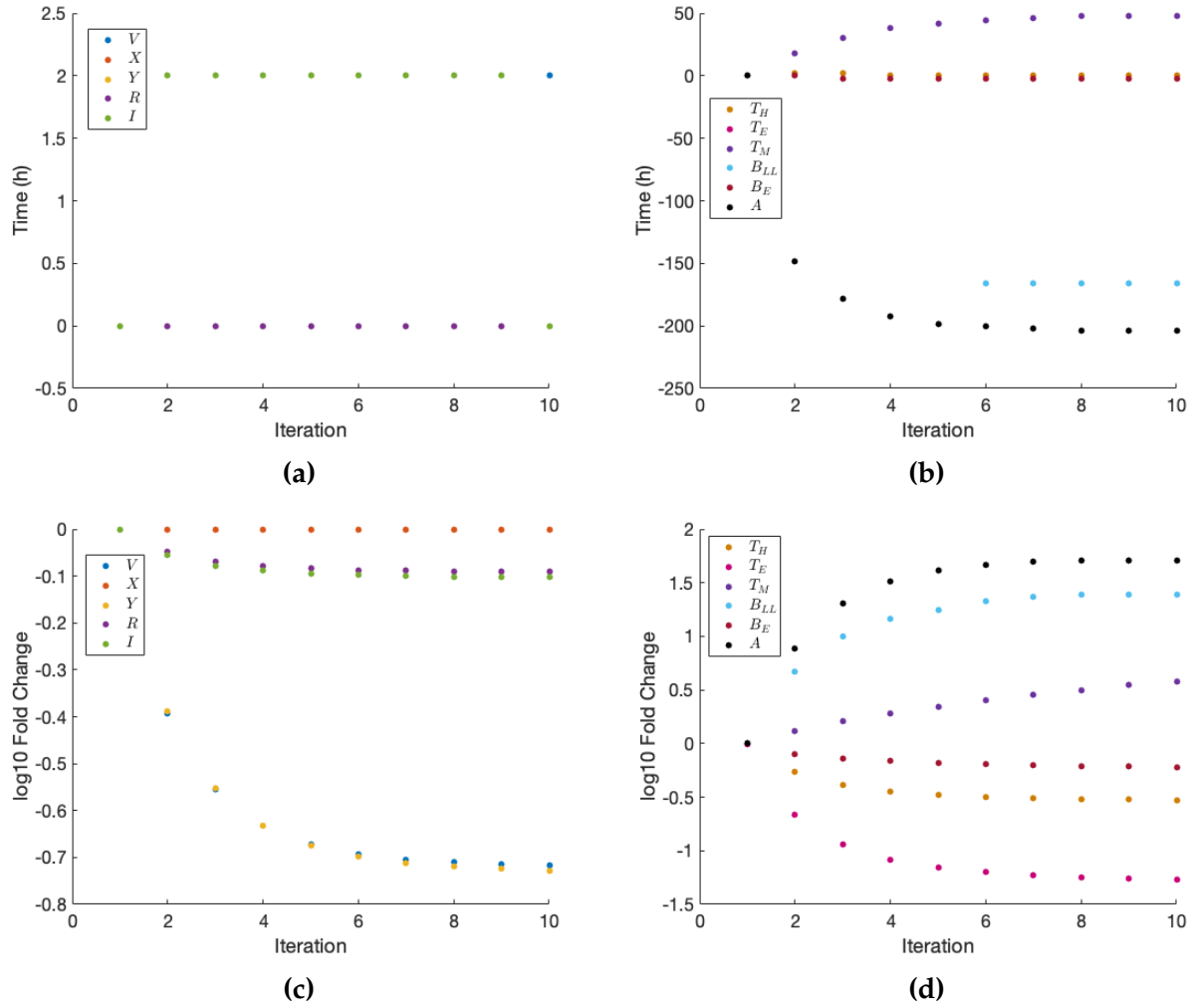

Figure 3.4: *Differences between initial model simulation presented in Figure 2.10 with regards to value of peak and timing of peak of all model variables of (2.1.1) for 10 infections. If the difference in peak time is negative, the peak occurred earlier than in Figure 2.10. If the difference in peak time is positive, the peak occurred later. (a) Difference in peak timing for viral and innate immune components described by (2.1.1a)-(2.1.1e). (b) Difference in peak timing for adaptive immune components described by (2.1.1f)-(2.1.1k). (c) Difference in peak values for viral and innate immune components described by (2.1.1a)-(2.1.1e). (d) Difference in peak values for adaptive immune components described by (2.1.1f)-(2.1.1k).*

Together, Figures 3.4c and 3.4d show that even for monotonically increasing immunological memory, immunological memory and innate immune components are not enough to control the infection and the adaptive immune response is always triggered. This suggests that for an infection of this strength, high levels of previously acquired immunity are not enough to control the infection, as suggested in [30]. This is especially true because these scenarios do not account for cross-reactivity and waning antibody titers, which dampen immunological memory strength, as described in Section 3.1. This is in agreement with the fact that early control of infection growth is the result of IFN action, as discussed in Section 2.3.3 and shown in Figure 2.14. Indeed, there is no memory component to IFN action in this model as immunological memory results from adaptive immune components. However, in recent years a growing body of literature has suggested that innate immune components could have improved response upon reinfection, which would suggest the existence of IFN-related memory [92, 93].

3.2.1 *Case Study of A Reinfection Scenario*

The immune response to influenza is subject to many randomly distributed factors, as described in Section 3.1. We will thus study an example a scenario likely to occur: over the course of 10 exposures (which represents a few decades), an individual will be naturally infected and vaccinated multiple times and virus mutations will impact how immunity is preserved over time. In this case, the values of C_{Unif}, E_{Bern}, T_{Norm}, and S_{Bern}, presented in Sections 3.1.1-3.1.4, are sampled independently from their respective distributions each time the model is run. Figure 3.5 provides a diagrammatic representation of the algorithm implementation of the different scenarios, depending on the values these variables take.

For the $(i+1)$-th infection, we have the history functions defined by

$$\begin{aligned} X^0_{i+1} &= X^0 && \text{from (3.1.4)} \\ Y^0_{i+1} &= Y^0 && \text{from (3.1.5)} \\ T^0_{M,i+1} &= C_{Unif} T^*_{M,i} && \text{from (3.1.7)} \\ B^0_{LL,i+1} &= \frac{d_A A^0_{i+1}}{k_{B_{LL}A}} && \text{from (3.1.6)} \\ A^0_{i+1} &= C_{Unif} A^*_i e^{-aT} && \text{from (3.1.11).} \end{aligned} \tag{3.2.2}$$

All other variables are zero for $-\tau \leq t < 0$, which is their steady state value defined in (2.2.45).

We will examine a case study of this scenario, i.e. a single realization of the random variables, with the values of C_{Unif}, E_{Bern}, T_{Norm}, and S_{Bern} presented in Table 3.2. In this

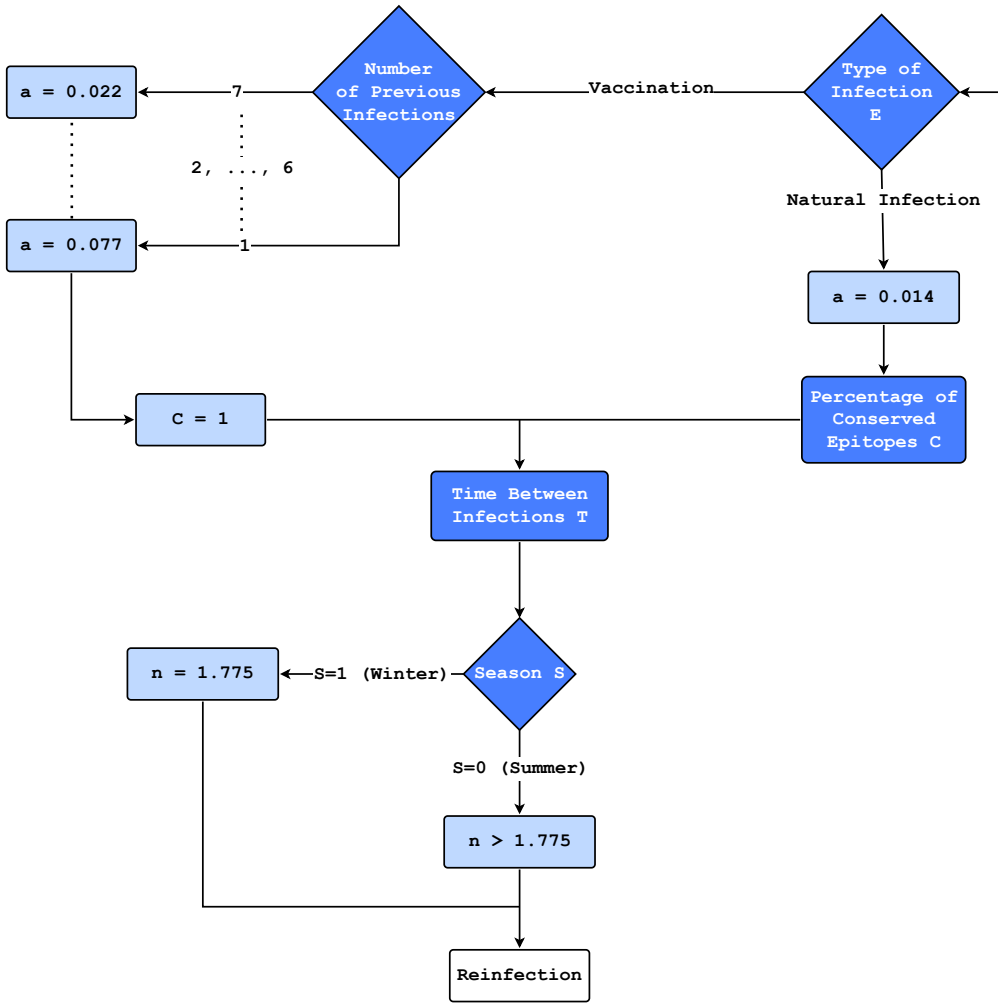

Figure 3.5: *Flow diagram of how various parameters and variables are chosen for reinfection scenarios. Diamonds represent decision nodes and rectangles represent processes and operations. Random variables are in dark blue. Flow lines indicate which parameter value was chosen. The probability distribution of the variables and the probability of each event was omitted from this flow diagram and values were stated to two significant figures for clarity.*

case, the history functions for T_M, B_{LL}, and A for each infection (iteration) were computed using the formulas in (3.2.2). In this case, we also choose

$$n = 1.86375$$

when $S_{Bern} = 0$, i.e. it is summer and n is subject to the constraint defined in (3.1.12).

For iterations where vaccination occurs, it does not make sense to plot infection curves for viral and innate immune components as well as helper T cells, effector CD8+ T cells, and effector B cells, i.e. all transient compartments, because no infection actually occurs.

i	Conserved Epitopes C_{Unif}	Type E_{Bern}	Time Elapsed T_{Norm}	Season S_{Bern}
1	1	Vaccination	39	Summer
2	0.64	Natural	47	Winter
3	0.90	Natural	43	Winter
4	1	Vaccination	39	Winter
5	1	Vaccination	50	Winter
6	0.80	Natural	12	Winter
7	1	Vaccination	35	Winter
8	1	Vaccination	10	Winter
9	0.87	Natural	25	Winter
10	0.66	Natural	28	Winter

Table 3.2: *Values of the randomly generated variables for reinfections for a single realization of the probabilistic model. Values are stated to the nearest month and percentage value.*

Indeed, as described in Section 3.1.2, the model (2.1.1) does not produce accurate time courses for vaccinations but accurately describes how antibody and long-lived B-cell titers are boosted. Moreover, as described in (3.1.8) in Section 3.1.2, post-vaccination, memory T cells are at the same level as before vaccination and for this reason T_M time courses will not be plotted for iterations where vaccination occurs. Thus, only B_{LL} and A are plotted for the iterations for which vaccination occurs, which are found in Table 3.2.

In Figure 3.6a, we can see that due to high levels of conserved epitopes, the memory T-cell populations stays relatively constant over the years, despite not being boosted when the individual is vaccinated. Conversely, because long-lived B cells and antibody are boosted by both vaccination and natural infection and because they wane much faster than memory T cells, the steady state values B_{LL}^* and A^*, defined in (2.2.44) and (2.2.43), respectively, show a lot more variability over time, as shown in Figures 3.6b and 3.6c. Time courses for all variables not presented in Figure 3.6 are similar to those presented in Figures 3.2 and 3.3, which is why they are omitted.

In Figure 3.7a, we can see that when a natural infection occurs, the innate immune components are stimulated to the same degree for each successive infection. However, due to an increased adaptive immune response, viral and infected cell peaks are much lower. Indeed, as shown in 3.7b, both vaccination and natural infection contribute to antibody and long-lived B-cell increases. Due to numerous vaccinations which do not boost memory T-cell levels, the population of memory T cells stays relatively constant over exposures, providing long-lasting immunity. Figure 3.7 shows that even when taking into account cross-reactivity of different influenza strains, declining immunity over time, vaccinations,

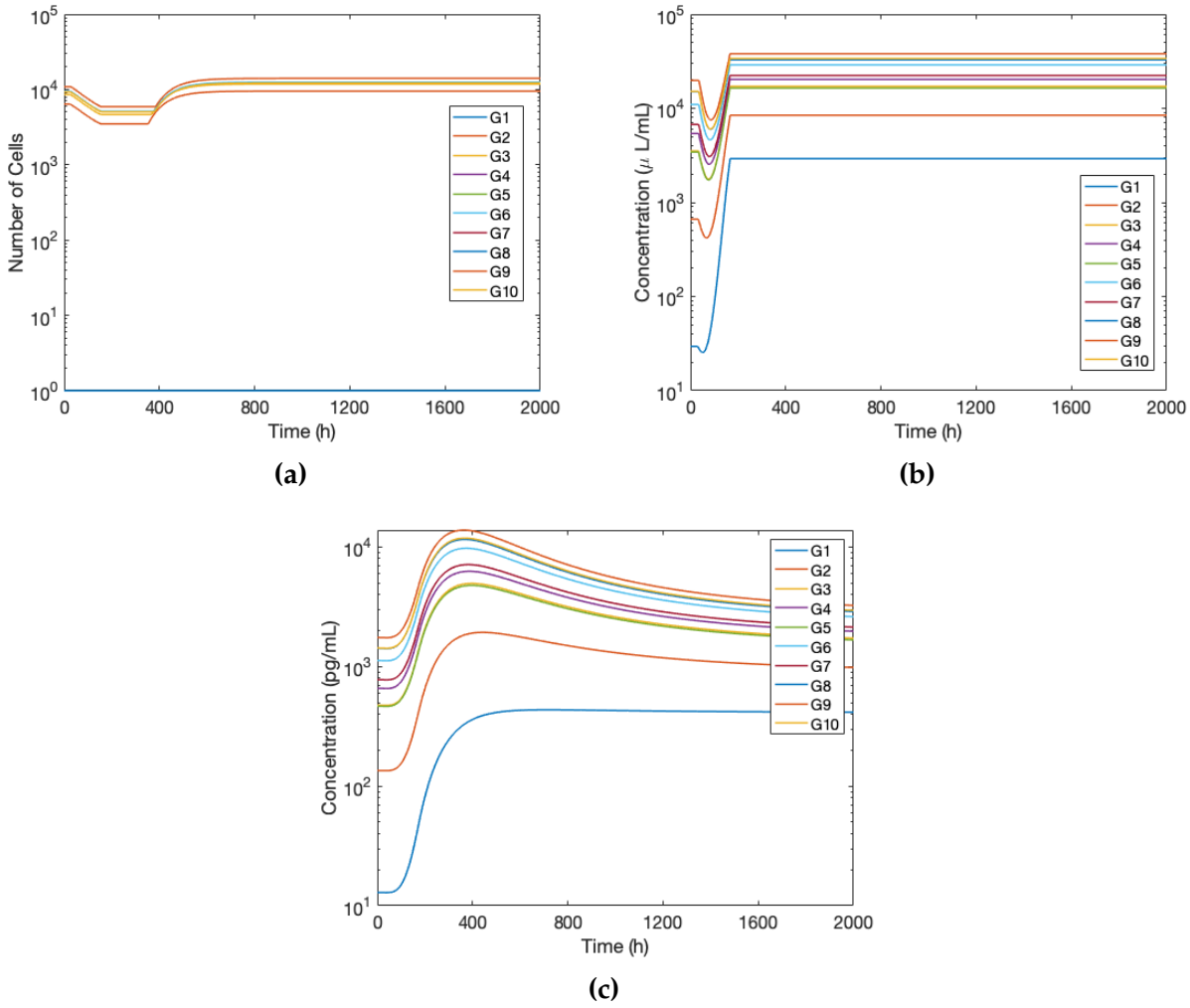

Figure 3.6: *Time courses of 10 successive exposures with random factors defined in Table 3.2, parameter values defined in Tables 2.4-2.7 (except for n), and history functions defined in (3.2.2). (a) Memory T cells T_M. (b) Long-lived B cells B_{LL}. (c) Antibody A.*

and seasonal influence, repeated exposures to influenza reduce the magnitude of peak viral titers and the number of infected cells, without increasing inflammation (IFN levels).

The differences in peak timing are similar to those presented in Figures 3.4a and 3.4b and so they are omitted.

Other realizations of the random variables resulted in similar time courses for T_M, B_{LL}, and A, as those presented in Figure 3.6. The differences between peak values also show similar dynamics as those presented in Figure 3.7. Due to these similarities, plots showing additional single realization time courses or peak differences are omitted.

The next logical step would have been to sample the random variables from their respective distributions and perform Monte-Carlo analysis to forecast long-term outcomes such as survival curves, as has been done in previous models [11, 57, 94–96]. Indeed, this

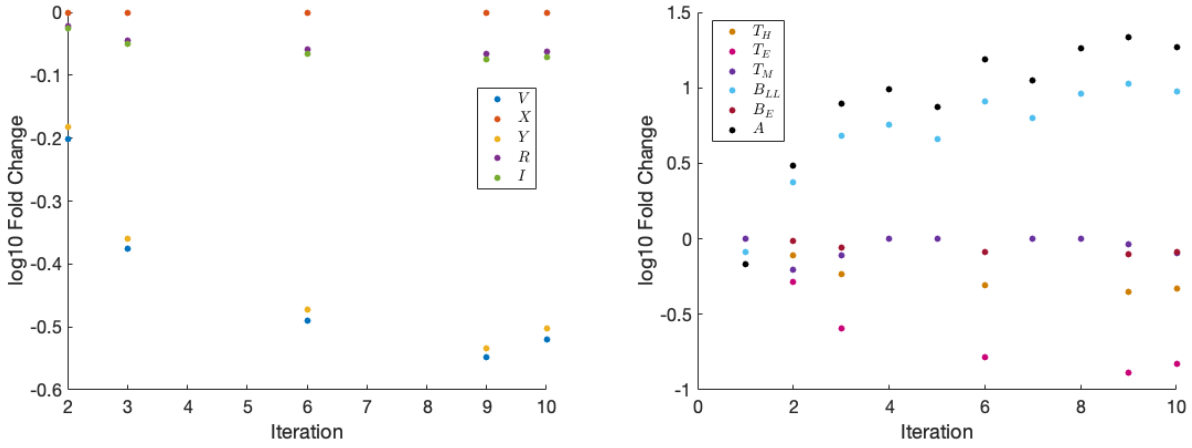

(a) **(b)**

Figure 3.7: *Differences between initial model simulation presented in Figure 2.10 with regards to value of peak for all variables of (2.1.1) for 10 exposures, subject to random factors presented in Table 3.2. (a) Difference in peak values for viral and innate immune components described by (2.1.1a)-(2.1.1e). (b) Difference in peak values for adaptive immune components described by (2.1.1f)-(2.1.1k).*

would allow us to examine the survival distributions, i.e. the occurrence of distinct events, such as time between infections, in groups who undergo to different types of exposure, e.g. frequency of vaccination. Moreover, we could also examine additional deterministic scenarios, such as the magnitude of the infection after a fixed number of vaccinations. However, time and space limitations preclude us from pursuing these directions in this thesis.

3.3 IMPACT OF SEX

Various biological sex differences affect the human immune response. Sex differences include sex chromosomes, reproductive tissues, and concentrations of sex steroids (hormones) such as androgens, which include testosterone, oestrogens, and progesterone. There is growing evidence that differences in both gene expression and sex hormones can lead to sex-biased immune cell function. The influence of genetic components on the immune response has not been as well characterized as the influence of sex hormones but a study suggests that sex chromosome complement does not impact influenza infections [97, 98]. Many immune cells, such as T cells and B cells, have sex hormone receptors and, as a result, the presence or absence of sex hormones or changes in concentrations of sex hormones can alter the immune response [97, 99, 100]. This suggests that sex hormones may directly cause polymorphic immune responses. Generally androgens and progesterone are anti-inflammatory, i.e. they supress several immune response components necessary

for inflammation. Estradiol (oestrogen) has different effects: low concentrations of estradiol are pro-inflammatory whereas high concentrations of estradiol lead to diminished production of pro-inflammatory cytokines [97, 99, 100].

We examined whether sex chromosome complement affects susceptibility to influenza A virus infection and found that sex chromosome complement did not affect influenza pathogenesis

These differences have wide-ranging implications on immune responses to a different pathogens. Specifically when considering viral infections, heightened pro-inflammatory responses, induced by low oestrogen concentrations, may increase the risk of chronic inflammation in females, described for the model (2.1.1) by the steady state expression (2.2.44), with $I^* \neq 0$ [98, 100]. Conversely, anti-inflammatory responses, resulting from androgen production, may increase the risk of persistent viral infection in male individuals.

IFN activity in immune cells at the disease free steady state with no chronic inflammation, defined in (2.2.45), is greater in females than in males, which may lead to more rapid antiviral immune responses in females exposed to virus or vaccines [100]. Females usually clear infections faster than males but they are more likely to be symptomatic [97, 100].

When considering influenza infections specifically, data supports the hypothesis that the sex-biased immune response to influenza is predominately mediated by sex steroid hormones, as opposed to sex chromosomes [98]. Females usually show increased T-cell activation and proliferation during an infection [99]. They also generally have higher levels of antibody (at least twice as strong) post-infection or post-vaccination to influenza than males [99, 100]. This is also associated with higher antibody specificity and avidity to the virus [100].

This leads to interesting questions as to whether increased levels of antibody in females lead to greater protection and whether protection against novel strains of influenza virus is greater in females than in males [100].

The concentrations of sex steroids change drastically over the course of an individual's life, and even fluctuate within shorter periods of time, e.g. during the menstrual cycle or pregnancy, which directly affects immunity [99, 100]. To simplify this modeling problem, we will only consider fixed concentration levels of each sex hormone.

Despite a stark increase in the last decade, there is very limited data regarding sex-biased differences in infection kinetics, as less than 10% of published papers in immunology report the sex of animal or human subjects [99]. Previous studies have used symptom scores to quantify sex differences in influenza, when more objective outcome measures, such as inflammatory markers, would allow for more specificity [98, 101]. Moreover, there are very few mathematical models of immune dynamics or more specifically of the within-

host immune response to infection that account for sex-biased differences. These models, two of which were published in the last year, usually represent sex-biased disparities with different parameter values [43, 102, 103]. This section will use the same methodology and we will determine new parameter values for females and males.

All parameter values which differ from those presented in Tables 2.4- 2.7 in Section 2.3.1.2 will be presented in Table 3.3, for both females and males, with the change with regard to the original parameter values. Going forward, we will refer to this combination of parameters, which results in the variable time courses presented in Figure 2.10, as the original model or original parameters.

We will suppose females have low estrogen production (pro-inflammatory) and males have high testosterone production (anti-inflammatory). As discussed in Section 2.1.2, IFN production resulting from a positive feedback loop can result in chronic inflammation, i.e. $I^* \neq 0$ in (2.2.44). This production occurs at a rate determined by the parameter b_2. The model is not structurally identifiable, so many parameter combinations could generate the desired increase in inflammation but we will model an increase in long-term inflammation in females by increasing b_2 and decreasing k_I, which represents the viral-induced IFN production rate. Decreasing b_2 and increasing k_I will represent anti-inflammatory action in males. Moreover, IFN inhibition of viral replication is induced more quickly in females, which in (2.1.1) is described by the delay τ_{IV}. As such, τ_{IV} will be greater for females than males.

T-cell production rates, k_{T_H} and k_{T_E} will be increased for females to depict increased T-cell proliferation and, conversely, will be decreased for males. d_{T_H} will also be modified so that T-cell population decline occurs within the correct time frame.

It is assumed females have greater antibody levels with higher antibody affinity than males. In (2.1.1), high-affinity antibody production is the result of antibody production by B_{LL}, which occurs at rate $k_{B_{LL}A}$. Because $k_{B_{LL}A}$, the production of antibody by long-lived B cells, was chosen to obtain the proper ratio of B_{LL} to A at steady state, as defined in (2.3.16), increased antibody production in females will be represented by increasing $k_{B_{LL}}$, the production rate of long-lived B cells. This is consistent with the fact that females usually have higher rates of B cells [99]. Conversely, $k_{B_{LL}}$ will be decreased to represent males' decreased antibody production.

The parameters k_{T_H} and d_{T_H} are still subject to the same constraints, as defined in (2.3.27) and (2.3.28). In Section 2.3.1.2, the parameter $k_{B_{LL}}$ was chosen to obtain the correct steady state value of B_{LL}^*, thus we expect the steady state values of B_{LL}^* to be different for females and males.

For the initial conditions defined in Table 2.1 in Section 2.3, the dynamics for females

Parameter	F Value	Change	M Value	Change
k_I	0.0585	0.65	0.09045	1.005
b_2	0.6675	4.45	0.1125	0.75
τ_{IV}	8	1.6	2	0.4
k_{T_H}	0.00452 $*$	1.19	0.00341 $*$	0.905
d_{T_H}	0.0081	1.35	0.0048	0.8
k_{T_E}	0.00161 $*$	1.07	0.00146 $*$	0.985
$k_{B_{LL}}$	0.00196 $*$	1.1	0.00167 $*$	0.95

Table 3.3: *Sex-biased parameter values and their fold change, when compared to the parameter values defined in Section 2.3.1.2. The values with a $*$ are stated to three significant figures but they are computed to full precision in the simulations.*

Variable	F Peak	M Peak	Original Peak
Free Virus V	$3.98 \cdot 10^5$	$1.37 \cdot 10^6$	$9.51 \cdot 10^5$
Infected Cells Y	$6.98 \cdot 10^8$	$4.76 \cdot 10^9$	$2.69 \cdot 10^9$
Recovered Cells R	$1.76 \cdot 10^1$	$1.81 \cdot 10^1$	$1.79 \cdot 10^1$
IFN I	$2.59 \cdot 10^1$	$2.61 \cdot 10^1$	$2.60 \cdot 10^1$
Helper T cells T_H	$5.42 \cdot 10^3$	$4.97 \cdot 10^3$	$5.18 \cdot 10^3$
Effector CD8+ T cells T_E	$6.15 \cdot 10^4$	$4.33 \cdot 10^4$	$5.20 \cdot 10^4$
Effector B cells B_E	$5.89 \cdot 10^2$	$9.19 \cdot 10^2$	$9.28 \cdot 10^2$

Table 3.4: *Comparison of peak values for simulations with original parameter values, for females, and males. This table only shows variables that are 0 at the disease free steady state, defined in (2.2.45), for original parameter values the of model. All values are stated to three significant digits, in their respective units defined in Table 1.2.*

and males are qualitatively similar with quantitative differences in the peak values and timings to those of the original model, shown in Figure 2.10, which we will consider to be representative of average human immune dynamics. Indeed, due to limited data, the parameters in Table 3.3 were chosen so that the peak values of I, T_H, and T_E and the steady state values A^* in the original model are the averages of female and male peak values. All other variables are considered to be free variables in this context, that is to mean their peak values or steady state values were not explicitly used to determine new parameter values. Peak values for the original model, females and males are presented in Table 3.4. Steady state values, for variables with non-zero steady state values, for the original model, females and males are presented in Table 3.5.

All variable peaks presented in Table 3.4 occur within the ranges presented in Table 1.1 for both female and male individual simulations. We consider the infection to be controlled

Variable	F Steady State	M Steady State
X^*	$3.55 \cdot 10^9$	$5.25 \cdot 10^9$
I^*	$1.56 \cdot 10^0$	0
R^*	$1.48 \cdot 10^0$	0
T_M^*	$1.65 \cdot 10^4$	$1.46 \cdot 10^4$
B_{LL}^*	$4.54 \cdot 10^3$	$2.58 \cdot 10^3$
A^*	$5.76 \cdot 10^2$	$3.77 \cdot 10^2$

Table 3.5: *Comparison of steady state values for simulations with original parameter values, for females, and males for the disease-free steady state* (2.2.44). *All values are stated to three significant digits, in their respective units defined in Table 1.2.*

when $Y(t) = 0$, which occurs after 340 hours in the original model, after 347 hours for males, and after 311 hours for females. Considering adaptive immune components determine the clearance of the infection, this asymmetrical change in infection length in females and males would suggest that increased T-cell proliferation and activation leads to faster clearance of the infection (by more than a day). Conversely, decreased T-cell proliferation does not markedly increase infection length, which would suggest that this effect is not directly proportional to T-cell proliferation but that high T-cell proliferation is required for shorter infection spans. Moreover, as we can see in Table 3.4, free virus, infected cell and effector B-cell populations decrease substantially in females, when compared to the original model. On the contrary, free virus and infected cell populations increase markedly in males, resulting in an infection that infects almost 90% of a male individual's lung, most likely causing death. Interestingly, the population of effector B cells in males does not increase very much to compensate for the decline in T cells.

There is minor increase in B-cell production and infection length in males compared to a stark decrease in B-cell production and infection length in females for changes of the same magnitude in T-cell production. This would suggest that small increases in T-cell production have a limited impact, until the magnitude of the T-cell response reaches a certain level, at which point the length and magnitude of the infection are markedly reduced. This could imply that the immune system is subject to different regimens under different conditions.

The peak value of IFNs is relatively constant across groups, by design, as only the source of IFN production has changed. As we can see in Table 3.5, this results in different steady state values for I in females and males. The steady state value of I for females is non-zero, which differs from original simulations of the model, shown in Figure 2.10. However, in females, the steady state $I^* \neq 0$ is very small and represents a value which

can occur in healthy individuals [14]. Compared to the steady state values of the original model presented in Table 2.2, steady state values of antibody and long-lived B cells are increased in females and decreased in males. The changes in memory T-cell populations are roughly proportional to the changes in effector CD8+ T-cell populations, for both female and male populations.

In the case where immunological memory is perfectly preserved, females and males' immune components exhibit the same trends after multiple reinfections as the original model, which was shown in Figure 3.4, respective to their specific peak values, so figures illustrating this are omitted. In this case, virus and infected cell populations plateau lower in females than in males.

In Figure 3.8, we consider the change in immune levels in females and males over 10 exposures, when compared to the original model for a single realization of the random variables, the values for which are presented in Table 3.2. All innate and adaptive components exhibit the same trends over 10 re-exposures as those shown in Figure 3.4. There are however some notable differences.

As we can see in Figure 3.8c, viral titers and infected cells are consistently higher in males, when compared to the original model peaks. Conversely, they are consistently lower in females, as shown in Figure 3.8a. The IFN peaks seem quite similar across all groups, which means the chronic inflammation present in females, defined by a non-zero I^* steady state value in (2.2.44) does not have an impact on IFN production during an infection. It could however contribute to keeping virus titers lower by inducing IFN production more quickly on reinfection. Moreover, adaptive immune components, shown in Figures 3.8b and 3.8d for females and males, respectively, exhibit similar trends as the original model, with antibody and B-cell populations higher in females than in males. Females exhibit lower levels of killer T cells over time compared to the original model, despite greater T-cell proliferation and memory T-cell levels, which bound CTL levels, seeming relatively constant across exposures (across all groups). This is likely due to increased antibody production, which limit viral titer peaks.

Similarly as for scenarios which do not consider sex as a variable, presented in Section 3.2, it would be interesting to study probabilities of long-term outcomes and perform survival analysis. Once more, time and space constraints prevent us from doing so.

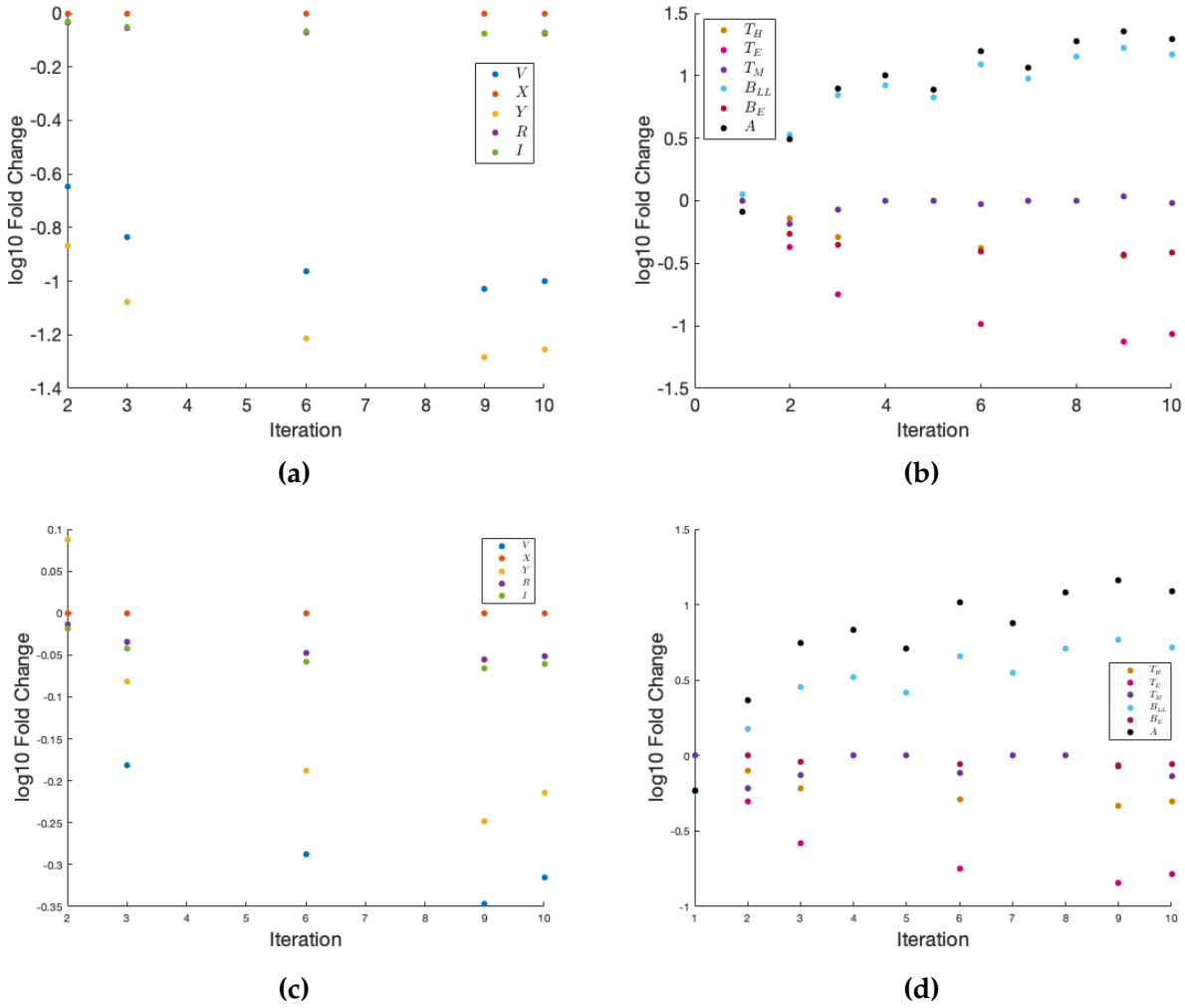

Figure 3.8: *Differences between initial model simulation presented in Figure 2.10 with regards to value of peak and timing of peak of all variables of (2.1.1) for 10 exposures, subject to random factors presented in Table 3.2. (a) Difference in peak values for viral and innate immune components described by (2.1.1a)-(2.1.1e) for females. (b) Difference in peak values for adaptive immune components described by (2.1.1f)-(2.1.1k) for females. (c) Difference in peak values for viral and innate immune components described by (2.1.1a)-(2.1.1e) for males. (d) Difference in peak values for adaptive immune components described by (2.1.1f)-(2.1.1k) for males.*

CHAPTER 4

CONCLUSION

In Chapter 1, we present an overview of the biological mechanisms that govern influenza infection dynamics. In Chapter 2 we developed an 11 delay differential equation model of within-host flu infections, described by (2.1.1a)-(2.1.1k). This model describes multiple phases of the immune response during the infection and post-infection. During the early stages of the infection, only the innate immune response, ascribed to I, the IFN population, is activated. Modeling innate immune components as a single compartment of the system (2.1.1) allows for more detailed and complex modeling of adaptive immune and memory components, without having an excessive number of compartments, which would make analysis of the model arduous. The innate immune response slows viral growth but is usually not strong enough to clear the infection. As such, when viral levels exceed a certain threshold V_T, the adaptive immune response is activated, the acute phase of which is described by helper T cells T_H, killer T cells T_E, and effector B cells B_E. The immunological memory components, which contribute to long-lasting immunity (years, decades) are described by memory T cells T_M, long-lived B cells B_{LL}, and antibody A. The long-lived B cell compartment represents a consolidation of multiple B cell populations and the single antibody compartment encapsulates antibodies of varying affinity to virus. These simplifications result in fewer model compartments and parameters, making the determination of parameter values for which no clinical values are known and sensitivity analysis easier. The adaptive immune response allows the immune system to clear the infection. Post-infection, memory T cells are produced, which allows for the maintenance of immunological memory.

To study these different phases of the immune response and their impact on infection time-courses, we first study two submodels. A three-equation submodel (2.1.2a)-(2.1.2c) of viral dynamics, excluding the immune response, is studied in Section 2.2.1, and allows us to define an R_0, analogous to the epidemiological R_0, which characterizes the stability of disease-free and endemic disease steady states. A five-equation submodel (2.1.3a)-(2.1.3e) of innate immune dynamics is studied in Section 2.2.2, in which we define two different types of disease-free steady states: the healthy steady state, where $I^* = 0$, and the chronic inflammation steady state, where $I^* \neq 0$. These two types of steady state also exist for the full model, including both the innate and adaptive immune responses, described by (2.1.1a)-(2.1.1k). For both the innate immune system submodel (2.1.3a)-(2.1.3e) and the full

model (2.1.1), the endemic disease steady state is not studied algebraically because it is not evident how to determine closed-form expressions for most variables. One notable exception is memory T cells which are zero at the endemic disease steady state, indicating that the absence of memory T cells is necessary for the persistence of elevated viral titers.

Numerical simulations of (2.1.1) are performed in Section 2.3 and various pathological scenarios are considered to study the impact of various immune components on disease outcome (infection clearance vs individual death), e.g. no innate immune response, no T cell response, etc. The model fails to accurately produce infection time courses for these scenarios, i.e. some cell populations exceed what is biologically possible. This is the result of having an artificially high turnover rate of target cells (high production rate and high decay rate) to produce correct time courses, meaning there is always a big reservoir of new cells that can be infected. However, these simulations still allow us to determine the most important components to each phase of the infection. Notably, the innate immune response is essential to control the early stages of the infection and the adaptive immune response, specifically the T cell response, controls infection clearance. Moreover, in Section 2.3.3, the joint impact of disease infectiousness and the viral replication rate on disease outcome is studied by performing a sensitivity analysis of the system with regard to these parameters.

In Chapter 3, we consider various scenarios related to repeated infections and vaccinations to study how immunological memory impacts the immune response over time. The strength of the immune recall depends on the similarity between different flu strains, the type of exposure (natural infection or vaccination) and the time between exposures, and the season during which the exposure occurs. These factors impact how cross-reactive the immune response is and allow us to described antibody waning in between infections (years), which is not explicitly accounted for in the model (2.1.1), developed in Chapter 2. We discuss how these factors are implemented in reinfection modeling in Section 3.1. We also investigate the (unrealistic) scenario where immunological memory is perfectly conserved and cross-reactive, which allows us to study open questions in immunology. Notably, these simulations show that high levels of pre-existing immunity do not result in sterilizing immunity, i.e. the adaptive immune response is always triggered. Immunological memory does reduce the magnitude of the infection monotonically across infections, though the infections peak at around the same time.

In Section 3.3, we consider the impact of sex hormones on the immune response during flu infections and how sex-specific immune responses evolves over the course of multiple infections or vaccinations. Model parameters are adapted to reflect differences in sex hormones such as increased T cell proliferation in female individuals and decreased inflammation in male individuals. However, because the model is not structurally identifiable

and there is a lack of data regarding sex differences in immunology, other parameters that are considered to be sex-independent in this model might not be, i.e. sex differences might have a larger impact than what was considered in the modeling done in this thesis. These sex-differences result in lower magnitude infections in female individuals and higher magnitude infections in male individuals. The most striking difference that results from these changes is that female individuals are able to clear the infection 36 hours before male individuals.

One aspect of the model (2.1.1) which is not thoroughly investigated in this thesis is the impact of the delays on infection time courses. Considering many of the delays are of similar magnitude, it might be possible to simplify the model further by omitting some of them and still obtain realistic time courses. Parameter fitting, which was not done rigorously, by using an objective function and optimization algorithm to determine the best parameters would be interesting to explore. Similarly, the inclusion of random variables, while making for an interesting modeling problem, in not studied at length. Consequently, the study of additional deterministic scenarios representing different types of exposures to influenza over time could have provided additional insight. An interesting question to explore would be the impact of changing levels of sex hormones over time. Indeed, the modeling in Section 3.3 assumes all sex hormone levels are constant and thus their impact on the immune response is constant. However, this is highly unrealistic as hormone levels vary a lot with time, especially oestrogens which have both immune-activating and immune-dampening effects, depending on present levels.

BIBLIOGRAPHY

1. Beauchemin, C. A. & Handel, A. A review of mathematical models of influenza A infections within a host or cell culture: lessons learned and challenges ahead. *BMC Public Health* **11 (Suppl 1),** S1–S7 (2011).
2. Eftimie, R., Gillard, J. & Cantrell, D. Mathematical Models for Immunology: Current State of the Art and Future Research Directions. *Bulletin of Mathematical Biology* **78,** 2091–2134 (2016).
3. Janeway Jr, C. A., Travers, P., Walport, M. & Shlomchik, M. J. in *Immunobiology: The Immune System in Health and Disease. 5th edition* (Garland Science, 2001).
4. Marshall, J. S., Warrington, R., Watson, W. & Kim, H. L. An introduction to immunology and immunopathology. *Allergy, Asthma & Clinical Immunology* **14,** 1–10 (2018).
5. Rouse, B. & Sehrawat, S. Immunity and immunopathology to viruses: what decides the outcome. *Nature Reviews Immunology* **10,** 514–526 (2010).
6. Abu-Shah, E. *et al.* Human CD8+ T cells exhibit a shared antigen threshold for different effector responses. *The Journal of Immunology* **205,** 1503–1512 (2020).
7. Henrickson, S. E. *et al.* T cell sensing of antigen dose governs interactive behavior with dendritic cells and sets a threshold for T cell activation. *Nature Immunology* **9,** 282–291 (2008).
8. Miao, H. *et al.* Quantifying the early immune response and adaptive immune response kinetics in mice infected with influenza A virus. *Journal of Virology* **84,** 6687–6698 (2010).
9. Alberts, B. *et al.* in *Molecular Biology of the Cell. 4th edition* (Garland Science, 2002).
10. Han, A., de Jong, S. & Russell, C. Co-evolution of immunity and seasonal influenza viruses. *Nature Reviews Microbiology* **21,** 805–817 (2023).
11. Smith, A. M. Host-pathogen kinetics during influenza infection and coinfection: insights from predictive modeling. *Immunological Reviews* **285,** 97–112 (2018).

12. Smith, A. M. & Perelson, A. S. Influenza A virus infection kinetics: quantitative data and models. *Wiley Interdisciplinary Reviews: Systems Biology and Medicine* **3,** 429–445 (2011).

13. Dobrovolny, H. M., Reddy, M. B., Kamal, M. A., Rayner, C. R. & Beauchemin, C. A. Assessing mathematical models of influenza infections using features of the immune response. *PLOS One* **8** (2 2013).

14. Galani, I.-E. *et al.* Untuned antiviral immunity in COVID-19 revealed by temporal type I/III interferon patterns and flu comparison. *Nature Immunology* **22,** 32–40 (2021).

15. Powell, T. J. *et al.* CD8+ T cells responding to influenza infection reach and persist at higher numbers than CD4+ T cells independently of precursor frequency. *Clinical Immunology* **113,** 89–100 (2004).

16. Myers, M. A. *et al.* Dynamically linking influenza virus infection kinetics, lung injury, inflammation, and disease severity. *eLife* **10,** e68864 (2021).

17. Brown, D. M., Román, E. & Swain, S. L. *CD4 T cell responses to influenza infection* in *Seminars in Immunology* **16** (2004), 171–177.

18. Krammer, F. The human antibody response to influenza A virus infection and vaccination. *Nature Reviews Immunology* **19,** 383–397 (2019).

19. Walker, F. C., Sridhar, P. R. & Baldridge, M. T. Differential roles of interferons in innate responses to mucosal viral infections. *Trends in Immunology* **42,** 1009–10023 (11 2021).

20. Ivashkiv, L. B. & Donlin, L. T. Regulation of type I interferon responses. *Nature Reviews Immunology* **14,** 36–49 (2014).

21. Ivanov, A. & Sharkovsky, A. in *Dynamics Reported: Expositions in Dynamical Systems* 164–224 (Springer, 1992).

22. Park, A. & Iwasaki, A. Type I and type III interferons–induction, signaling, evasion, and application to combat COVID-19. *Cell Host & Microbe* **27,** 870–878 (2020).

23. Lee, A. J. & Ashkar, A. A. The dual nature of type I and type II interferons. *Frontiers in Immunology* **9,** 2061 (2018).

24. Mertowska, P., Smolak, K., Mertowski, S. & Grywalska, E. Immunomodulatory role of interferons in viral and bacterial infections. *International Journal of Molecular Sciences* **24,** 10115 (2023).

25. Cui, W. & Kaech, S. M. Generation of effector CD8+ T cells and their conversion to memory T cells. *Immunological Reviews* **236,** 151–166 (2010).

26. Regoes, R. R., Yates, A. & Antia, R. Mathematical models of cytotoxic T-lymphocyte killing. *Immunology & Cell Biology* **85,** 274–279 (4 2007).

27. Nowak, M. A. & May, R. *Virus Dynamics: Mathematical Principles of Immunology and Virology* (Oxford University Press, 2000).

28. Wherry, E. & Ahmed, R. Memory CD8 T-cell differentiation during viral infection. *Journal of Virology* **78,** 5535–45 (11 2004).

29. Antia, R., Bergstrom, C. T., Pilyugin, S. S., Kaech, S. M. & Ahmed, R. Models of CD8+ responses: 1. What is the antigen-independent proliferation program. *Journal of Theoretical Biology* **221,** 585–598 (2003).

30. Antia, R., Ganusov, V. & Ahmed, R. The role of models in understanding CD8+ T-cell memory. *National Review of Immunology* **5,** 101–11 (2005).

31. Seder, R., Darrah, P. & Roederer, M. T-cell quality in memory and protection: implications for vaccine design. *Nature Reviews Immunology* **8,** 247–258 (2008).

32. Morel, P. A., Ta'asan, S., Morel, B. F., Kirschner, D. E. & Flynn, J. L. New insights into mathematical modeling of the immune system. *Immunologic Research* **36,** 157–165 (1-3 2006).

33. Hart, Y. *et al.* Paradoxical Signaling by a Secreted Molecule Leads to Homeostasis of Cell Levels. *Cell* **158,** 1022–1032 (2014).

34. Nutt, S. L., Hodgkin, P. D., Tarlinton, D. M. & Corcoran, L. M. The generation of antibody-secreting plasma cells. *Nature Reviews Immunology* **15,** 160–171 (2015).

35. Khodadadi, L., Cheng, Q., Radbruch, A. & Hiepe, F. The maintenance of memory plasma cells. *Frontiers in Immunology* **10,** 721 (2019).

36. Larson, E. W., Dominik, J. W., Rowberg, A. H. & Higbee, G. A. Influenza virus population dynamics in the respiratory tract of experimentally infected mice. *Infection and Immunity* **13,** 438–447 (1976).

37. Baccam, P., Beauchemin, C., Macken, C. A., Hayden, F. G. & Perelson, A. S. Kinetics of influenza A virus infection in humans. *Journal of Virology* **80,** 7590–7599 (2006).

38. Möhler, L., Flockerzi, D., Sann, H. & Reichl, U. Mathematical model of influenza A virus production in large-scale microcarrier culture. *Biotechnology and Bioengineering* **90,** 46–58 (2005).

39. Smith, A. M. *et al.* Effect of 1918 PB1-F2 expression on influenza A virus infection kinetics. *PLOS Computational Biology* **7,** e1001081 (2011).

40. Tan, J., Pan, R., Qiao, L., Zou, X. & Pan, Z. Modeling and dynamical analysis of virus-triggered innate immune signaling pathways. *PLOS One* **7** (10 2012).

41. Handel, A., Longini Jr, I. M. & Antia, R. Towards a quantitative understanding of the within-host dynamics of influenza A infections. *Journal of the Royal Society Interface* **7,** 35–47 (2010).

42. Zarnitsyna, V., Lavine, J., Ellebedy A Ahmed, R. & Antia, R. Multi-epitope Models Explain How Pre-existing Antibodies Affect the Generation of Broadly Protective Responses to Influenza. *PLOS Pathology* **12** (6 2019).

43. Liparulo, T. S. & Shoemaker, J. E. Mathematical Modeling Suggests That Monocyte Activity May Drive Sex Disparities during Influenza Infection. *Viruses* **16,** 837 (2024).

44. Bocharov, G. & Romanyukha, A. Mathematical model of antiviral immune response III. Influenza A virus infection. *Journal of Theoretical Biology* **167,** 323–360 (1994).

45. Gilpin, S. E., Charest, J. M., Ren, X. & Ott, H. C. Bioengineering lungs for transplantation. *Thoracic Surgery Clinics* **26,** 163–171 (2016).

46. Hartley, G. E. *et al.* Influenza-specific IgG1+ memory B-cell numbers increase upon booster vaccination in healthy adults but not in patients with predominantly antibody deficiency. *Clinical & Translational Immunology* **9,** e1199 (2020).

47. Glass, D. S., Jin, X. & Riedel-Kruse, I. H. Nonlinear delay differential equations and their application to modeling biological network motifs. *Nature Communications* **12,** 1788 (2021).

48. Smith, H. *An introduction to delay differential equations with applications to the life sciences* (Springer, 2011).

49. Shampine, L. F. & Thompson, S. Solving ddes in matlab. *Applied Numerical Mathematics* **37,** 441–458 (2001).

50. Barton, D. A. Stability calculations for piecewise-smooth delay equations. *International Journal of Bifurcation and Chaos* **19,** 639–650 (2009).

51. Bernardo, M., Budd, C., Champneys, A. R. & Kowalczyk, P. *Piecewise-smooth dynamical systems: theory and applications* chap. Qualitative theory of non-smooth dynamical systems (Springer Science & Business Media, 2008).

52. Bellen, A. & Zennaro, M. *Numerical methods for delay differential equations* (Numerical Mathematics and Science, 2013).

53. Spijker, M. N. Stiffness in numerical initial-value problems. *Journal of Computational and Applied Mathematics* **72,** 393–406 (1996).

54. The MathWorks Inc. *MATLAB version: 9.13.0 (R2022b)* Natick, Massachusetts, United States, 2022. https://www.mathworks.com.

55. Agrawal, V., Zhang, C., Shapiro, A. D. & Dhurjati, P. S. A dynamic mathematical model to clarify signaling circuitry underlying programmed cell death control in Arabidopsis disease resistance. *Biotechnology Progress* **20,** 426–442 (2004).

56. Przedborski, M. *venetoclax-tedizolid* https://github.com/mprzedborski/venetoclax-tedizolid. 2022.

57. Price, I. *et al.* The inflammatory response to influenza A virus (H1N1): an experimental and mathematical study. *Journal of Theoretical Biology* **374,** 83–93 (2015).

58. Pascucci, E. & Pugliese, A. Modelling immune memory development. *Bulletin of Mathematical Biology* **83,** 118 (2021).

59. Billeskov, R., Beikzadeh, B. & Berzofsky, J. A. The effect of antigen dose on T cell-targeting vaccine outcome. *Human Vaccines & Immunotherapeutics* **15,** 407–411 (2019).

60. Rahil, Z. *et al.* Landscape of coordinated immune responses to H1N1 challenge in humans. *The Journal of Clinical Investigation* **130,** 5800–5816 (2020).

61. Kaech, S. M. & Ahmed, R. Memory CD8+ T cell differentiation: initial antigen encounter triggers a developmental program in naive cells. *Nature Immunology* **2,** 415–422 (2001).

62. Van den Broek, T., Borghans, J. A. & Van Wijk, F. The full spectrum of human naive T cells. *Nature Reviews Immunology* **18,** 363–373 (2018).

63. Van Stipdonk, M. J., Lemmens, E. E. & Schoenberger, S. P. Naive CTLs require a single brief period of antigenic stimulation for clonal expansion and differentiation. *Nature immunology* **2,** 423–429 (2001).

64. Allan, M. J., Callard, R., Stark, J. & Yates, A. Comparing antigen-independent mechanisms of T cell regulation. *Journal of Theoretical Biology* **228,** 81–95 (2004).

65. Macallan, D. C., Busch, R. & Asquith, B. Current estimates of T cell kinetics in humans. *Current Opinion in Systems Biology* **18,** 77–86 (2019).

66. Kaech, S. M., Wherry, E. J. & Ahmed, R. Effector and memory T-cell differentiation: implications for vaccine development. *Nature Reviews Immunology* **2,** 251–262 (2002).

67. Weisstein, E. W. Bolzano's Theorem. *https://mathworld. wolfram. com/* (2008).

68. Schuh, L., Markov, P. V., Veliov, V. M. & Stilianakis, N. I. A mathematical model for the within-host (re) infection dynamics of SARS-CoV-2. *Mathematical Biosciences* **371,** 109178 (2024).

69. Bodewes, R. *et al.* Prevalence of antibodies against seasonal influenza A and B viruses in children in Netherlands. *Clinical and Vaccine Immunology* **18,** 469–476 (2011).

70. Hall, E. *Chapter 12: Influenza* https://www.cdc.gov/pinkbook/hcp/table-of-contents/chapter-12-influenza.html. 2024.

71. Stewart, W. *The Interferon System* (Springer Vienna, 2012).

72. Arnheiter, H., Haller, O. & Lindenmann, J. Host gene influence on interferon action in adult mouse hepatocytes: specificity for influenza virus. *Virology* **103,** 11–20 (1980).

73. Vitale, G. *et al.* Effects of type I interferons on IGF-mediated autocrine/paracrine growth of human neuroendocrine tumor cells. *American Journal of Physiology-Endocrinology and Metabolism* **296,** E559–E566 (2009).

74. Vieira, P. & Rajewsky, K. The half-lives of serum immunoglobulins in adult mice. *European Journal of Immunology* **18,** 313–316 (1988).

75. Rawlins, E. L. & Hogan, B. L. Ciliated epithelial cell lifespan in the mouse trachea and lung. *American Journal of Physiology-Lung Cellular and Molecular Physiology* **295,** L231–L234 (2008).

76. Staneková, Z. & Varečková, E. Conserved epitopes of influenza A virus inducing protective immunity and their prospects for universal vaccine development. *Virology* **7,** 1–13 (2010).

77. Wahl, I. & Wardemann, H. Sterilizing immunity: understanding COVID-19. *Immunity* **55,** 2231–2235 (2022).

78. Patel, M. M., York, I. A., Monto, A. S., Thompson, M. G. & Fry, A. M. Immune-mediated attenuation of influenza illness after infection: opportunities and challenges. *The Lancet Microbe* **2,** e715–e725 (2021).

79. Amanna, I. J. & Slifka, M. K. Mechanisms that determine plasma cell lifespan and the duration of humoral immunity. *Immunological Reviews* **236,** 125–138 (2010).

80. Jansen, J. M., Gerlach, T., Elbahesh, H., Rimmelzwaan, G. F. & Saletti, G. Influenza virus-specific CD4+ and CD8+ T cell-mediated immunity induced by infection and vaccination. *Journal of Clinical Virology* **119,** 44–52 (2019).

81. Pizzolla, A. & Wakim, L. M. Memory T cell dynamics in the lung during influenza virus infection. *The Journal of Immunology* **202,** 374–381 (2019).

82. Sridhar, S. *et al.* Cellular immune correlates of protection against symptomatic pandemic influenza. *Nature Medicine* **19,** 1305–1312 (2013).

83. Eickhoff, C. S. *et al.* Highly conserved influenza T cell epitopes induce broadly protective immunity. *Vaccine* **37,** 5371–5381 (2019).

84. Bui, H.-H., Peters, B., Assarsson, E., Mbawuike, I. & Sette, A. Ab and T cell epitopes of influenza A virus, knowledge and opportunities. *Proceedings of the National Academy of Sciences* **104,** 246–251 (2007).

85. Sridhar, S. *et al.* Longevity and determinants of protective humoral immunity after pandemic influenza infection. *American Journal of Respiratory and Critical Care Medicine* **191,** 325–332 (2015).

86. Petrie, J. G., Ohmit, S. E., Johnson, E., Truscon, R. & Monto, A. S. Persistence of antibodies to influenza hemagglutinin and neuraminidase following one or two years of influenza vaccination. *The Journal of Infectious Diseases* **212,** 1914–1922 (2015).

87. Zelner, J., Petrie, J. G., Trangucci, R., Martin, E. T. & Monto, A. S. Effects of sequential influenza A (H1N1) pdm09 vaccination on antibody waning. *The Journal of Infectious Diseases* **220,** 12–19 (2019).

88. Vorvick, L. J. *Flu (Influenza)* 2022. https://www.pennmedicine.org/for-patients-and-visitors/patient-information/conditions-treated-a-to-z/flu-influenza#:~:text=Most%20people%20get%20a%20cold,usually%20not%20the%20actual%20flu..

89. Hoa, L. N. M. *et al.* Influenza A (H1N1) pdm09 but not A (H3N2) virus infection induces durable seroprotection: results from the Ha Nam cohort. *The Journal of Infectious Diseases* **226,** 59–69 (2022).

90. Tsang, T. K. *et al.* Reconstructing antibody dynamics to estimate the risk of influenza virus infection. *Nature Communications* **13,** 1557 (2022).

91. Boonarkart, C., Suptawiwat, O., Sakorn, K., Puthavathana, P. & Auewarakul, P. Exposure to cold impairs interferon-induced antiviral defense. *Archives of Virology* **162,** 2231–2237 (2017).

92. Netea, M. G. *et al.* Defining trained immunity and its role in health and disease. *Nature Reviews Immunology* **20,** 375–388 (2020).

93. Hajishengallis, G., Netea, M. G. & Chavakis, T. Innate immune memory, trained immunity and nomenclature clarification. *Nature Immunology* **24,** 1393–1394 (2023).

94. Yang, W., Karspeck, A. & Shaman, J. Comparison of filtering methods for the modeling and retrospective forecasting of influenza epidemics. *PLOS Computational Biology* **10,** e1003583 (2014).

95. KhudaBukhsh, W. R., Choi, B., Kenah, E. & Rempała, G. A. Survival dynamical systems: individual-level survival analysis from population-level epidemic models. *Interface Focus* **10,** 20190048 (2020).

96. Lukens, S. *et al.* A large-scale immuno-epidemiological simulation of influenza A epidemics. *BMC Public Health* **14,** 1–15 (2014).

97. Forsyth, K. S., Jiwrajka, N., Lovell, C. D., Toothacre, N. E. & Anguera, M. C. The conneXion between sex and immune responses. *Nature Reviews Immunology,* 1–16 (2024).

98. Klein, S. L., Hodgson, A. & Robinson, D. P. Mechanisms of sex disparities in influenza pathogenesis. *Journal of Leukocyte Biology* **92,** 67–73 (2012).

99. Klein, S. L. & Flanagan, K. L. Sex differences in immune responses. *Nature Reviews Immunology* **16,** 626–638 (2016).

100. Dunn, S. E., Perry, W. A. & Klein, S. L. Mechanisms and consequences of sex differences in immune responses. *Nature Reviews Nephrology* **20,** 37–55 (2024).

101. Giurgea, L. T. *et al.* Sex differences in influenza: the challenge study experience. *The Journal of Infectious Diseases* **225,** 715–722 (2022).

102. Cotra, S., Kohandel, M. & Przedborski, M. Sex-Related Differences in the Immune System Drive Differential Responses to Anti-PD-1 Immunotherapy. *Biomolecules* **14,** 1513 (2024).

103. Bogaards, J. A. *et al.* Sex-specific immunization for sexually transmitted infections such as human papillomavirus: insights from mathematical models. *PLOS Medicine* **8,** e1001147 (2011).